3-11-2024

Role of Glia in Diurnal Rhythms in Neuroinflammation and Blood-Brain Barrier Breakdown

Jennifer Hoi-Ping Lawrence
Washington University in St. Louis

WASHINGTON UNIVERSITY IN ST. LOUIS

Division of Biology and Biomedical Sciences
Neurosciences

Dissertation Examination Committee:
Erik Musiek, Chair
Marco Colona
Richard Daneman
Jason Ulrich
Gregory Wu

Role of Glia in Diurnal Rhythms in Neuroinflammation and Blood-Brain Barrier Breakdown

by
Jennifer Lawrence

A dissertation presented to
Washington University in St. Louis
in partial fulfillment of the
requirements for the degree
of Doctor of Philosophy

May 2024
St. Louis, Missouri

Table of Contents

List of Figures

Acknowledgments

I would first like to thank my thesis advisor, Dr. Erik Musiek for always supporting my scientific development and for always being in my corner. Thank you for allowing me to pursue the most interesting scientific questions and for building such a caring community. Thank you to everyone in the Musiek Lab for always going above and beyond to help me with experiments at all hours of the day, especially my fellow graduate students. A special note to Julie Dimitry for keeping things running and always being willing to help troubleshoot problems, none of this would be possible without you.

To my parents, thank you for encouraging my love of learning and science from an early age. I feel incredibly fortunate to have inherited your passion for asking and answering questions. And to my brother, it has always meant a lot to know that you were there if I needed you.

A huge thank you to all the people I have had the privilege of calling friends. I cannot thank you all enough for all the words of encouragement, laughs, and great memories you have all given me. Another special note to my partner, Pat Sheehan, who faithfully supported both me and my science from the very beginning.

Jennifer Lawrence

Washington University in St. Louis

May 2024

Dedicated to my parents. For always supporting me.

Abstract of the Dissertation

Role of Glia in Diurnal Rhythms in Neuroinflammation and Blood-Brain Barrier Breakdown

by

Jennifer Lawrence

Doctor of Philosophy in Biology and Biomedical Sciences

Neurosciences

Washington University in St. Louis, 2024

Professor Erik Musiek, Chair

While inflammation is an important mechanism for the return to homeostasis post insult or injury, inflammation in the central nervous system (CNS) can lead to irreparable damage. To mitigate this process, the brain is protected from circulating neurotoxic molecules as well as peripheral immune cells through the tightly regulated blood-brain barrier (BBB). The balance between pro- and anti- inflammation in the CNS rapidly shifts towards a neurotoxic proinflammatory state during acute bacterial or viral infections or chronic neuroinflammatory diseases. Excessive inflammatory responses are also coupled with extensive BBB leakage and breakdown, allowing rampant entry of peripheral inflammatory cells and mediators into the brain. Recent evidence suggest that many aspects of immune function exhibit pronounced 24-hour rhythms which are controlled by the circadian system. Immune cell activation and trafficking, cytokine production, and pgp-transporter efflux across the BBB are all modulated by circadian rhythms. Using a mouse model of sepsis, we found that there is diurnal variation in the severity of inflammatory BBB breakdown and that this evening susceptibility is driven through the activation of glial cells – including microglia and astrocytes. Neurodegenerative diseases,

such as Alzheimer's disease (AD), are characterized by chronic rather than acute inflammation still have rhythms in immune response. We found that the pro-inflammatory chemokine CXCL5 is rhythmically expressed in astrocytes, under the control of the molecular clock, and increases in expression in mouse models of AD. Using an astrocyte-specific overexpression model, we observed that increased levels of CXCL5 induces greater amyloid-beta plaque load. This increase in disease pathology was due to an increase in plaque count and occurred independently of glial activation, suggesting astrocyte-derived CXCL5 induces loss of glial support and increased amyloid-beta deposition. Altogether, these data highlight the importance of considering all aspects of circadian biology when studying chronic and acute inflammation in both the periphery and CNS.

Chapter 1: Introduction

1.1 Circadian Rhythms and Immunity

1.1.1 Circadian Rhythms – Zeitgebers and Sleep

Circadian rhythms exist in almost all living organisms, from complex mammals to cyanobacteria (Ouyang et al., 1998; Takahashi, 2017). These rhythms help an organism predict changes to its environment which improve its overall fitness (Takahashi, 2017). Daily biological or behavioral rhythms begin and end within a 24-hour period of time, leading to the term "circadian" - which stems from the Latin words "*circa*" and "*diem*", translating to "about day" (Sehgal, 2017). The circadian clock is synchronized to the external environment by cues termed "zeitgebers", the German word for "time-giver" (Etain et al., 2011). Light is the primary zeitgeber, although many other environmental factors like social cues and feeding time also serve as zeitgebers (Etain et al., 2011). Canonically, light passes through the eye and strikes the retina, where it activates rods and cones and sends visual information to the occipital lobe via the optic nerve (Hattar et al., 2002). However, light also activates intrinsically photosensitive retinal ganglion cells in the retina. These cells encode for non-visual information and instead project along the retinohypothalamic tract directly to the suprachiasmatic nucleus (SCN) in the hypothalamus of the brain (Hendrickson et al., 1972; Moore & Lenn, 1972). The SCN is the primary internal clock in mammals, it is a collection of 20,000 neurons which transduce environmental information into both neuronal and humoral signals (Takahashi et al., 2008). This diverse output allows the SCN to control a variety of behavioral functions ranging from hormone release to body-temperature fluctuations (Takahashi et al., 2008). Experiments conducted in the 1970s found that lesioning the SCN ablated behavioral and hormonal rhythms in rodents (Moore

& Eichler, 1972; Stephan & Zucker, 1972). It is important to note that these studies found that the SCN was necessary for the *temporal* control of the behavior rather than the behavior itself, as lesioned animals had no change in ability to conduct these behaviors (Moore & Eichler, 1972; Stephan & Zucker, 1972). In example, one such study found that SCN-lesioned rats had no change in the total amount they slept; however, their sleep was no longer consolidated to one time (Ibuka & Kawamura, 1975). This study was key in disentangling sleep and circadian rhythms as two distinct processes.

Sleep-wake cycles are an intrinsic part of all animals, they are defined by two behavioral states – adaptive behavior (activity/wakefulness) and behavioral quiescence (rest/sleep) (Moore, 2007). The balance between sleep and wake is determined by the interplay of two opposing forces – homeostatic sleep drive and the circadian drive for arousal (Moore, 2007). Homeostatic sleep drive is the aggregate of all sleep-promoting substances. These substances are defined as anything that incrementally increase over time and are reset post-sleep. Conversely, arousal factors are under circadian control and are defined as substances that promote wakefulness. In diurnal animals, such as humans, homeostatic sleep drive is at its nadir in the early morning after we wake and increases continually with time. Rather than increase linearly, arousal is under circadian control – increasing after we wake and peaking midday before decreasing during the evening. At a critical point, the mounting homeostatic pressure to sleep outweighs the waning circadian drive for arousal, inducing sleep. This pattern is inverted in nocturnal animals, such as mice and rats.

1.1.2 Circadian Rhythms – Entrainment and the Molecular Clock

The balance between sleep and wake is tightly temporally regulated, since diurnal and nocturnal animals are specifically suited to navigate either the day or night. Researchers can

measure bouts of animal activity per unit time as a gross measurement of wake vs sleep states, these measurements are termed “actigraphy”. A common method to track actigraphy is a simplified, automated form of the open field test which uses infrared sensors attached to individually housed animals’ home cages (J. Park et al., 2021). As the animal freely roams the cage, the sensors record movement and, over the course of several days, patterns in the onset and offset of the animal’s behavior appear (LeGates & Altimus, 2011). While these data cannot give an in-depth understanding of sleep structure, they are a non-invasive, affordable method for recording the timing of an animal’s sleep and wake states (J. Park et al., 2021). The timing of these sleep-wake cycles is tightly tied to when zeitgebers are presented (LeGates & Altimus, 2011). When controlling for other variables, such as the presence or absence of food, light becomes the primary zeitgeber (Etain et al., 2011). Measuring how closely activity onset tracks with the presence of light gives a definition for how “entrained” an animal is. In nocturnal animals, such as mice, fully entrained animals will wake immediately upon the onset of dark and sleep during the light (LeGates & Altimus, 2011).

While zeitgebers are critical for the *synchronization* of circadian rhythms, it was found as early at 1729 that rhythms persist in constant conditions (Sehgal, 2017). Mice kept in constant darkness with *ad libitum* access to food and water continue to have defined periods of wake and sleep (F. C. Davis & Menaker, 1981; Ebihara et al., 1978; Wee et al., 2002). However, while mice continue to be rhythmic, the onset of activity is no longer entrained to occur at set time each day. Without the presence of a zeitgeber, animals wake and sleep depending on their own individual period – this is called “free-running” (Ameen et al., 2022). Most mice have a period slightly shorter than 24 hours, so they begin to wake up slightly earlier each day when in constant darkness (F. C. Davis & Menaker, 1981). An animal’s internal period is species

dependent, with even individual strains of mice having slightly altered patterns in free-running (Ebihara et al., 1978). Free-running (or organism-dependent circadian rhythms in constant conditions) is distinct from being arhythmic, which is the complete lack of rhythms characterized by fragmented bouts of sleep and arousal states (Zheng et al., 1999). Adding further complexity, arhythmic mice can mask – showing entrained rhythms if presented with a strong enough zeitgeber, despite their fragmented behavior when kept in constant conditions. These studies highlight the complicated relationship in between internal rhythms (an animal's innate period) and environmental cues (the presence or absence of zeitgebers).

Internal rhythms are maintained by cell-autonomous clocks, ruled by ubiquitously expressed clock genes (Lowrey & Takahashi, 2004; Takahashi et al., 2008). The molecular clock is driven by a transcription-translation feedback loop (TTFL) comprised of the core clock genes as well as downstream enhancers and repressors. The core clock proteins, CLOCK (*Clock*) and BMAL1 (*Arntl1*), form a heterodimer which binds to regulatory elements of the DNA, driving the upregulation of rhythmic genes – including their own repressors PERIOD (*Per1, Per2, Per3*) and CRYPTOCHROME (*Cry1, Cry2*)[2]. The CLOCK:BMAL1 complex acts as the positive arm of the molecular clock, increasing during the day, while PER and CRY act as the negative arm of the clock, reaching peak levels during the early evening (Takahashi, 2017). The TTFL will continue to cycle throughout a 24-hour period without external input, driving rhythmic functions despite a lack of environmental cues; however, SCN output is critical for ensuring individual cells in the body are able to synchronize functions with one another (Ramkisoensing & Meijer, 2015). Further studies are needed to fully elucidate what physiological functions are affected by the interplay between internal and external circadian rhythms.

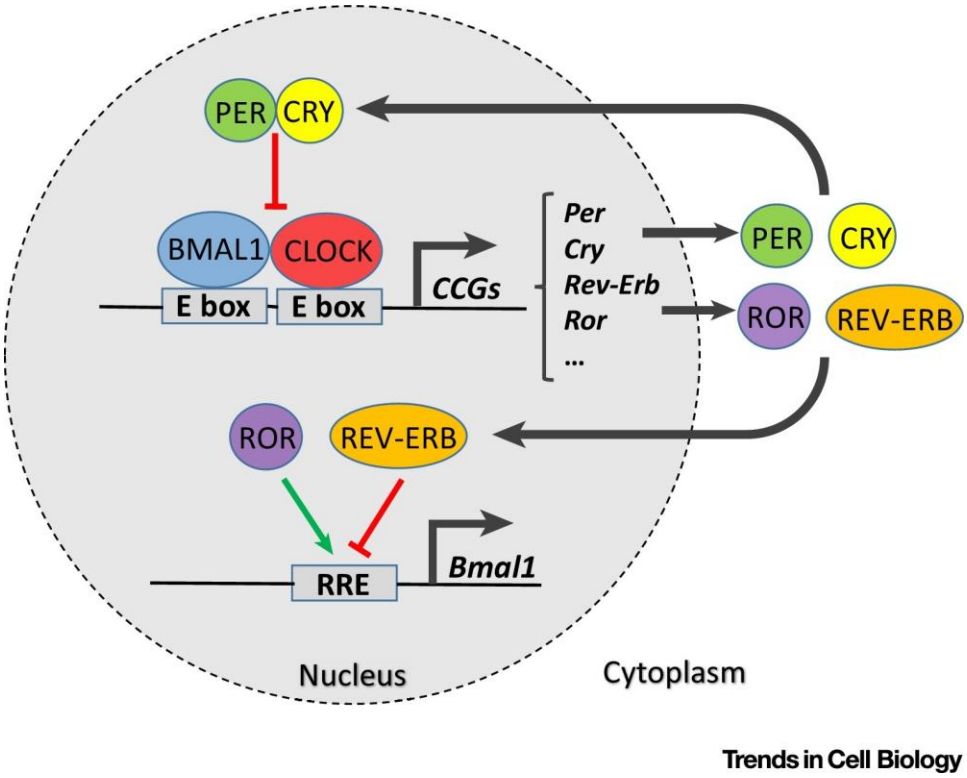

Figure 1.1: The transcription-translation feedback loop and the core circadian clock. The intracellular molecular clock is formed by a "positive" and "negative" arm of a transcription-translation feedback loop (TTFL). The positive arm is formed by the BMAL1 and CLOCK proteins, which drive the expression of the downstream genes *Per*, *Cry*, *Rev-Erb*, and *Ror*. These genes encode for proteins involved in the negative arm of the loop, with PER and CRY inhibiting BMAL1 and REB-ERB acting as a negative repressor. Figure from: (Gaucher et al., 2018)

1.1.3 Peripheral Inflammation and Rhythms in Adaptive Immunity

When an inflammatory insult or injury occurs, it is critical for the body to have mechanisms to both combat the injury as well as return to homeostasis. This basic introduction to the immune system is in reference to Janeway's Immunobiology, 8th edition (Murphy et al., 2017). The immune system is comprised of leukocytes, commonly referred to as "white blood cells". Leukocytes are produced by hematopoietic stem cells that reside in bone marrow. These pluripotent stem cells can become either a myeloid or lymphoid progenitor cell, this division grossly divides the downstream cell lineages into innate or adaptive immune response cells.

Myeloid progenitor cells generate innate immune cells, including monocytes (dendritic cells and macrophages) as well as granulocytes (eosinophils, basophils, and neutrophils). Lymphoid progenitor cells produce lymphocytes (T cells and B cells) - the adaptive immune response cells. Natural killer cells also come from the lymphoid progenitor cell line but unlike other cells within the lineage do not have antigen specificity.

The adaptive immune system responds to antigens present on pathogens, allowing it to mount a robust, targeted response. However, this process can take on the scale of days to produce, creating a need for a more immediate response. This is where the innate immune system comes in. In addition to granulocytes, monocytes and macrophages are the primary innate immune cells. Monocytes circulate throughout the blood, migrating into tissues where they can then mature into macrophages. Circulating monocytes and tissue-resident macrophages act as a first line of defense, engulfing pathogens through a process called phagocytosis.

While macrophages lack the antigen specificity of adaptive immune cells, they express pattern recognition receptors (PRRs) that recognize molecular patterns commonly found on pathogens. PRRs allow innate immune cells to quickly differentiate between “self” and “non-self” cell-to-cell interactions and identify harmful pathogens. An example of a PRR is toll-like receptor 4 (TLR-4) which specifically responds to lipopolysaccharide (LPS), a component of gram-negative bacteria such as *E. coli*. As immediate responders, another important role of macrophages is to recruit and activate other leukocytes. They do this through the production of cytokines. These cytokines often act as autocrine or paracrine signaling molecules, inducing local responses like vasodilation. However, more stable cytokines can act in an endocrine manner – triggering wide-spread behavioral effects such as fever. Specific cytokines called chemokines induce chemotaxis, recruiting additional leukocytes to the site of infection or

inflammation. Altogether, this process of pathogen-induced cytokine release is called "inflammation".

Rhythms in immune response may confer an evolutionary advantage of ensuring maximum immunity during daily times at which animals are at the greatest risk of injury or infection (Curtis et al., 2014). However, any sensitization of the innate immune response must be under tight control. Increased leukocyte recruitment and excessive release of pro-inflammatory cytokines could quickly lead to a detrimental, pro-inflammatory positive feedback loop. In order to keep immune sensitization in check, both adaptive and innate immune cells have rhythmic functions dependent upon BMAL1-driven cellular clocks, although these rhythmic functions vary by cell type (Boivin et al., 2003; Bollinger et al., 2011; Keller et al., 2009; Silver et al., 2012).

The impact of rhythms on adaptive immune cell function is a burgeoning field of circadian biology. The most well understood example of this is in Multiple Sclerosis (MS). There are two subtypes of MS, relapsing remitting MS (RRMS) and primary progressive MS (PPMS). Both forms are a chronic autoimmune condition characterized by T cell-dependent destruction of the myelin sheath along neurons. Researchers model MS through Experimental Autoimmune Encephalitis (EAE), an ascending paralytic autoimmune disease induced through immunizing mice with myelin peptides, Freud's Adjuvant, and pertussis toxin (Wiedrick et al., 2021). This cocktail of drugs triggers the migration of activated, myelin-specific T cells into the central nervous system (CNS), where they produce widespread inflammation and peripheral monocyte infiltration. Together these adaptive and innate immune cells create demyelinating perivascular CNS white-matter lesions – leading to hindlimb weakness after 12-15 days and eventual

paraplegia, severe ataxia, and in some cases death by 35 days post-immunization (Wiedrick et al., 2021).

Light and circadian rhythms drive EAE disease progression, with the time-of-day (TOD) of immunization impacting disease progression (Druzd et al., 2017) and constant light (L:L) or dark (D:D) showing ameliorated disease severity (Moriguchi et al., 2021). Researchers found that mice immunized with EAE 8 hours after the onset of light (zeitgeber time 8, ZT8) had significantly worse disease progression than those immunized at ZT20, and these differences persisted up to 30 days post-immunization (Druzd et al., 2017). They also found that this phenomenon was due to TOD differences in the trafficking of T and B cells to lymph nodes (LNs). There is a peak in lymphocyte homing towards LNs during the onset of night, coupled with an antiphase peak in egress during the day. The increase in lymphocytes in LNs during the night allows the adaptive immune system to mount a stronger immune response, leading to increased T cell CNS-infiltration and overall worsened disease severity in mice immunized at ZT8. They found rhythmic LN homing – and the subsequent disease severity – were both circadian and under BMAL1 control. Rhythmic LN homing persisted in D:D and was completely abrogated with genetic *Bmal1* deletion, or "knockout" (BmKO), in specifically T cells. BmKO T cells became "stuck", unable to properly exit LNs and re-enter the lymphatic system – clamping the TOD difference in a protective "ZT20-like" state (Druzd et al., 2017). However, while EAE immunization occurs acutely, MS in humans is a chronic progressive disease with no clear time of disease onset. Despite this difference, circadian rhythms may still prove to be a vital consideration for treating MS. When comparing RRMS patients there are only significant differences in disease-associated gene expression between those relapsing or in remission when

their blood is tested at night – indicating that disease severity and immune cell infiltration in MS are still closely tied to circadian rhythms (Huang et al., 2021).

1.1.4 Impact of Light and Circadian Rhythms on Acute Infections

While chronic peripheral inflammatory diseases such as atherosclerosis, MS, arthritis, and obesity all have established circadian effects, acute onset inflammatory diseases – such as sepsis – have also been linked to sleep and circadian rhythm disturbances (Almalki et al., 2022; Cox et al., 2022; Curtis et al., 2014). Sepsis is not a disease itself, but is rather a dysregulated immune response to an underlying pathogen, leading to rampant inflammation throughout the body (S. R. Bennett, 2015). Sepsis is a leading cause of death in the United States and the mortality rate for patients with sepsis is 15%, increasing to 40-50% in patients with severe, multi-organ dysfunction sepsis (Quartin et al., 2008). In one mouse model of sepsis, mice are given an injection of LPS, mimicking the pathogen pattern of gram-negative bacteria and stimulating TLR4 receptors and inducing an inflammatory response (Munford, 2010). TLR4 is expressed by antigen-presenting cells, including macrophages and epithelial cells. LPS, along with its co-factor LBP, bind to the membrane-bound receptor Cluster Differentiation 14 (CD14) on the surface of dendritic cells (Radulovic et al., 2018). Once attached to CD14, LPS is shuttled to Lymphocyte Antigen 96 (MD-2) which is attached to the extracellular portion of the TLR4 receptor. The MD-2/TLR4 complex is now able to induced downstream intracellular signaling in response to LPS binding, leading to activation of the Nuclear Factor KappaB pathway and the upregulation of proinflammatory cytokines such as *Tnfα*, *Il-6*, and *Il-1β* (Radulovic et al., 2018).

LPS responses have a strong TOD effect, with increased release of pro-inflammatory cytokines and chemokines when mice are treated with LPS at ZT12 compared to ZT0 (J. E.

Gibbs et al., 2012). A study in 2009 found that many of these rhythmic patterns of inflammatory cytokine production are dependent on cell-intrinsic macrophage circadian clocks (Keller et al., 2009). The researchers isolated leukocytes from the spleens of mice kept in D:D and found that, depending on the TOD they were isolated, splenocytes have different cytokine production post-LPS stimulation. In particular, TNFα and IL-6 were both rhythmically secreted, peaking at circadian time 8-12 (CT8-12). They found that these rhythms persisted in *ex vivo* cell cultures – indicating that the rhythmic production of proinflammatory cytokines is occurring independently from systemic factors.

This intrinsic rhythmicity in peripheral macrophage response may confer an evolutionary advantage; however, it could also increase the risk of an overactive immune response if an inflammatory stimulus occurs at the wrong time of day – ultimately harming an animal's fitness. Early studies from the 1960s and 70s found time-of-day variability in LPS induced mortality, with increased lethality at the end of the resting phase – 2h before the onset of activity (Halberg et al., 1960; Shackelford & Feigin, 1973). This data has been further supported by a recent study that found mortality post-LPS is highly rhythmic, with a peak in death when LPS is administered at ZT8 and a trough at ZT20 (Lang et al., 2021). The peak in LPS mortality coincides with peak entry of circulating leukocyte into peripheral tissues (which peak at ZT13), suggesting that circadian rhythms in LPS lethality are due to rhythms in cytokine production (J. E. Gibbs et al., 2012; Scheiermann et al., 2012). However, this phenomenon is more complex than this hypothesis can explain. Rhythms in LPS-mortality are light *dependent* and myeloid cell clock *independent*, as rhythms in mortality are ablated in mice kept in D:D but persist in myeloid cell BmKO mice (Lang et al., 2021). Additionally, rhythms in inflammatory cytokine production are not required for TOD differences in mortality, as cytokine production remained rhythmic in D:D,

with only slight alterations to the time at which expression peaks (Lang et al., 2021). In fact, rhythmic homing of peripheral immune cells to lymph nodes persisted in both D:D and myeloid BmKO conditions – indicating LPS-induced mortality is caused by a complex, multicellular circadian immune response (Lang et al., 2021).

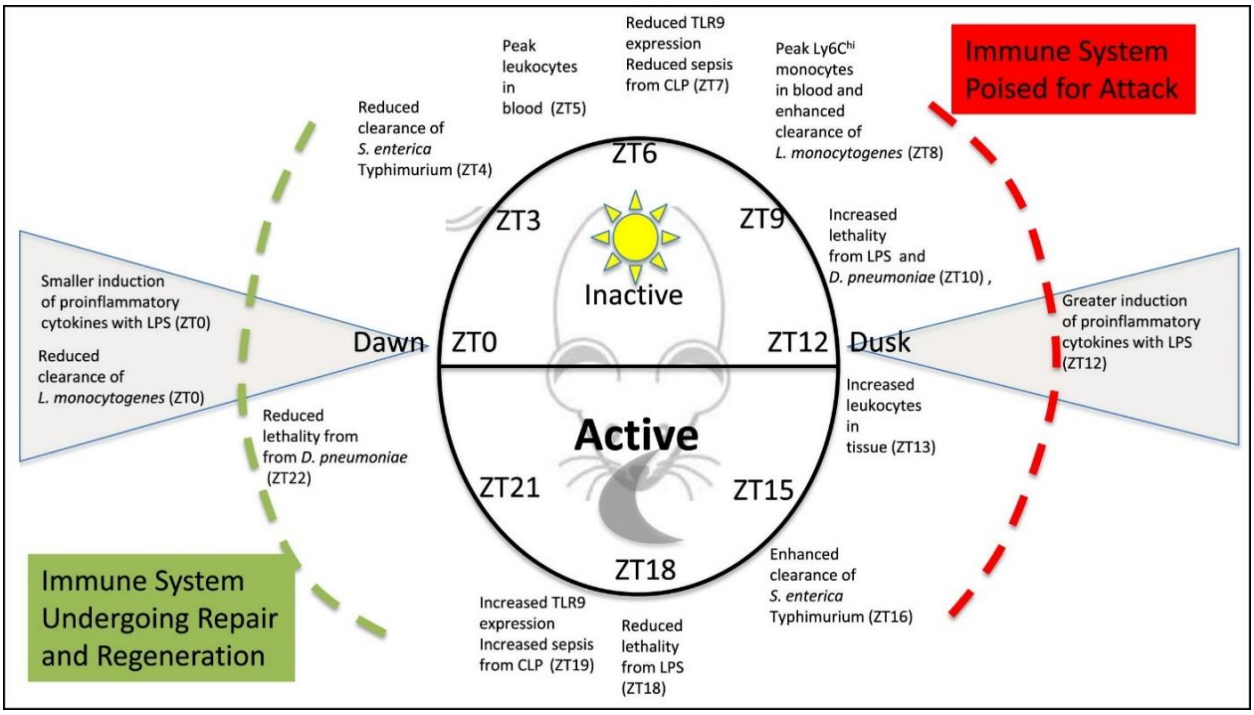

Figure 1.2: Rhythms in the murine immune response to acute infection. Mice are nocturnal, in that they are inactive during the day (from ZT0-ZT12) and active during the evening (ZT12-ZT24). The time of day at which the organism encounters various pathogens determines the severity of their immune response, with the greatest immune response during the onset of evening, at the beginning of their active phase. Figure from: (Curtis et al., 2014)

While bacterial endotoxins, such as LPS, have been used to model sepsis for many years, there are caveats. LPS is only one component of a bacterium, and other factors in true infection may concurrently activate additional pathways. There is also a large discrepancy in LPS response across species, with humans, horses, and rabbits having up to a 100,000-fold increase susceptibility to LPS compared to baboons, mice, rats, and chickens (Munford, 2010). The underlying mechanism for this difference is not yet known, although it is thought to be due to species-dependent macrophage responses to secreted serum factors (Munford, 2010). This

interspecies variability is a critical factor to consider for any translational research. Even within humans there is variability, healthy subjects treated with LPS maintain cerebrovascular autoregulation, but patients with severe sepsis do not – this could be due to differences in hypoxia and fever between the two models (Berg et al., 2013). Another caveat to consider is that there is proposed immune feedback regulation of the circadian system as some inflammatory cytokines can promote sleep (Paladino et al., 2010). These factors complicate studying the circadian effects, since sleep and inflammation may have a bidirectional interaction.

1.2 Rhythms in Blood Brain Barrier Function

1.2.1 Introduction to the Blood Brain Barrier

At baseline the CNS is generally considered "immune privileged", although this term has come under fire in recent years. While peripheral immune cells such as macrophages or T cells are generally restricted from the brain parenchyma in a healthy animal, there are resident immune cells in the brain the form of glia: astrocytes, microglia, and oligodendrocytes (further discussed in 1.2.2 Rhythms in the Neurovascular Unit). The strict separation between the CNS and peripheral blood compartment occurs through a series of tightly controlled barriers and serves not only to protect the brain from peripheral immune cells, but also other circulating proteins and other molecules in the blood, some of which may be neurotoxic. These barriers include both the blood cerebrospinal fluid barrier (BCSB) and blood brain barrier (BBB).

The brain is contained within the skull and meninges. While the skull is similar to peripheral bone in that it contains bone marrow niches, which allow for both the maintenance and production of adaptive and innate immune cells, the meningeal layers are more complex (Mazzitelli et al., 2022). There are three meningeal layers: the dura, arachnoid, and pia mater.

The dura mater is immune rich, full of leukocytes as well as lymphatic and fenestrated “leaky” blood vessels. Conversely, the arachnoid mater has an inner layer of epithelial cells that are connected by tight junctions (TJs), forming a restrictive barrier (Alcolado et al., 1988; Hannocks et al., 2018). Between the arachnoid and pia mater, together coined the leptomeninges, is the cerebrospinal fluid (CSF). CSF is produced by the choroid plexus and bathes the brain, flowing around the surface and within ventricles. The BSCB occurs at the intersection of the CSF and blood and is formed by ependymal cells, a type of ciliated neuroepithelial cell that have TJs (Buckley & McGavern, 2022).

There are two main arteries that supply blood to the CNS, the internal carotid and cerebral arteries – giving rise to anterior and posterior circulation respectively (Mastorakos & McGavern, 2019). These subarachnoid blood vessels branch off into penetrating arterioles that dive into the brain parenchyma while still being surrounded by the final meningeal layer, the pia mater. These blood vessels are the start of the CNS vascular tree. Penetrating arterioles branch off into capillaries, where the diameter of the vessel is small enough to allow for only a single red blood cell to pass (C. Wang et al., 2022). Post-capillary venules then carry the blood towards larger venules and draining veins, which have more incomplete coverage by the pia mater (Mastorakos & McGavern, 2019). At each level of the vascular tree, brain endothelial cells (BECs) express TJs which connect them to neighboring endothelial cells - creating a high-resistance barrier with low paracellular leakage. However, coverage by supporting cells differs depending on the vascular order. BECs in both arterioles and venules are adhered to the endothelial basement membrane and ensheathed by pericytes; however, only arteries and branching arterioles have additional smooth muscle cells. Almost all of the cerebrovascular surface is covered by astrocytic endfeet (Mathiisen et al., 2010). As penetrating blood vessels

enter the brain, the perivascular space between BECs and the surrounding pia mater becomes enclosed by astrocyte endfeet – referred to as the glial limitans – rather than the pia mater (Mastorakos & McGavern, 2019). Perivascular macrophages (PVMs) live in this perivascular (sometimes also called Virchow-Robin) space around arterioles and venules (T. Yang et al., 2019). This space is critical for immune surveillance (further discussed in 1.2.3 The BBB in disease).

At the smallest order, capillaries can be further divided into three major groups: (1) continuous non-fenestrated capillaries, (2) continuous fenestrated, and (3) discontinuous capillaries. The CNS contains continuous non-fenestrated capillaries where the endothelial and astrocyte basement membranes are directly adhered to one another, leaving little to no perivascular space (Mastorakos & McGavern, 2019). Bulk flow and cellular properties dictate that the majority of solute exchange occurs at the capillary level; however, intravenous tracer injections do not enter the brain parenchyma – despite being found in the leptomeninges, choroid plexus, and perivascular spaces (Mastorakos & McGavern, 2019; Yuan & Rigor, 2010). This restriction of entry from the blood to peri-capillary compartments is due to the blood-brain barrier (BBB) and indicates there are more complex mechanics at play than simple osmotic pressure. The BBB is formed by a series of distinct BEC properties, including continuous nonfenestrated vessels, decreased pinocytosis, the presence of junctional proteins, and additional regulatory elements that allow for the selective movement of solutes between the blood and CNS (Daneman, 2012).

BECs are connected to one another by TJs and Adherens junctions (AJs), the general biochemical properties of both are summarized from the following 2009 review (Hartsock & Nelson, 2008). AJs initiate and stabilize cell-cell adhesion, eventually leading to the assembly of

TJs – which in turn serve to control paracellular movement. Both AJs and TJs rely on cytoskeletal and transmembrane proteins. AJs are formed by E-cadherins, which have extracellular repeat domains that form weak, calcium-dependent interactions between neighboring cells. Intracellularly, p120-catenin binds to juxtamembrane domains on E-cadherin, regulating its recruitment to the plasma membrane as well as its internalization and degradation – allowing for temporal control over cell adhesiveness. Conversely, β-catenin – which is necessary for E-cadherin to exit the endoplasmic reticulum – binds with such high affinity that it is unknown if the two proteins ever dissociate. TJs are created by two transmembrane proteins, occludin and claudin, along with multiple associated intracellular proteins. Occludin helps regulate paracellular permeability by the binding of claudin and junctional adhesion molecules to a 20 amino acid sequence in its second extracellular loop. Through these cell-cell interactions, claudin can induce occludin protein turnover and decreased TJ localization, triggering increased ion flux. Claudins also form links between neighboring membranes, creating a paracellular "fence" that restricts solute movement. However, depending on the type of claudin present in the TJ there are varying degrees of ion permeability, allowing for paracellular TJ channels or "gates". TJs in the CNS are formed primarily by claudin-5 and claudin-1, although there is also claudin-3 and claudin-12 found in certain circumstances (Sladojevic et al., 2019). Other critical BBB junctional proteins include zonula occludin-1 (ZO-1), ZO-2, and ZO-3, which are scaffolding proteins that may link AJs and TJs through their ability to bind both occludin and p120-catenin (Utepbergenov et al., 2006).

Select small (400-500 Da) molecules can cross the BBB via passive paracellular and transcellular diffusion; however, efflux pumps exist to remove certain diffusible molecules – further limiting CNS entry (Wong et al., 2019). Large or polar molecules must enter through

facilitated diffusion or active transport (Fischer et al., 1998). Carrier-mediated transport requires protein receptors to shuttle molecules across the endothelial layer. Large molecules, such as glucose and amino acids, bind to specific protein transporters on the luminal side of the membrane. This binding induces a conformational change which allows the compound to pass through in the direction of the concentration gradient (Y. Chen & Liu, 2012). Unlike carrier-mediated transport, receptor-mediated transcytosis relies on a finite number of transmembrane receptors rather than a concentration gradient (Lajoie & Shusta, 2015). Macromolecular ligands bind to specific receptors on the luminal endothelial wall, triggering membrane invagination, pinching off an intracellular vesicle containing both the receptor and ligands (Wong et al., 2019). This vesicle is then transported across the endothelium, releasing its contents into the CNS. Adsorptive-mediated transcytosis does not involve protein receptors. Instead, positively charged molecules interact with the endothelial membrane, inducing endocytosis (Pardridge, 1992). Due to the lack of specificity, this method leads to a general adsorption of molecules from the blood to the brain. Once through the endothelium, molecules must then cross the glial limitans before entering the brain parenchyma. A combination of the basement membrane and tight 20nm gaps between astrocyte endfeet creates a restrictive barrier, allowing select entry depending on lipophilicity, concentration gradients, and astrocytic transport mechanisms (Mastorakos & McGavern, 2019). Some molecules (0.7 to 70 kDa) can pass through this additional layer; however, larger molecules (150 to 2,000 kDa) remain trapped in the perivascular space (Bedussi et al., 2015; Hannocks et al., 2018; Iliff et al., 2012). Understanding the dynamics of BBB transport is critical in both health and disease.

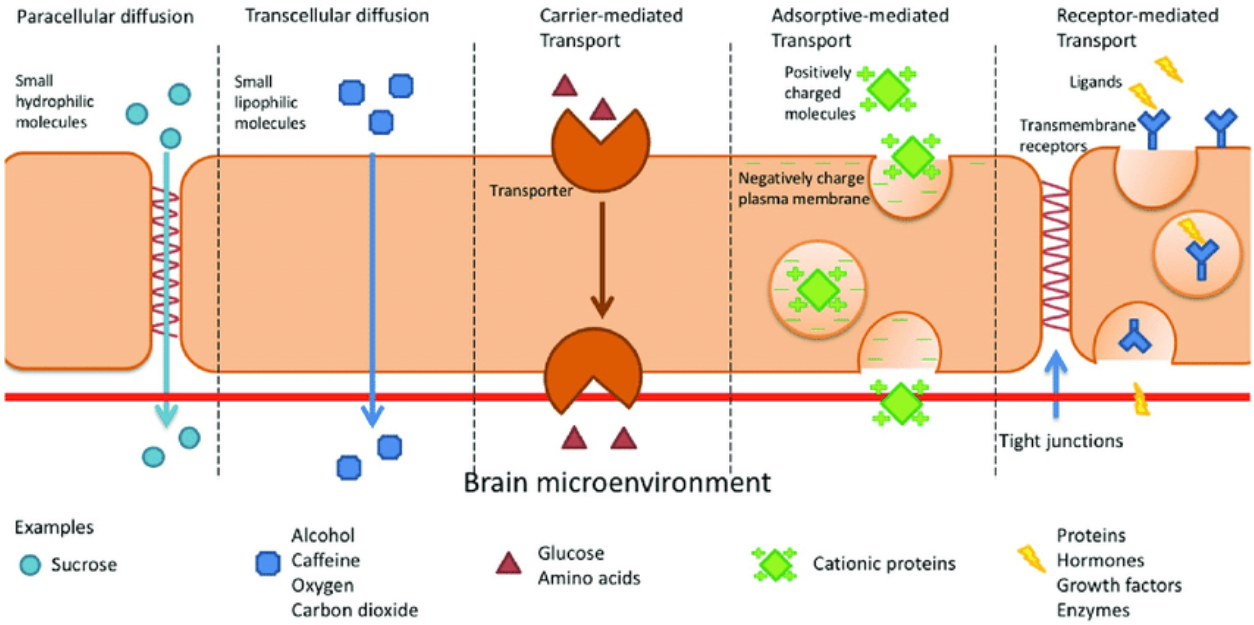

Figure 1.3: Methods of transport between blood and brain compartments. Depending on the biochemical structure of the molecule, there are various ways in which they can pass through the restrictive blood-brain barrier. There is (1) paracellular diffusion of small, hydrophilic molecules, (2) transcellular diffusion of small lipophilic molecules, (3) carrier-mediated transport of certain molecules dependent upon specific transporter proteins, (4) adsorptive-mediated transport of positively charged molecules, and (5) receptor-mediated endocytosis of certain molecules. Figure from: (Wong et al., 2019)

Proper BBB function is necessary for protecting the CNS from exogenous substances and maintaining brain homeostasis; however, it also creates a barrier in the delivery of therapeutics. While direct administration of drugs to the CNS allows more flexibility in drug formulation, there is an inherent risk of brain damage and infection (Choi et al., 2011; Wong et al., 2019). Instead, there is an ongoing struggle to find minimally invasive methods for safe and effective CNS drug delivery. One potential method is hijacking receptor-mediated transcytosis to allow therapeutics in the peripheral blood to enter the CNS, an example of this is the Alzheimer's disease (AD) investigational antibody treatment trontinemab. Trontinemab is a monocolonal anti-amyloid-beta (Aβ) treatment that binds to Aβ similarly to its predecessor gantenerumab, while also being taken up by the human transferrin receptor 1 (TfR1) (Hp et al., 2023). Transferrin receptors are widely expressed transmembrane glycoproteins found throughout the

periphery as well as in BECs, neurons, and glia. Recent human studies have found that targeting trontinemab to TfR1 reduced amyloid-related imaging abnormalities (ARIA), an anti-Aβ immunotherapy induced form of edema/hemorrhage, while also increasing drug efficacy (*Trontinemab | ALZFORUM*, n.d.). However, an important caveat to consider is that transferrin receptors are saturated by endogenous transferrin in the blood and further burdening this system reduces the uptake of iron by the brain (de Boer & Gaillard, 2007; Y. Zhang & Pardridge, 2001).

1.2.2 Rhythms in the Neurovascular Unit

Adapted from: Li W.*, Tiedt S.*, Lawrence J. H., Harrington M., Musiek E. S., Lo E. H. 2024. Circulation Research

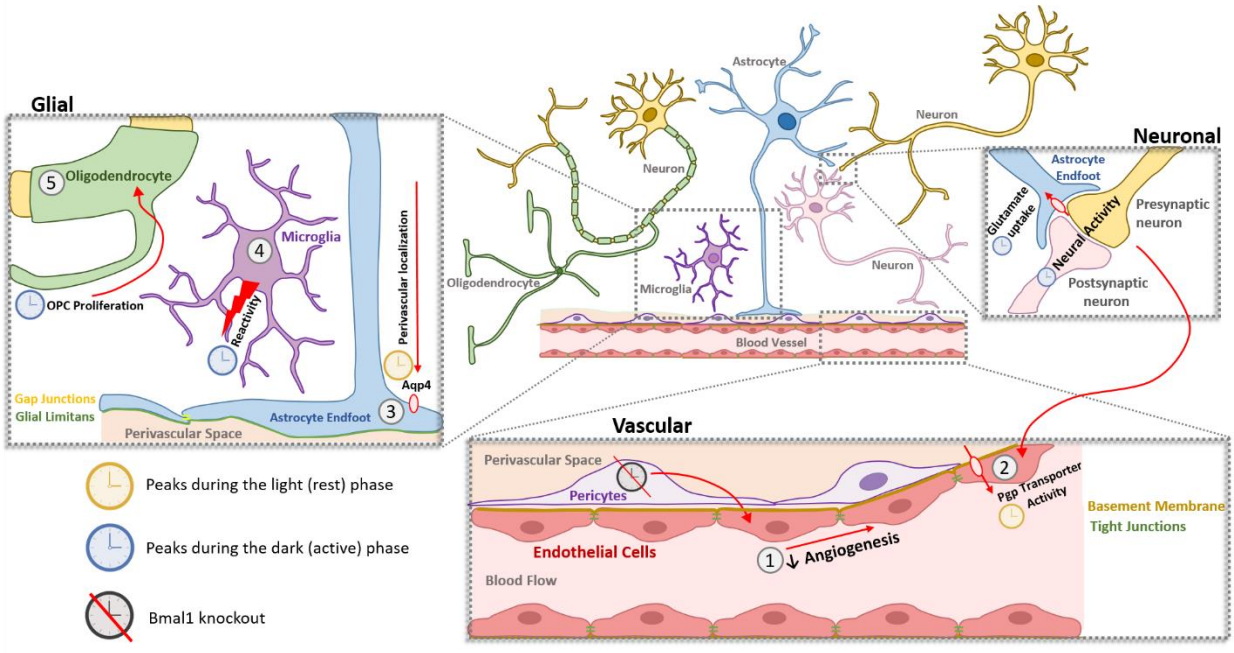

Figure 1.4: Circadian Rhythms at the Neurovascular Unit. Circadian Rhythms exist in all compartments of the NVU: Vascular, Neuronal, and Glial. (1) Bmal1 deficient pericytes lose rhythmic secretion of lactate, inducing decreased angiogenesis, (2) Neuronal activity during the active phase increases endothelial pgp-transporter activity, (3) Perivascular localization of astrocyte endfoot channel AQP4 increases during rest, (4) Microglial phagocytosis increases in the evening, and (5) OPC proliferation increases during sleep.

The neurovascular unit (NVU) provides a conceptual framework for investigating coordinated signaling between neuronal, glial and vascular compartments. Since it was first proposed in 2003, this concept has undergone several revisions and updates. A second iteration of the concept incorporated the idea that the NVU is highly dynamic and plastic. Potential targets may be biphasic and change as the brain shifts from initial injury into delayed recovery (Lo, 2008; Moskowitz et al., 2010). Since then, the concept has been further refined to include the emerging recognition that that CNS is not isolated but remains in close communication with peripheral organs (Lo, 2014). Therefore, it is critical to also consider the role of crosstalk between the CNS and systemic biology, including responses in the immune system, cardiovascular function, lymphatics and microbiome (Tiedt et al., 2022). The NVU is highly dynamic, with daily oscillations in neuronal and glial activity and blood flow all requiring a constantly adaptive balance in metabolic supply-and-demand. However, the exchange of nutrients and waste products in and out of the brain is a tightly regulated process with the BBB forming a selectively permeable barrier. Consequently, there arises a necessity for time-of-day variations within vascular-specific functions but also how glial cells support neuronal survival and function (Paschos & FitzGerald, 2010). This is orchestrated by the circadian clock. The core circadian clock proteins BMAL1, CLOCK, NPAS2, PER, and CRY– are all expressed and oscillating in vascular tissue, glial cells, and neurons.

Rhythms in peripheral endothelial cell function are well established. Assessment of human endothelial function in brachial artery through flow-mediated dilation reveals a circadian variation, reaching its lowest point in the morning and peaking at night (Maruo et al., 2006; Otto et al., 2004). This aligns with the observed morning peak in cardiac and vascular events (N. Takeda & Maemura, 2016). Further studies on human subjects demonstrate significant circadian

variations in endothelium-dependent vasodilation, associated with oscillating levels of nitric oxide (NO) and endothelin-1 (Elherik et al., 2002; Z. Zhang et al., 2020). Additionally, endothelial NO synthase (eNOS) expression displays daily oscillations, peaking at noon and declining in the morning (Kunieda et al., 2008). Notably, cerebral blood flow (CBF) also exhibits circadian oscillations under stable conditions of blood pressure and physical activity (Conroy et al., 2005). In retinal blood vessels, CLAUDIN-2, CLAUDIN-4, and CLAUDIN-5 are found to be highly dynamic and regulated in a circadian manner (Hudson et al., 2019; Louer et al., 2020), and both *Occludin* and *Claudin-1* mRNA levels exhibit daily oscillations that are inversely associated with intestinal permeability (Oh-oka et al., 2014). These findings suggest circadian rhythms may also influence brain endothelial cell (BEC) function - including tight junction formation and BBB permeability; however, specific BBB-related studies are limited. BECs play essential functions within the CNS, including regulating CBF, maintaining BBB integrity, and supporting overall brain health (Li et al., 2018). Notably, recent research proposed that phosphorylation of ZO-1 promotes PER1 nuclear translocation, thus regulating the circadian clock during feeding (Y. Liu et al., 2020). Increased ZO-1 phosphorylation correlated with impaired BBB integrity in dystrophic mice brains and mouse brain microvascular endothelial cells (W. Chen et al., 2019; Nico et al., 2007). Understanding the interaction between circadian genes and endothelial junctional proteins hold promise for designing therapies targeting disrupted circadian rhythm and dysfunctional BBB in brain diseases.

Beyond the BECs that comprise the blood vessels themselves, there are the surrounding mural cells – also known as smooth muscle cells and pericytes – which play vital roles in maintaining the brain's vascular health and functionality. The existing literature investigating the circadian influence on mural cells primarily focus on peripheral tissues; however, since pericytes

are embedded in the basement membrane they could directly contact endothelial cells (Gerhardt & Betsholtz, 2003) . Synchronizing the clock in pericytes in co-culture with endothelial cells promotes endothelial BMAL1 rhythmicity, enhancing vessel-like structures (Mastrullo et al., 2022). These studies suggest that crosstalk signals from mural cells may influence endothelial rhythms, but careful in vivo validation of this cell biology is required. Other considerations are the impact of sleep/wake on neuronal firing, changing nutrient and CBF demand. Our brains conduct a divergent set of tasks across a 24-hour cycle: during wake, integrating sensory input to coordinate motoric output, while during sleep consolidating memory. This indicates considerable differences in activity at a network and single neuron level between day and night. Upon reception of direct or indirect input from the SCN, cell-intrinsic clocks govern neuronal phenotypes at the molecular, morphological, and functional level. The extent of transcriptional and translational circadian oscillation in neurons has recently been uncovered: 67% of synaptic forebrain mRNAs show circadian oscillations with a mean amplitude of about twofold and peaking in anticipation of either wake or sleep: synaptic signaling preceded wake while metabolism and translation preceded sleep (Noya et al., 2019).

The final compartment of the NVU are formed by glial cells. Astrocytes have a multitude of processes which both wrap around blood vessels as well as integrate into the synaptic cleft, forming “tripartite” synapses with neurons (Allen et al., 2012; Blanco-Suarez et al., 2018; Christopherson et al., 2005; Ezan et al., 2012). This distinct morphology allows astrocytes to act as mediators between nutrient uptake, waste efflux, and neuronal activity. Astrocytes interact with neurons through tightly regulating the extracellular milieu, including the uptake and release of gliotransmitters such as glutamate. Through these mechanisms, in the SCN, astrocytes play critical roles in maintaining the behavioral rhythms of an organism. Genetically abrogating

circadian rhythms specifically in astrocytes disrupts SCN neuronal firing and alters behavioral rhythms (Barca-Mayo et al., 2017; Brancaccio et al., 2019; Tso et al., 2017). Studies have shown that astrocytic glutamate uptake is dependent upon the circadian proteins CLOCK and PER2 and that glutamine synthetase, a glial-derived enzyme critical for glutamate synthesis, is decreased in the SCN during rest (Barca-Mayo et al., 2017; Beaulé et al., 2009; Leone et al., 2015). Additionally, as early as 1993 it was discovered that the localization of the astrocyte marker glial fibrillary acidic protein (GFAP) in the SCN changes over the course of a day (Fernandez-Galaz et al., 1999; Lavialle & Servière, 1993).

In extra-SCN regions of the brain, astrocytic circadian rhythms are necessary for brain homeostasis. Distribution of the astrocytic water channel Aquaporin-4 (Aqp4) exhibits circadian rhythmicity, leading to time-of-day changes in glymphatic function (Hablitz et al., 2020; Lananna et al., 2018; Mestre et al., n.d.; Pizarro et al., 2013). Translating ribosome affinity purification (TRAP) experiments done in Drosophila have found that 293 genes in the astrocyte translatome are rhythmic – indicating that there are many more astroglial functions under circadian control (You et al., 2021). In vitro studies have shown that astrocytes continue to have rhythmic gene expression even in complete isolation from other cells, and these rhythms are ablated by the disruption of core molecular clock proteins such as Bmal1 (Marpegan et al., 2011; Prolo et al., 2005). Deletion of astrocytic Bmal1 induces cell-autonomous astrocyte activation in vivo, with morphological changes, enhanced expression of GFAP, and widespread transcriptomic changes (Lananna et al., 2018). Bmal1-deficient astrocytes show increased expression of lysosomal proteins and enhanced endocytosis in vitro (McKee et al., 2023). Systemically, deleting Bmal1 in astrocytes causes metabolic imbalance, disrupted glutamate and GABA levels, and decreased life span (Barca-Mayo et al., 2020). In mouse models of tau and

alpha-synuclein proteinopathy, astrocyte-specific Bmal1 deletion can increase macroautophagy and mitigate toxic protein aggregation (Sheehan et al., 2023). It is important to consider that BMAL1 can mediate non-circadian functions, and it remains unclear which effects of Bmal1 deletion in astrocytes are due to abrogated cellular circadian rhythms, as opposed to non-rhythmic phenomena. However, these data show that disrupting the core molecular clock in astrocytes via Bmal1 deletion can have striking effects on astrocyte gene expression, morphology, and activation state, and can strongly influence brain pathology.

Microglia are dynamic cells, with highly motile processes which constantly surveil their environment. While microglia originate from yolk sac erythro-myeloid progenitors, they have similar properties as hematopoietic stem cell derived peripheral macrophages (F. C. Bennett et al., 2018; Epelman et al., 2014; van Furth & Cohn, 1968). Microglia are proficient at phagocytosis and are critical for clearing tissue debris and pruning neural synapses – ensuring CNS immunity, proper circuitry development, and preventing hyper-excitability (Merlini et al., 2021; Paolicelli et al., 2011; Schafer et al., 2012). Previously, it was considered that the presentation of certain stimuli polarized microglial cells into two states: a "classical" pro-inflammatory (M1) or an "alternative" anti-inflammatory (M2) state (Guzmán-Ruiz et al., 2023). While this concept has recently been challenged (Ransohoff, 2016), it highlights the importance of understanding variability in microglial responses to inflammatory stimuli. Additionally, microglial responses vary across the circadian day, further complicating their pro- or anti-inflammatory profile.

Similarly to astrocytes, microglial cells have persisting cellular rhythms when cultured in isolation, and they upregulate the clock proteins Per1 and Per2 in response to exogenous glucocorticoids or ATP - both of which are rhythmically produced in vivo (Fonken et al., 2015;

Nakazato et al., 2011). One key circadian microglial function is adult synaptic pruning. Synaptic pruning is necessary to support time-of-day changes in neural activity and is, in part, dependent upon the microglia-specific protease Cathepsin S (CatS). Disruption of the Clock gene leads to loss of rhythmic microglial CatS expression, decreased refinement of neuronal circuitry, and altered diurnal locomotion (Hayashi et al., 2013). Microglia-specific Bmal1 deletion leads to accelerated brain aging phenotypes including impaired synaptic pruning, learning and memory deficits, and disrupted sleep (Iweka et al., 2023). Interestingly, the effects of microglial Bmal1 deletion may actually be mediated by its downstream transcriptional target, REV-ERBα. Diurnal oscillations in microglial synaptic phagocytosis occur in-phase with BMAL1 and antiphase of the negative feedback repressor REV-ERBα, with REV-ERBα deletion abrogating these rhythms and locking the cell into a tonic state of increased phagocytosis, leading to loss of hippocampal synapses (Griffin et al., 2020). In the setting of high fat diet-induced stress, the increased synaptic phagocytosis imparted by microglial Bmal1 deletion actually preserves memory (X.-L. Wang et al., 2021), suggesting that the microglial circadian clock may serve different functions under basal conditions and in the setting of stress or disease.

Global germline deletion of REV-ERBα causes increased microglial phagocytic activation and pro-inflammatory cytokine release, while LPS-mediated neuroinflammation can be mitigated using using a pharmacological REV-ERBα agonist (Griffin et al., 2019). Microglia from aged mice show altered circadian rhythms coupled with tonically-elevated cytokine production, which may contribute to age-related inflammation (Fonken et al., 2016). In a mouse Alzheimer's Disease model, microglia display disrupted circadian gene expression which is associated with NF-kB activation and inflammation (Ni et al., 2019). While the exact mechanisms are under debate, microglial circadian rhythms are clearly an important contributing

factor in neuroinflammation and synaptic pruning and should be taken into consideration when studying neuronal circuitry and disease.

The third glial cell, oligodendrocytes, are responsible for myelinating CNS axons, a critical aspect of neuronal health since the loss or dysregulation of myelination is connected to a myriad of neurodevelopmental and neurological disorders, including multiple sclerosis (K. L. Davis et al., 2003; Dwork et al., 2007; Onnink et al., 2015; Podbielska et al., 2013). Both oligodendrocytes and oligodendrocyte precursor cells (OPCs, also known as NG2-glia) serve other functions besides myelination, including the regulation of neuroinflammation, synaptic formation, and neural signaling (Bergles et al., 2000; Fernández-Castañeda et al., 2020; S. Lin & Bergles, 2004). Additionally, oligodendrocyte function – including proliferation, myelin formation, migration, and differentiation – is depending upon neural derived-factors. Immediately following CNS injuries, such as ischemic stroke, there is widespread oligodendrocyte cell death and loss of this critical neural-oligodendrocyte support (Hamanaka et al., 2018).

While oligodendrocytes show time-of-day differences in gene transcription and proliferation in vivo, they are relatively understudied in the circadian field (Bellesi et al., 2013; Matsumoto et al., 2011). It is unknown if these phenomena are due to intrinsic circadian function or a result of sleep/wake cycles, since oligodendrocyte function and proliferation are also both tied to neural activity (Butt et al., 2014; De Angelis et al., 2012; Williamson et al., 1998). Recent work shows that OPCs possess intrinsic circadian clocks which mediate rhythmic gene expression in vivo (Dean et al., 2022). Ablating Bmal1 in OPCs can reduce OPC proliferation under basal conditions and in response to brain injury (Dean et al., 2022). OPC-specific Bmal1 deletion also dysregulates oligodendrocyte development, migration, morphology,

and function, ultimately leading to reduced myelination and fragmented sleep architecture (Rojo et al., 2023). Current research suggests that there may be circadian regulation of OPC differentiation, lipid synthesis, and mitochondrial function although these areas of research have yet to be fully explored (Colwell & Ghiani, 2019; Rojo et al., 2022).

Rhythms in cellular function within these NVU compartments each collectively contribute to rhythms in BBB function. The BBB is not the impenetrable barrier as believed for a long time, it rather serves as an interface that regulates the uptake of a plethora of plasma molecules through ligand-specific, receptor-based transcytosis, even under physiological conditions (A. C. Yang et al., 2020). Growing evidence suggests that this permeability shows a circadian rhythm and is regulated by the molecular clock: for example, after intravenous injection of RHB, a substrate of p-glycoprotein, the level of RHB in the brain oscillates with a peak early after lights on and trough after lights off, indicating that p-glycoprotein-mediated efflux is highest during the active phase (S. L. Zhang et al., 2021). Of note, the cycling of efflux activity is regulated by endothelial magnesium levels (S. L. Zhang et al., 2021). In adult Drosophila, endocytosis is increased in BBB glia during sleep with the peak at the early night when sleep predominates (Artiushin et al., 2018). Further, tight junction proteins such as CLAUDIN-5 and OCCLUDIN oscillate and are under transcriptional control of *Clock* and *Bmal1* in peripheral endothelial cells (Hudson et al., 2019; Oh-oka et al., 2014). Illustrating how the activity of one cell type can affect the clock of another, a recent study unraveled how neuronal activity regulates circadian clock genes within brain endothelial cells, which in turn mediate the activity-dependent control of BBB efflux transport (Pulido et al., 2020).

A constitutive *Bmal1* knockout of NESTIN-positive cells induces increased BBB breakdown, which was attributed to the disruption of pericyte circadian rhythms . However, it

was recently found that there was no increase in small molecule leak in Bmal1 deficient OPCs, using a mouse line that also targeted $NG2^{+}$ pericytes – suggesting that the previous phenotype may be due to embryonic effects (Rojo et al., 2023). Microglial ablation studies have found that microglia are deleterious during inflammatory blood-retina barrier breakdown but are protective in models of both ischemic stroke and micro-bubble induced intraparenchymal hemorrhage (Jin et al., 2017; Kokona et al., 2018; Mastorakos et al., 2021). This difference may be due to inflammation induced nitric oxide (NO) synthase production vs mechanical-injury repair-associated microglia formation (Leal et al., 2007; Mastorakos et al., 2021; M. Takeda et al., 2001). However, little is known about circadian rhythms in capillary associated microglia, especially in the context of inflammatory BBB breakdown.

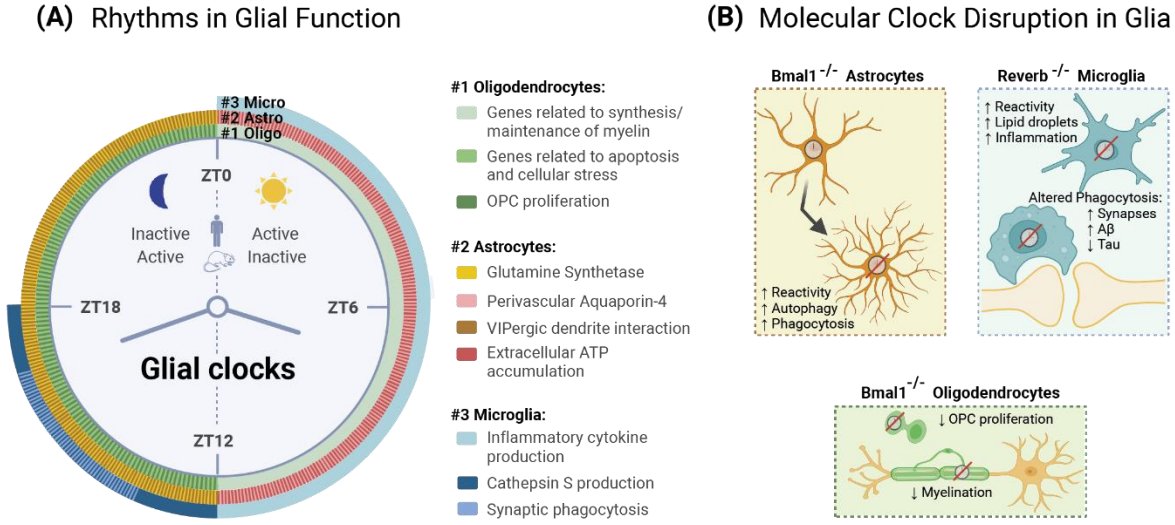

Figure 1.5: Rhythmic Glial Functions. (A) Many biological processes are rhythmic at baseline in oligodendrocytes (#1), astrocytes (#2), and microglia (#3)*. #1. Sleep/wake studies have found that OPC proliferation and myelin/apoptosis pathways have time-of-day differences in oligodendrocytes (Bellesi et al., 2013; Matsumoto et al., 2011). #2. During the dark (active) phase there is increased astrocytic glutamine synthase and VIPergic dendrite coverage in the SCN (Beaulé et al., 2009; Becquet et al., 2008; Leone et al., 2015). Conversely, during the light (rest) phase, astrocytes have increased perivascular localization of AQP4 and extracellular ATP accumulation (Hablitz et al., 2020; Lananna et al., 2018; Mestre et al., n.d.; Pizarro et al., 2013; Womac et al., 2009). #3. Microglial pro-inflammatory cytokine release and synaptic phagocytosis both peak during the dark (active) phase, whereas CathepsinS production is highest during the light (rest) phase (Griffin et al., 2020; Hayashi et al., 2013). (B) Deletion of the core molecular clock proteins BMAL1 or REV-ERBα induce morphological and functional changes in glial cells **. Bmal1 deletion in astrocytes leads to astrogliosis, with increased reactivity, autophagy/lysosomal degradation, and phagocytosis (McKee et al., 2023; Sheehan et al., 2023). REV-ERBα deficient microglia have a more variable response. There is increased reactivity, lipid droplet formation, and synaptic/Aβ phagocytosis; however, there is less extracellular Tau phagocytosis (Griffin et al., 2019; J. Lee et al., 2020, 2023). Deletion of Bmal1 in oligodendrocyte precursor cells decreases OPC proliferation and myelin coverage (Rojo et al., 2023).

* All studies were conducted in nocturnal rodents. Additionally, for in vivo experiments not done in constant conditions, it is possible the observed diurnal variations are due to neuronal activity, sleep, or light effects. **There is some glial cell crosstalk using cell-specific gene deletion models; however, this seems to be highly cell dependent. Microglial-specific Rev-erbα deletion induces astrogliosis in the hippocampus, while astrocyte-specific Bmal1 deletion does not significantly increase DAM markers (J. Lee et al., 2023; Sheehan et al., 2023)

1.2.3 The BBB in disease

Both systemic and central inflammation can induce BBB dysfunction. Treating with systemic LPS induces cerebrovascular vasodilation, neuroinflammation, as well as altered TJ function and vesicular processes (Banks et al., 2015). LPS can triggers BBB leakage across multiple brain regions, including the frontal and parietal cortices, striatum, midbrain, thalamus, hippocampus, and cerebellum (Banks et al., 2015). During peripheral inflammation BBB breakdown can also be coupled with leukocyte extravasation, although this process is made more complex by the CNS's inherent immune privilege and the discontinuous nature of perivascular spaces. Injecting virus directly into the brain parenchyma does not elicit an adaptive immune response (Matyszak & Perry, 1998; Stevenson et al., 1997). This is because parenchymal capillaries have minimal perivascular space, leading to an inability of immune cells to traffic from the brain parenchyma, along blood vessels, and into draining lymph nodes where they can present antigen to resident adaptive immune cells. Conversely, leukocytes in the CSF act more similarly to those in the periphery, freely moving along large perineuronal pathways where they egress into lymphatic vessels and enter lymph nodes (Louveau et al., 2018). This perivascular structure creates a unique problem. While antigen presenting cells (APCs), such as macrophages or dendritic cells, in the dura and choroid plexus are able to readily exit into peripheral circulation, border-resident APCs in the perivascular space, along leptomeningeal vessels, or in the subarachnoid space are trapped (Mastorakos & McGavern, 2019). In order to mount an adaptive immune response, leukocytes must somehow gain direct access to these static CNS compartments where the APCs reside.

Leukocyte entry into the CNS is tightly regulated through the expression of specific cell adhesion molecules. This allows select activated $CD8^+$ and $CD4^+$ T cells, but not B cells or

innate immune cells, to roll along the luminal wall where they eventually completely adhere to – and begin migrating across – the endothelial cell layer (Engelhardt & Ransohoff, 2012). This extravasation occurs along postcapillary venules, rather than capillaries, since the perivascular space creates a double layer of insulation between the blood and parenchyma (Wolburg et al., 2005). If the activated T cells recognize antigen presented by the perivascular APCs, they begin the process of crossing the astrocyte basal lamina and glial limitans, finally entering the brain parenchyma (Greter et al., 2005; Lodygin et al., 2013). Peripheral immune responses may also dictate neuroinflammation independent of leukocyte migration across the BBB. Peripheral cytokines (for further background see 1.1.3 Peripheral inflammation and rhythms in adaptive immunity) can interact with luminal BEC receptors or directly enter the CNS through cytokine receptor -dependent or -independent mechanisms (Banks, 2005; Mastorakos & McGavern, 2019).

To examine a CNS-specific innate immune response, researchers have directly bathed the cerebral surface of the brain in LPS and found that pial arterioles increased in both diameter and blood flow. This vasodilation was due to the production of inducible nitric oxide synthase (iNOS) since it was prevented by co-treatment with the iNOS inhibitor aminoguanidine (AG). iNOS is an enzyme that catalyzes L-arginine into nitric oxide (NO) (Mayhan, 1998). NO is a signaling molecule involved in neurotransmission, blood-pressure, and vascular tone that is made on demand since its gaseous form is easily diffusible (Thiel & Audus, 2001). NO is routinely made in small (picomolar) quantities by multiple cell types, including endothelial cells and neurons, produced by eNOS (*Nos1*) and nNOS (*Nos3*) respectively. Conversely, iNOS, encoded by *Nos2*, is rarely produced in healthy cells and is calcium-independent, producing large (micromolar) amounts of NO, often in the setting of inflammation (Thiel & Audus, 2001).

Notably, both astrocyte and microglia produce iNOS in response to LPS and independently of one another (Kong et al., 1996), with NO appearing to be upstream of the astrocyte activation marker GFAP (Brahmachari et al., 2006).

Systemic LPS may impact the BBB both directly (by binding to endothelial cells) or indirectly (through pro-inflammatory cytokine production and loss of trophic support) (Peng et al., 2021). LPS interacting directly with $TLR4^+$ BECs triggers increased paracellular leak through (1) impairing TJ and AJ formation, (2) inducing matrix metalloproteinase 9 (MMP9) degradation of existing TJs, and (3) decreasing P-gp transporter activity – leading to a buildup of toxic molecules that diffused into the CNS (Peng et al., 2021). Direct LPS-BEC interaction may also impact transcytosis across the BBB through the phosphorylation of caveolae-1. It is thought that BBB breakdown and influx of inflammatory factors is what causes sepsis-associated encephalopathy, a debilitating neurological disorder that leads to long term cognitive impairments (Silva et al., 2020). Inhibiting iNOS as a means to protect against BBB breakdown is an active area of research. Treating mice with the iNOS inhibitor L-NG-nitro arginine methyl ester (L-NAME) during the early stages of EAE protects against infiltrating $CD4^+$ T cells. Researchers found also found that administering AG systemically after an acute surgical brain injury significantly reduced BBB leakage as well as loss in TJ proteins (Fan et al., 2011). However, it is important to note that both the delivery and timing of these treatments are critical to determine its efficacy. Long term treatment of rats with L-NAME for 4 weeks prior to the onset of a seizure actually increased mortality and BBB breakdown (Kalayci et al., 2006). It's hypothesized that this increase in BBB disruption is due to a feedback mechanism where prolonged inhibition led to increased production of NO (T. Liu et al., 2019). Additionally, a study looking at the response to peripheral LPS injections on the anterior pituitary gland and

medial basal hypothalamus, found that intracerebroventricular (i.c.v.) AG treatment protected against iNOS production in both brain regions; however, intraperitoneal (i.p.) AG only protected the anterior pituitary gland but not in the medial basal hypothalamus (Mohn et al., 2002). When dealing with CNS-specific neuroinflammation, such as with intracisternal LPS infusions, co-infusing AG almost completely protected against all BBB breakdown (Boje, 1996; Chung et al., 2021). While another iNOS inhibitor, L-NMMA, was cleared for clinical trials for cancer treatment in the periphery, there is still conflicting information about its barrier penetration properties – suggesting we are still years away from iNOS inhibitors being used to treat CNS inflammation (Chung et al., 2021).

1.2.4 Conclusion

In summary, while circadian rhythms are inarguably a critical component of an organism's overall fitness, there are many unanswered questions regarding their role in peripheral and central immunity. Glial cells, primarily microglia and astrocytes, are known to interact with the BBB and have highly circadian responses to inflammatory stimuli. Beyond answering the basic scientific questions of how extrinsic factors such as light can control central immune responses, this area of research has important translational considerations for patients with inflammatory diseases coupled with BBB disruption.

Chapter 2: Time of Day determines severity of inflammatory BBB disruption and endothelial morphology

2.1 Abstract

The blood-brain barrier (BBB) is critical for maintaining brain homeostasis but is susceptible to inflammatory breakdown. Permeability of the BBB to lipophilic molecules shows circadian variation due to rhythmic transporter expression, while basal permeability to polar molecules in non-rhythmic. Whether daily timing influences BBB permeability in response to inflammation is unknown. Here, we induced systemic inflammation through repeated lipopolysaccharide (LPS) injections either in the morning (ZT1) or evening (ZT13) under standard lighting conditions, then examined BBB permeability to a polar molecule. We observed clear diurnal variation in inflammatory BBB permeability, with a striking increase in BBB breakdown specifically following evening LPS injection. The diurnal variation in BBB permeability was both light dependent as well as under circadian control, as the phenomenon persisted after light-inversion and was ablated during constant darkness. Ultrastructural analysis suggests that the increase in small molecule leak may be due to increased transcytosis. Using transcriptomics, we found that the top pathways with both a treatment and time-of-day interaction were involved with BBB and extracellular matrix (ECM) maintenance.

2.2 Introduction

The blood brain barrier (BBB) plays a critical role in restricting certain blood-borne molecules from the brain, helping protect the central nervous system (CNS) from circulating

neurotoxic molecules as well as peripheral immune cells (Buckley & McGavern, 2022; Peng et al., 2021; Persidsky et al., 2006). The BBB is a multicellular structure, consisting of endothelial cells, mural cells (pericytes and smooth muscle cells), and astrocytes - collectively referred to as the neurovascular unit (NVU). Outside of the NVU, microglia and neurons also impact BBB function (Mastorakos et al., 2021; Pulido et al., 2020). In the setting of peripheral or central inflammation, the BBB can become more permeable due to transporter dysfunction, breakdown of endothelial cell tight and adherens junctions, and increases in transcytosis (Erickson et al., 2023; Jana et al., 2022). These mechanisms of BBB breakdown occur in both acute neuroinflammatory conditions, such as encephalitis and stroke, as well as in neurodegenerative diseases, and can exacerbate neuroinflammation and brain injury (Banks et al., 2015; Jana et al., 2022, p. 1; Knowland et al., 2014). Thus, factors which regulate inflammatory BBB breakdown have clear implications for brain homeostasis and health.

The central nervous system exhibits circadian dynamics, with diurnal oscillations in neuronal activity and metabolic demand creating a need for time-of-day variations in vascular function. Circadian rhythms govern behavioral and physiological functions and allow an organism to predict daily changes in its environment, improving its overall fitness (Ouyang et al., 1998; Takahashi, 2017). The circadian clock is synchronized to the external environment by cues termed “zeitgebers”, with light serving as the primary zeitgeber (Etain et al., 2011). Peripheral gut and retinal barriers are known to be controlled by clocks (Eum et al., 2023; Hudson et al., 2019; Oh-oka et al., 2014) and all components of the BBB express core clock genes and exhibit circadian rhythms (Bhatwadekar et al., 2017; Griffin et al., 2020; Lananna et al., 2018; Mastrullo et al., 2022; Nakazato et al., 2017; Nonaka et al., 2001). BBB permeability to lipophilic molecules has been reported and is dependent on circadian expression of specific transporter

proteins such as p-glycoprotein (Pulido et al., 2020; S. L. Zhang et al., 2021). However, the BBB does not show daily rhythms in permeability to polar molecules under basal conditions (Pan et al., 2002; Pan & Kastin, 2001; Pulido et al., 2020; S. L. Zhang et al., 2018). Since many biological functions gain or lose rhythms in the presence of chronic inflammation or disease, we asked if BBB permeability to polar molecules in response to inflammation, termed inflammatory BBB breakdown, exhibits diurnal rhythmicity (Blacher et al., 2022; Haspel et al., 2014).

Importantly, the circadian system also has a strong influence over immune responses. In mice, inflammatory responses to a variety of inflammogens, including lipopolysaccharide (LPS), bacterial, and viral infection, all show striking time-of-day effects. Mice treated with systemic LPS in the evening have much higher mortality than those treated in the morning, and this time-of-day difference can be ablated by deleting the key clock gene Bmal1 (Lang et al., 2021). However, LPS-induced inflammatory response and mortality are governed not only by the circadian clock, but also but a host of other factors including exposure to light and time of feeding, and do not seem to rely on the circadian function of monocytes (Geiger et al., 2021; J. Gibbs et al., 2014; Lang et al., 2021; Silver et al., 2018). Here, we have investigated how inflammatory BBB breakdown and brain and peripheral inflammation are influenced by exposure to intraperitoneal LPS injection at different times of day.

2.3 Results

2.3.1 Time-of-Day (TOD) Strongly Regulates Inflammatory BBB Breakdown

We first sought to determine if exposure to an inflammatory stimulus at different times of day can differentially impact BBB permeability. To induce robust inflammatory BBB

breakdown, we gave daily intraperitoneal (i.p.) injections of 2 mg/kg LPS or PBS control to 2-month-old male C57bl/6 mice for two days in a row at either 7am or 7pm (Figure 2.1A). In a 12-hour light cycle, these times correspond to 1 hour after the onset of light (ZT1) and 1 hour after the lights turn off (ZT13). We chose these times because they roughly correspond to the nadir and peak of diurnal behavioral rhythms, as well as circadian gene expression in most organs (R. Zhang et al., 2014). To measure BBB breakdown, we administered tracers on the third day at the same time of day as prior LPS injections and quantified the amount of tracer found in the hippocampus, cortex, and cerebellum relative to the amount found in the serum (Figure 2.1A). First, in order to identify gross size exclusion properties in LPS-induced BBB breakdown, we examined BBB permeability to two tracers of varying size – with mice treated only at ZT13, the time at which there is greatest LPS-induced mortality (Lang et al., 2021). Evans Blue (EB) is a relatively small azo dye (961 Da) that binds with high affinity to serum albumin, creating a high molecular weight (mw) tracer of 69 kDa (Yao et al., 2018). Conversely, sodium fluorescein (NaFL) is a small mw (376 Da) inert fluorescent molecule that weakly binds to endogenous proteins and has no known endothelial cell transporters, allowing it to serve as a sensitive BBB permeability tracer (Saunders et al., 2015). Neither PBS nor LPS-treated mice showed any visible leak of EB, indicating there is no gross hemorrhaging in this model of inflammation (Figure 2.1B). While there was no NaFL seen in the brain at baseline in PBS control mice, there was robust NaFL leak in ZT13 LPS treated mice (Figure 2.1B). These data suggest that LPS induces a relatively small molecule leak, through either paracellular diffusion or receptor-independent transcellular transport. All further tracer experiments were conducted using NaFL.

We next examined the effect of time-of-day (TOD) of LPS exposure on BBB permeability. As expected, there was minimal permeability of NaFL in PBS-treated mice at

either ZT1 or ZT13 (Figure 2.1C), supporting previous studies stating that basal permeability to polar molecules does not show diurnal variation (Pulido et al., 2020; S. L. Zhang et al., 2018). However, mice treated with LPS in the evening (ZT13) had greater NaFL leak across multiple brain regions than those treated in the morning (ZT1), with the cerebellum having the greatest absolute leak and the cortex having the strongest TOD effect (Figure 2.1C). Of note, while LPS treatment at ZT1 only slightly increased BBB permeability to NaFl in the cortex and hippocampus, permeability was significantly increased in all brain regions after LPS exposure at ZT13.

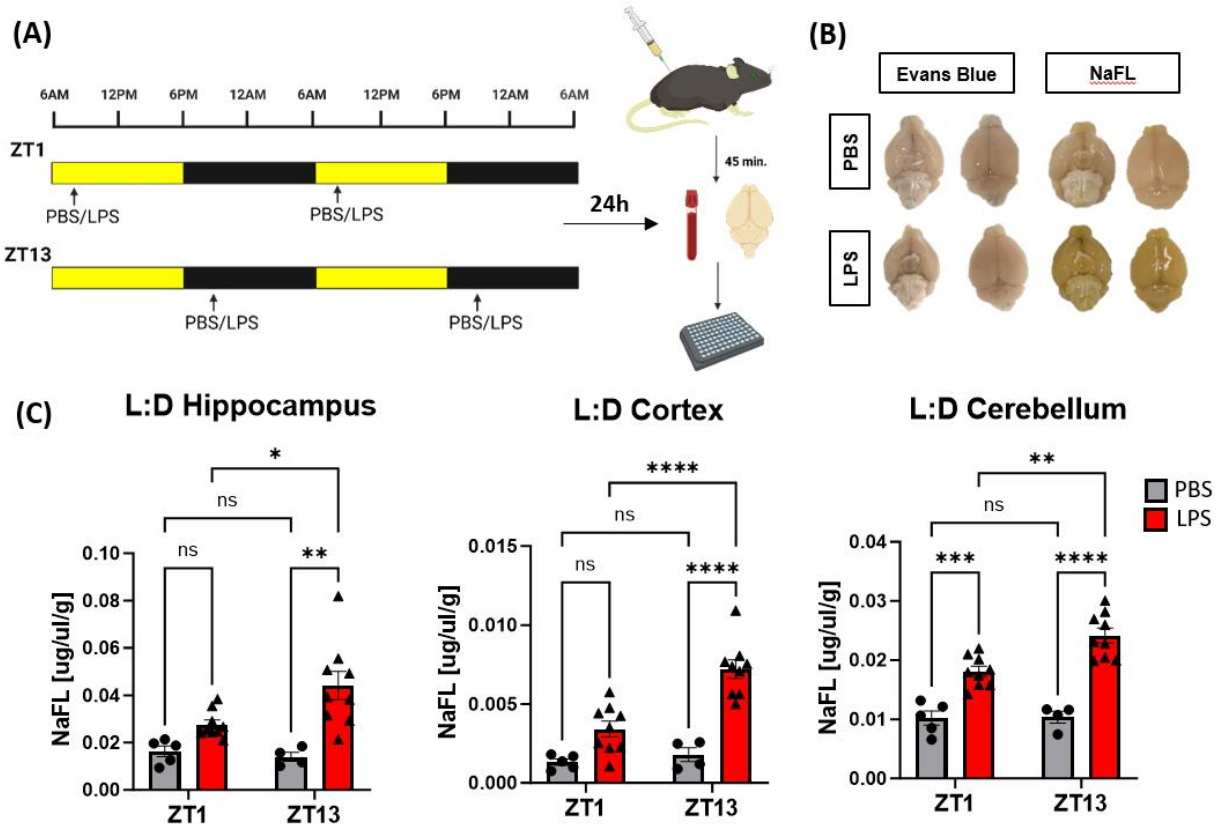

Figure 2.1: Diurnal variation in small molecule leak during inflammatory BBB breakdown. (A) Schematic of the 2-hit LPS experimental paradigm used for diurnal BBB permeability experiments using sodium fluorescein (NaFL). (B) Representative images of dorsal and ventral view of whole brains from mice injected with PBS and LPS as in A, then given either Evans Blue or NaFL tracer. (C) Quantification of diurnal differences in LPS-induced NaFL leak in the hippocampus, cortex, and cerebellum. n = 4-9 mice per group.

2.3.2 Interaction of Light and Circadian Rhythms Drive Diurnal Variation in Inflammatory BBB Breakdown

Previous studies have found that the presence of light is necessary to drive rhythms in LPS-induced mortality, indicating that the diurnal variation in BBB leakage may be due to either light or circadian rhythms (Lang et al., 2021). Since there is an effect of constant darkness on LPS response (Lang et al., 2021), we instead used an inverted dark:light (D:L) light cycle to test if diurnal differences in NaFL leak are driven through the onset of light or through intrinsic circadian mechanisms. Following a 12-hour shift in lighting schedule, the circadian clock takes several days to entrain to the new zeitgeber, allowing us to disentangle the effect of light and an organism's internal circadian rhythm (Figure 2.2A, B). The diurnal difference in LPS-induced BBB breakdown persisted after 1 day of light inversion, with LPS still inducing greater NaFL leak in the evening – 7pm now being 1 hour after lights-on (ZT1) (Figure 2.2C). These data indicate that internal circadian rhythms - rather than the onset of light - are responsible for driving diurnal fluctuations in LPS-induced BBB breakdown. It also shows that behavioral activity can be dissociated from the diurnal differences in LPS-induced BBB breakdown. For all D:L experiments, control littermate mice kept in L:D showed the same ZT13 LPS-induced BBB breakdown. However, we next found that the diurnal differences in LPS-induced NaFL leak were ablated in mice kept in 24-hours of constant darkness (D:D) (Figure 2.2D), a finding consistent with previous studies of LPS-induced mortality. This suggests that there is a complex interaction between light and circadian rhythms in driving LPS-induced inflammatory BBB breakdown. Interestingly, since mice free-run during D:D, their period of consolidated activity continues to occur primarily during the night for the first weeks. This suggests that neural activity alone is insufficient to drive this phenotype. Altogether, these data indicate that the underlying circadian mechanism of LPS-induced BBB breakdown is separate from behavioral

activity, may be impacted by the presence of light, and entrains to new light schedules slower than sleep/wake cycles.

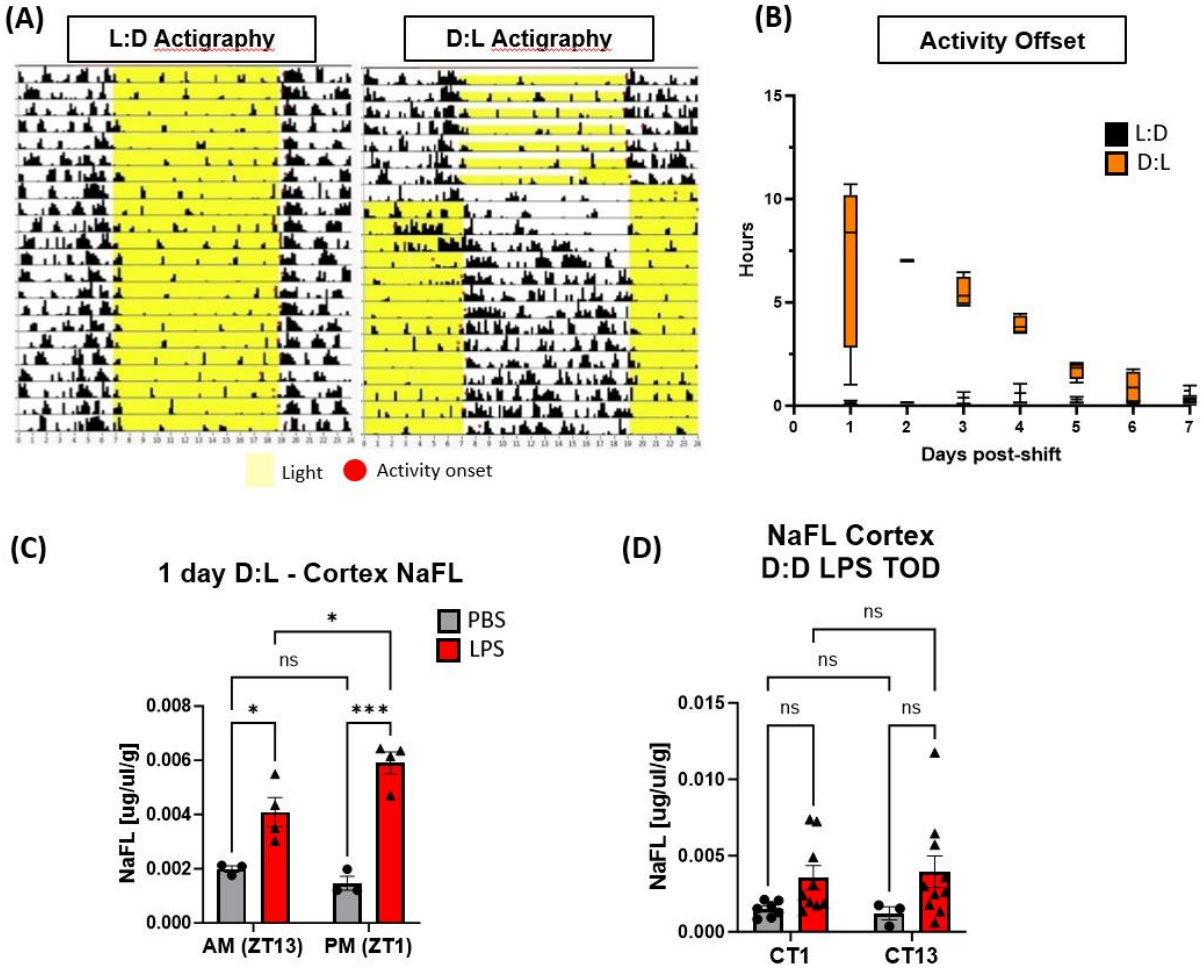

Figure 2.2: Interaction of light and circadian rhythms drive diurnal variation in inflammatory BBB breakdown. (A) Representative actigraphy from L:D and D:L single-housed mice. (B) Hours of activity onset from beginning of darkness for 1 week after light inversion. (C) TOD differences in LPS-induced NaFL leak in the cortex of D:L mice, ZT13 is 7am and ZT1 is 7pm. (D) TOD differences in LPS-induced NaFL leak in the cortex of D:D mice, CT1 is 7am and ZT13 is 7pm. n = 3-9 mice per group.

2.3.3 Evening LPS Exposure Disrupts Endothelial Cell Morphology

Solutes can cross the BBB in a myriad of ways including passive paracellular or transcellular diffusion as well as adsorptive-, carrier-, or receptor-mediated transport. Inflammatory BBB breakdown occurs primarily through either disruption of endothelial tight

junctions (TJs) or an increase in transcytosis (Banks et al., 2015). To characterize diurnal changes in capillary ultrastructure in response to LPS, we used transmission electron microscopy (TEM) to image cortical vessels from mice treated as in Fig. 1. While we saw no gross disruption of the neurovascular unit (NVU), there was significant diurnal variation in vasodilation, with an increase in capillary diameter in mice treated with LPS at ZT13 as compared to ZT1 (Figure 2.4A, B). We next measured the average tight junction (TJ) length per vessel and saw no change based on time or treatment (Figure 2.4C, D). In addition, there were no changes in blood vessel coverage with the TJ protein CLAUDIN5, despite known circadian rhythms in *Claudin5* gene expression (Figure 2.3A) (Hudson et al., 2019). These data are supported by previous studies showing LPS-induced inflammation does not affect TJs, although we did note select disrupted TJs imaged in the LPS treatment group in low prevalence (Figure 2.3B) (Erickson et al., 2023).

LPS treatment is also known to increase transcytosis, as indicated by the number of micro- and macro-pinocytic vesicles in endothelial cells (Erickson et al., 2023). We quantified the number of vesicles per capillary, only counting actively invaginating vesicles from the luminal side, and found a significant increase in the percentage of vessels containing at least one vesicle in LPS treated mice at ZT13 only (Figure 2.4E, F). Previous TEM studies have also found that LPS induces luminal plasma membrane ruffling, which has been implicated as a mechanism bacteria and viruses use to increase infection of endothelial cells (Erickson et al., 2023; Espinal et al., 2022; X. P. Lin et al., 2020). We found a significant increase in severe luminal irregularity in LPS treated mice at ZT13 only. While there is a slight increase in severe luminal irregularity between ZT1 and ZT13 LPS treated mice, the significant effect at ZT13 is primarily driven through increased plasma membrane smoothness in the PBS mice (Figure 2.4G). However, it is important to differentiate that the cilia-like structures seen in ZT1 PBS

mice are morphologically distinct from the severe luminal irregularity seen in both the ZT1 and ZT13 LPS treated mice, which is characterized by deeper plasma and basement membrane disruption (Figure 2.4G). Altogether, these ultrastructural abnormalities indicate evening LPS exposure induces increased luminal diameter as well as a disrupted endothelial cell morphology that is consistent with increased transyctotic particle uptake.

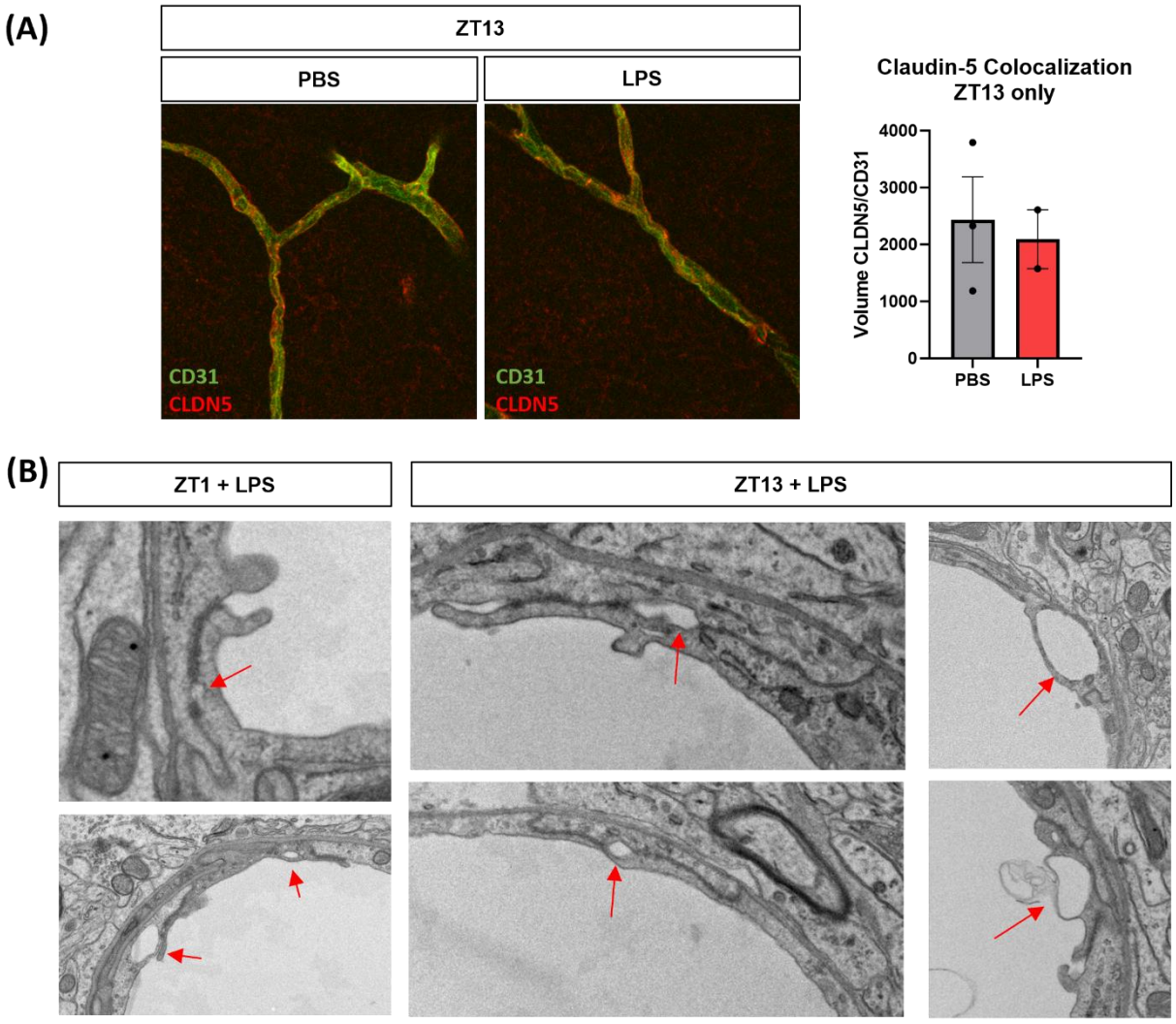

Figure 2.3: Tight junction disruption in select LPS-treated mice. (A) Effects of LPS on Claudin-5 co-localization with CD31 at ZT13. (B) Examples of TJ disruption and vacuole-like structures present in LPS treated mice at both ZT1 and ZT13, denoted by red arrows.

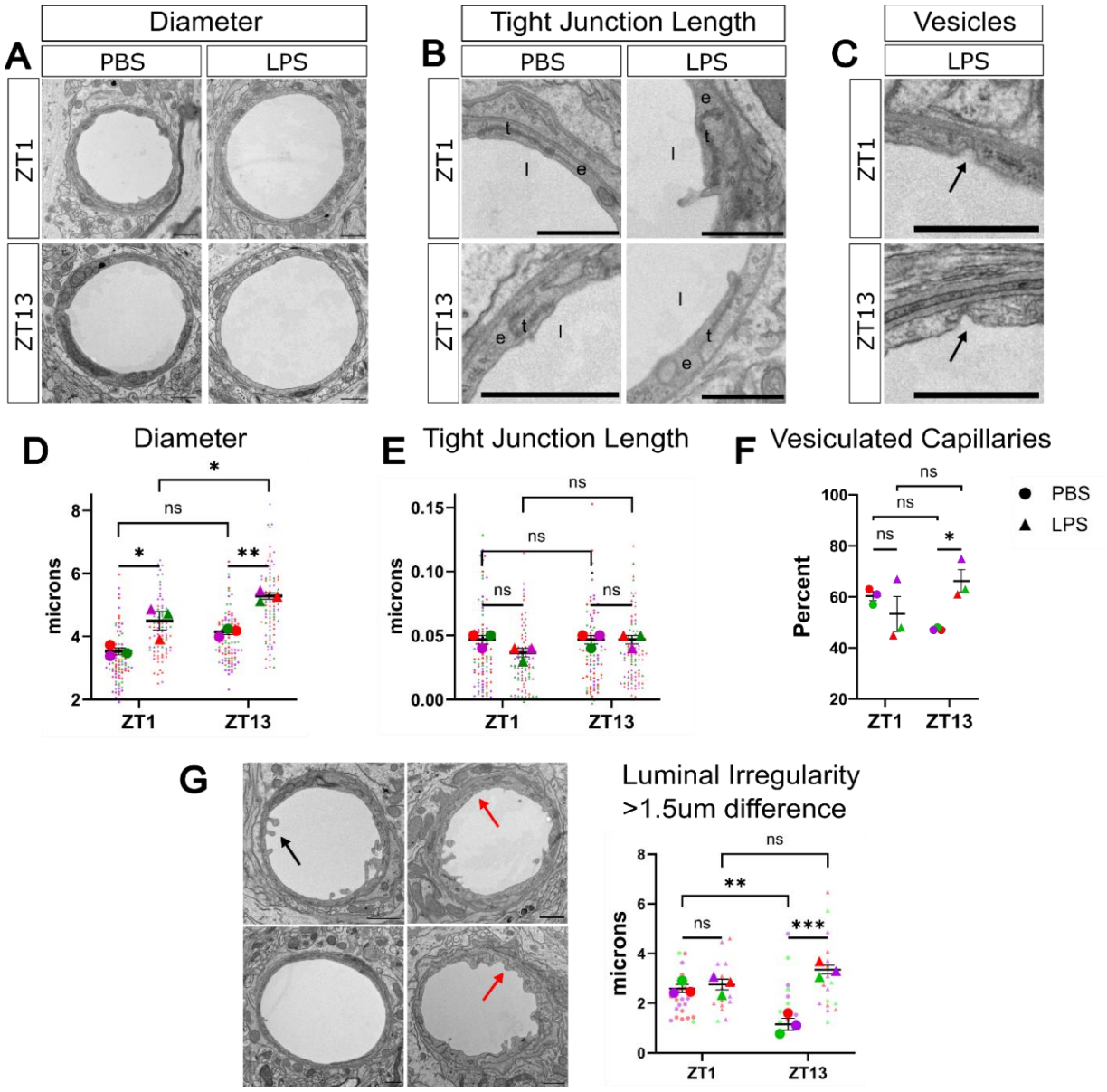

Figure 2.4: Evening LPS exposure disrupts endothelial cell morphology. (A,B) Representative images and quantification of diameter across cortical capillaries. Main effect of LPS was significant, but interaction was not by 2-way ANOVA. (C,D) Representative images and quantification of average tight junction length per capillary; e = endothelial cell, l = lumen, t = tight junction. No effects were significant by 2-way ANOVA. (E,F) Inclusion criteria for vesicles (arrow indicating invaginating vesicles) and quantification of percentage of capillaries that contain one or more vesicles. Interaction was significant by 2-way ANOVA, and post-hoc test is shown. (G) Representative images and quantification of severe luminal irregularity (arrows: black showing blebbing at luminal surface, red showing plasma/basement membrane disruption). Main effect of TOD and Interaction were significant by 2-way ANOVA, and post-hoc test is shown For all graphs, N = 3 mice per group, 28-32 capillaries per mouse. Average for each mouse is shown in large dots, while technical replicates shown as smaller dots in similar color per mouse; Scale bar = 1 micron.

2.3.4 Evening LPS Exposure Specifically Enhances Neuroinflammatory and BBB-Related Gene Expression

While previous studies have characterized the brain inflammatory profile induced by LPS, none have considered diurnal variations in immune response to LPS exposure (Hasel et al., 2021; S. S. Kang et al., 2018; Pulido-Salgado et al., 2018). To account for this, we conducted bulk RNAseq on cortex samples from mice treated with i.p. LPS (or PBS control) at ZT1 and ZT13, as in Fig. 1. When comparing only LPS-treated mice between ZT1 and ZT13, we identified 209 differentially expressed genes (DEGs; 181 upregulated and 28 downregulated, adjusted $P<0.05$) in the ZT13 LPS compared to ZT1 LPS group (Figure 2.5A). Since the majority of DEGs were upregulated at ZT13, we next asked if LPS treatment induced more transcripts at ZT13 than at ZT1 by examining PBS vs. LPS at ZT1 and separately analyzing PBS vs. LPS at ZT13, then comparing the DEG lists. There were 3287 DEGs (1761 upregulated and 1526 downregulated) in LPS compared to PBS treated mice at ZT1 and 5398 DEGs (2756 upregulated and 2642 downregulated) in LPS compared to PBS treated mice at ZT13. Comparisons between these two datasets found that there were 2661 DEGs uniquely found in mice treated at ZT13, with only 550 DEGs unique to ZT1, and an additional 2737 DEGs found at both times (Figure 2.5B). KEGG pathway analysis for DEGs uniquely induced with ZT13 LPS treatment found that most of the top pathways were involved in inflammation and immunity, with the third pathway being adherens junctions (AJs) (Figure 2.5C).

We next used a 2-way ANOVA to examine statistical interaction between our two variables, time-of-day (TOD, ZT1 vs. ZT13) versus treatment (PBS vs. LPS). This method allowed us to control for baseline rhythms in gene expression in the PBS control groups. We then plotted only the DEGs with a significant TOD x LPS interaction on axes representing their

log_2fold change in AM (x-axis) versus PM (y-axis). This showed us that DEGs which are upregulated in response to LPS tend to be further upregulated when treated with LPS in the PM (Figure 2.5D). KEGG pathway analysis of all DEGs with a significant TOD x treatment interaction found dysregulation of several vascular related functions - focal adhesion and fluid shear stress and atherosclerosis - as well as inflammatory pathways, including leukocyte transendothelial migration and ECM-receptor interaction (Figure 2.5E). Many of the genes with a TOD x treatment interaction are involved in BBB function, including upregulation of the TJ- and AJ-associated proteins *Cldn5* and *Cdh5* (Figure 2.5D). Although opposing the directionality of the NaFL leak, this may serve as a compensatory mechanism during robust inflammation and BBB disruption. Congruent with the increase in capillary diameter, there was a diurnal increase in expression of the vasodilator-stimulated protein (*Vasp*) and inducible nitric oxide synthase (*Nos2*) genes, both of which have been implicated in BBB dynamics (Figure 2.5D) (Boje, 1996; Kraft et al., 2010). Altogether, while we saw significant changes in LPS-induced gene expression at both the ZT1 and ZT13 time points, BBB-associated genes were among the most significantly dysregulated pathways when considering the interaction of time and treatment.

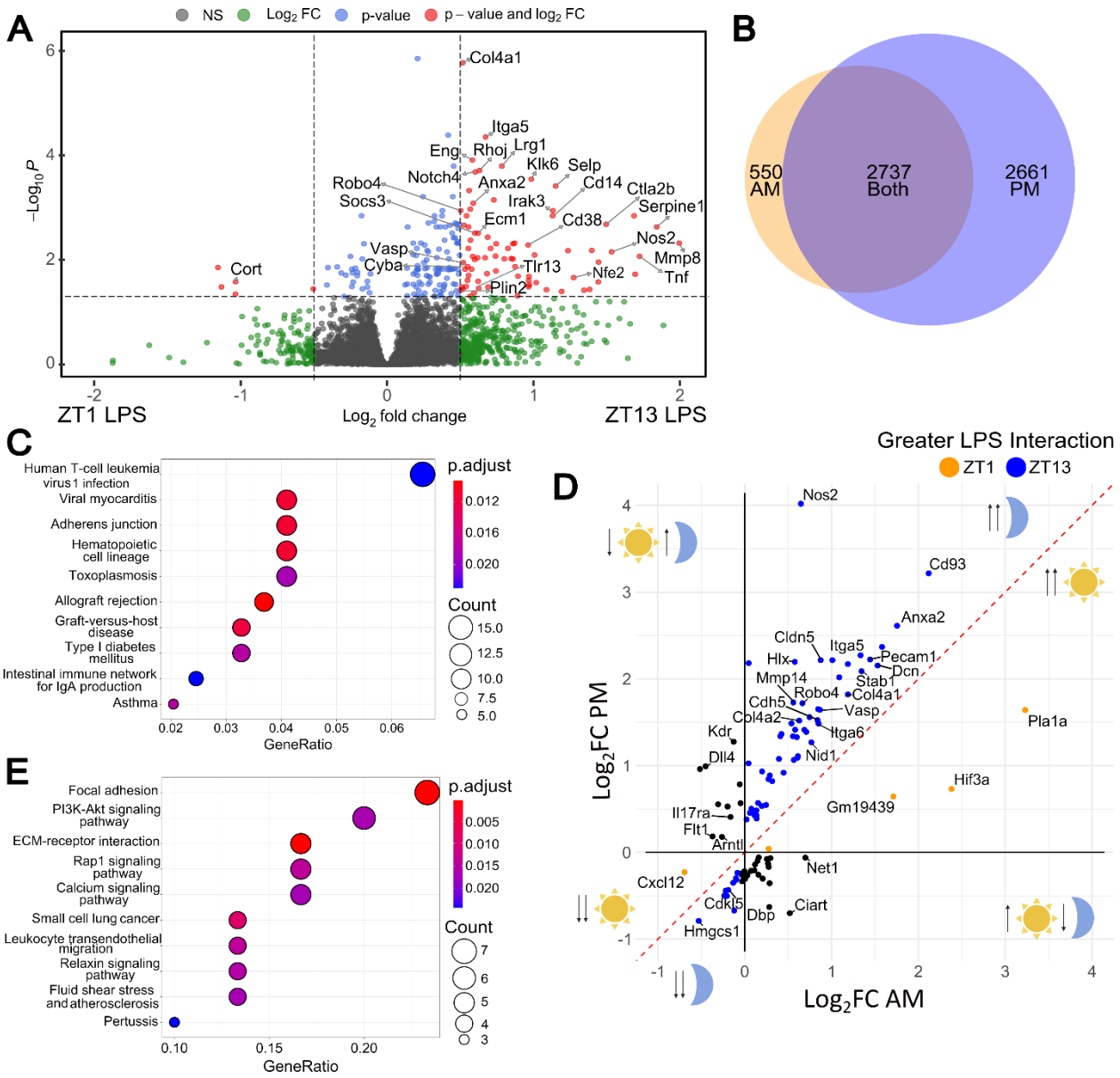

Figure 2.5: Evening LPS exposure specifically enhances neuroinflammatory and BBB-related gene expression. (A) Volcano plot of differentially expressed genes (DEGs) from bulk RNAseq in LPS-treated mouse cortex, comparing ZT1 vs. ZT13 treatment time. Red dots indicate transcripts with adjusted P value <0.05 and fold change >1.75 fold, and right upper area indicates higher expression in mice treated at ZT13 (B) Venn diagram showing overlap of DEGs upregulated after LPS in the ZT1 vs. ZT13 datasets. (C) ORA dotplot of the top pathways uniquely dysregulated at only ZT13. (D) XY plot of genes with a significant TOD and treated interaction by 2-way ANOVA. Log fold change (PBS vs. LPS) in the AM (ZT1) group is shown on X axis, and in the PM (ZT13) group on Y axis. Cartoons indicate the response of genes in that area to LPS (up or down arrow) in the AM (sun) or PM (moon). Genes shown above the red dotted line and right of the Y-axis were all upregulated in the PM, with Nos2 being the highest fold change. (E) ORA dotplot of the top dysregulated KEGG pathways using the full gene list from D. n = 3-5 mice per group

2.4 Discussion

While inflammatory BBB breakdown and circadian rhythms in barrier properties have both been explored independently, there is relatively little known about daily rhythms in neuroinflammation and BBB breakdown. Our current findings suggest that there are diurnal changes in the susceptibility of the BBB to inflammatory breakdown, beyond the known rhythms in transporter activity (Pan et al., 2002; Pan & Kastin, 2001; Pulido et al., 2020; S. L. Zhang et al., 2018). Ultrastructural imaging found increased nighttime vasodilation, membrane dysregulation, and vesicle formation – potentially contributing to transcytosis and small molecule leak. Transcriptomic analysis showed that these diurnal variations were coupled with dysregulated extracellular matrix, neuroinflammatory, and BBB associated processes, with greater inflammatory gene expression in mice treated with LPS in the evening (ZT13).

Rhythms in immune response may confer an evolutionary advantage by ensuring maximum immunity during times of day when animals are at the greatest risk of injury or infection (Curtis et al., 2014). Mortality post-LPS is highly rhythmic, with a peak in death when LPS is administered at ZT8 and a trough at ZT20 (Lang et al., 2021). This effect is light *dependent* and myeloid cell clock *independent*, as rhythms in mortality are ablated in mice kept in constant darkness (DD) and persist in mice deficient in the master circadian clock protein, BMAL1, in myeloid cells (Lang et al., 2021). Of note, constitutive brain-specific deletion of BMAL1 has been reported to induce BBB breakdown at baseline, further complicating the study of cellular circadian rhythms in inflammatory BBB leakage (Nakazato et al., 2017). Interestingly, inflammatory cytokine production may not be required for circadian rhythms in mortality, as one study found cytokine production remained rhythmic in DD while mortality did not (Lang et al., 2021). Rhythmic homing to lymph nodes also persisted in both DD and myeloid *Bmal1* deletion

conditions – indicating LPS-induced mortality may be caused by a complex, multicellular immune response (Lang et al., 2021). Altogether these data show that, while there are striking effects of timing on immune response, there is more work needed to disentangle the role of cellular clocks and external factors.

At the capillary level, there were structural abnormalities uniquely induced by evening LPS exposure. While there were no changes to average tight junction (TJ) length, there were select TJ disruptions seen in LPS treated mice as well as dysregulated TJ-associated protein expression. We also observed increased plasma membrane ruffling and vesicular transport in ZT13 LPS treated mice. These data open an interesting discussion on the exact mechanism of this small molecule leak. The initial size exclusion between NaFL and Evans Blue (EB) indicates leak is occurring paracellularly, whereas the observed structural changes associated with transcellular transport would not have the same size exclusion properties – suggesting there should be increased EB entry. Finally, there was a significant effect of both treatment as well as treatment x time on average luminal diameter. This increase in cerebrovascular blood flow, coupled with BBB dysregulation, may serve to increase peripheral immune cell surveillance and response during neuroinflammation (for further discussion on perivascular immune surveillance see 1.2.3 The BBB in disease).

The increase in vasodilation seen by TEM was further supported by transcriptomic data. RNA sequencing of cortical tissue identified *Nos2* as having the greatest fold change increase of any gene with a significant diurnal difference in response to LPS (Figure 2.5D). *Nos2* is highly expressed in microglia and encodes for inducible nitric oxide synthase (iNOS), which catalyzes nitric oxide (NO) production in response to pro-inflammatory cytokines (Boje, 1996; Fan et al., 2011; Kong et al., 1996; Mayhan, 1998). Importantly, inhibiting iNOS protects against LPS-

induced vasodilation and BBB leakage – highlighting its role in controlling endothelial cell function (Boje, 1996; Fan et al., 2011; Kong et al., 1996; Thiel & Audus, 2001). Another gene with a strong diurnal response to LPS was *Cybb*, also known as NADPH oxidase-2 (*Nox2*). *Nox2* is primarily expressed in microglia and induces the matrix metalloproteinases *MMP9* and *MMP12* in response to LPS – which are involved in TJ degradation and iNOS production respectively, and both of which have TOD differences (Figure 2.5D) (Chelluboina et al., 2015; J.-T. Lee et al., 2014). Altogether, this data shows that there is a robust effect of timing on LPS-induced neuroinflammation, and that evening inflammatory stimuli induces an altered pro-inflammatory profile that is more conducive to BBB dysfunction. However, the exact mechanisms of how peripheral inflammation induces BBB dysfunction as well as what cell types are involved have yet to be elucidated.

2.5 Materials and Methods

BBB assays: 100uL of 100mg/ml sodium fluorescein (Sigma-Aldrich: F6377) diluted in sterile PBS was injected subcutaneously, 45 minutes later mice were deeply anesthetized with i.p. pentobarbital (150mg/kg). 100uL of blood was collected by cardiac puncture before they were perfused with ice-cold PBS containing 3g/l heparin. Both hemispheres were dissected into regions and stored in pre-weighed tubes filled with 500uL PBS on ice. A small piece of peripheral and brain tissues were removed, flash frozen, and stored at -80°C for RNA analysis as described below. Tissue was weighed then homogenized for 3 minutes in a bullet blender and serum was added to a serum separator tube (BD Microtainer: 365967) before being spun down and diluted 1:200, tissue supernatant and serum were incubated 1:1 in 2% Trichloroacetic acid (Millipore Sigma: T9159) overnight (4°C). The samples were spun down again and diluted 1:1 in Borate Buffer (Honeywell: 33650) before being read on a plate reader along with a standard curve. Fluorescence per gram of CNS tissue was compared to fluorescence per uL of serum to determine the absolute amount of NaFL that crossed from the periphery to the brain for each mouse.

4uL/g body weight of 2% Evans Blue (Sigma-Aldrich, E2129) was injected retro-orbitally, 15 minutes later the mice were deeply anesthetized and perfused as described above. Whole brains were dissected out and imaged.

Circadian rhythm disruption models: For constant darkness experiments, mice were kept in standard 12:12 light:dark and after the lights turned off at 6pm they were kept off for the remainder of the experiment. For inverted light cycle experiments, the lights turned off at 6pm and were kept off for an additional 12h before turning on at 6pm the next day. Control mice were

littermates kept in standard 12:12 light cycle, turning on at 6am and off at 6pm. For all experiments when mice were injected during the dark phase, red light was used and they were kept in darkness until fully anesthetized. Actigraphy was recorded using PIR infrared wireless sensors (Actimetrics) and circadian analysis was done using ClockLab Analysis software, version 6.1.02.

Drug administration: LPS from *escherichia coli* O55:B5 (Sigma-Aldrich, L6529) was diluted to 2mg/ml in PBS and stored at -80°C. Immediately before each injection, LPS stock was thawed and diluted to 0.5mg/mL in PBS before being injected (i.p.) at a dose of 2mg/kg. Each LPS stock was not thawed more than twice before being discarded. To avoid batch effects, enough LPS was purchased at each time for an average of 3 experimental cohorts to be treated from the same stock. Mice were weighed each day prior to injection and the weight at the first day was used to determine dosing for the entire experiment.

RNA quantification: Tissue was homogenized in 500ul of Trizol with beads added before running in a bullet blender for 3 minutes. TRIzol samples were then subjected to chloroform extraction (1:6 chloroform:TRIzol, followed by thorough mixing, and centrifugation at (12500 x g for 15 minutes). RNA was then extracted from the aqueous layer using the PureLink RNA Mini Kit according to manufacturer's instructions. RNA concentration was measured on a Nanodrop spectrophotometer, then cDNA was made using a high-capacity RNA-cDNA reverse transcription kit (Applied Biosystems/Life Technologies) with 250ng-1 mg RNA per 20mL reaction. Real-time quantitative PCR was performed with ABI TaqMan primers and ABI PCR Master Mix buffer on ABI StepOnePLus or QuantStudio 12k thermocyclers. Taqman primers (Life Technologies) were used, and mRNA measurements were normalized to b-actin (Actb)

mRNA for analysis. For larger experiments, microfluidic qPCR array measurements were performed by the Washington University Genome Technology Access Center using a Fluidigm Biomark HD system, again using Taqman primers. RNA sequencing was performed and values normalized as previously described (McKee et al., 2022). Volcano plots were made using Enhanced Volcano R package, heatmaps were made using the Pretty heatmap package, and X-Y plots were made using ggplot. Over-representation analysis dot plots of KEGG pathways were generated using the ClusterProfiler and enrichplot R packages.

Transmission Electron Microscopy: Mice were anesthetized as described above and perfused with 10mL perfusion buffer (0.2mg/ml xylocaine and 20 units/ml heparin) then 20mL fixative solution (2.5% glutaraldehyde, 2% paraformaldehyde, and 0.15M cacodylate buffer with 2mM $CaCl_2$), all kept at 37°C. Tissue was then post-fixed in ice-cold fixative solution overnight at 4°C. The brains were embedded in epoxy resin and the region of interest were cut into a 1mm x 1mm squares 70nm thick.

All imaging was done on a JEOL JEM-1400Plus Transmission Electron Microscope at 3-5,000x magnification. Capillaries were identified by morphology (<8um in diameter) with a circularity ratio <2. Treatment groups were blinded to the investigator and TIFF image files were opened using ImageJ and analyzed using the measure tool. The scale for each image was set depending on the magnification used. Diameter was determined as the distance across the vessel at the shortest point, luminal irregularity was the measured length of the plasma membrane divided by the estimated circumference using the elliptical tool, TJ length was the average of each measured TJ per vessel divided by the circumference, and vesicles were only counted if actively invaginating from the luminal side.

Statistics: In all figures, graphs depict the mean + SEM, and N generally indicates the number of animals, unless otherwise noted in the figure legend. For TEM experiment, each datapoint depicts the mean for 28-32 technical replicates from one mouse, and each of these mean values is considered an N of 1. An F test was first performed for datasets with a single dependent variable and 2 groups, to determine if variances were significantly different. If not, 2-tailed unpaired T-test was performed. For datasets with 2 dependent variables, 2-way ANOVA was performed, and if main effect was significant, Tukey multiple comparisons test was then added for appropriate sets of variables. Outliers were identified using Grubbs test and were excluded. Statistical tests were performed with GraphPad Prism software, version 10.0.2. P values greater than 0.1 were noted as not significant (NS). $P<0.05$ was considered significant and was note with asterisks indicating the p-value: *$P<0.05$, **<0.01, ***<0.005, ****<0.00

Study approval: All animal experiments were approved by the Washington University IACUC and were conducted in accordance with AALAC guidelines and under the supervision of the Washington University Department of Comparative Medicine. 7-week-old male C57/bl6J littermate mice were all obtained from Jackson Labs (Bar Harbor, ME) and allowed to acclimate for one week in our facilities before all experiments. For viral injection experiments embryonic day 18 timed-pregnant CD1 mice were ordered from Charles River (Wilmington, MA). Mice were housed in a 12-hour light/dark cycle (lights on at 6am and off at 6pm) and allowed ad libitum access to food and water unless otherwise stated during circadian rhythm disruption models.

Chapter 3: Time-of-day differences in microglial activation and resolution drive inflammatory BBB breakdown

3.1 Abstract

Inflammatory BBB breakdown is much more severe following LPS exposure in the evening (ZT13) as compared to morning (ZT1); however, the exact mechanisms are unknown. We found that this diurnal variation is characterized by persisting astrocyte and microglial activation and cytokine production which is not observed in the morning and is not present in peripheral organs. The exaggerated evening neuroinflammation and BBB disruption could not be elicited through astrocyte activation, were suppressed by microglial depletion, and could be prevented in vivo by treatment with an iNOS inhibitor. Our data show that diurnal rhythms in microglial inflammatory responses to LPS drive daily variability in BBB breakdown, occurs independently of rhythms in peripheral inflammation, and reveals time-of-day as a key regulator of inflammatory BBB disruption.

3.2 Introduction

Peripheral immune cells rapidly mount an immune response after intraperitoneal (i.p.) LPS administration. After a single, large dose of i.p. LPS mice begin to show sickness behaviors 2 hours post injection (hpi). Disease scoring increases up to 6 hpi before returning to baseline by 24 hours. At the mRNA level, pro-inflammatory cytokines begin to increase between 0.5-2 hours post injection (hpi) and peak in expression between 2-4 hpi (Seemann et al., 2017). Plasma

corticosterone, the murine homolog of human corticosterone, began to increase after 2 hours and peaked 6 hpi. In the brain endothelium, *TLR4* was upregulated starting at 0.5h, peaking 3 hpi, and returning to homeostatic levels by 9 hpi. Interestingly, using mass spectrometry to quantify LPS protein, researchers found that 30 mins after LPS injection there was LPS within $TLR4^{+}$ endothelial cells but none within the brain parenchyma. This data suggest that peripherally derived cytokines pass through the BBB and enter the brain parenchyma where they induce neuroinflammation.

CNS immunity is largely conferred by resident glial cells. Previous studies have tried to disentangle the role of microglia in peripheral LPS-induced inflammation. Researchers treated mice with PLX5622, an antagonist for the myeloid receptor CSFR1, that induces microglia cell death (Vichaya et al., 2020). To control for off-target effects of PLX treatment, they also used a diphtheria toxin genetic ablation model. Mice lack the receptor for diphtheria, rendering them immune to the toxin; however, by crossing the diphtheria toxin receptor (DTR) to a microglial specific Cre driver (*Cx3xr1*), they were able to create mice with diphtheria-induced cell death specifically in microglia. They found that there was no effect on LPS-induced sickness behavior using either PLX5622 treatment or Cx3cr1-DTR ablation. Researchers did find PLX5622 treatment decreased levels of *IL-6* and *IL-10* in the CNS and *IL-10*, *TNFα*, and *Oas1a* in the liver, whereas Cx3cr1-DTR mice showed increased *IL-1β* and *TNFα* in the CNS and increased *IL-6*, *IL-1β*, and *TNFa* in the liver (Vichaya et al., 2020). Altogether, these data suggest that while the method of microglial depletion impacts the central and peripheral immune responses to LPS, $CSFR1^{+}$ cells are not required to mount LPS-induced sickness behavior. However, there is no known literature describing the effects of microglial ablation on LPS-induced BBB disruption.

3.3 Results

3.3.1 Evening LPS causes persisting expression of inflammatory and glial activation transcripts

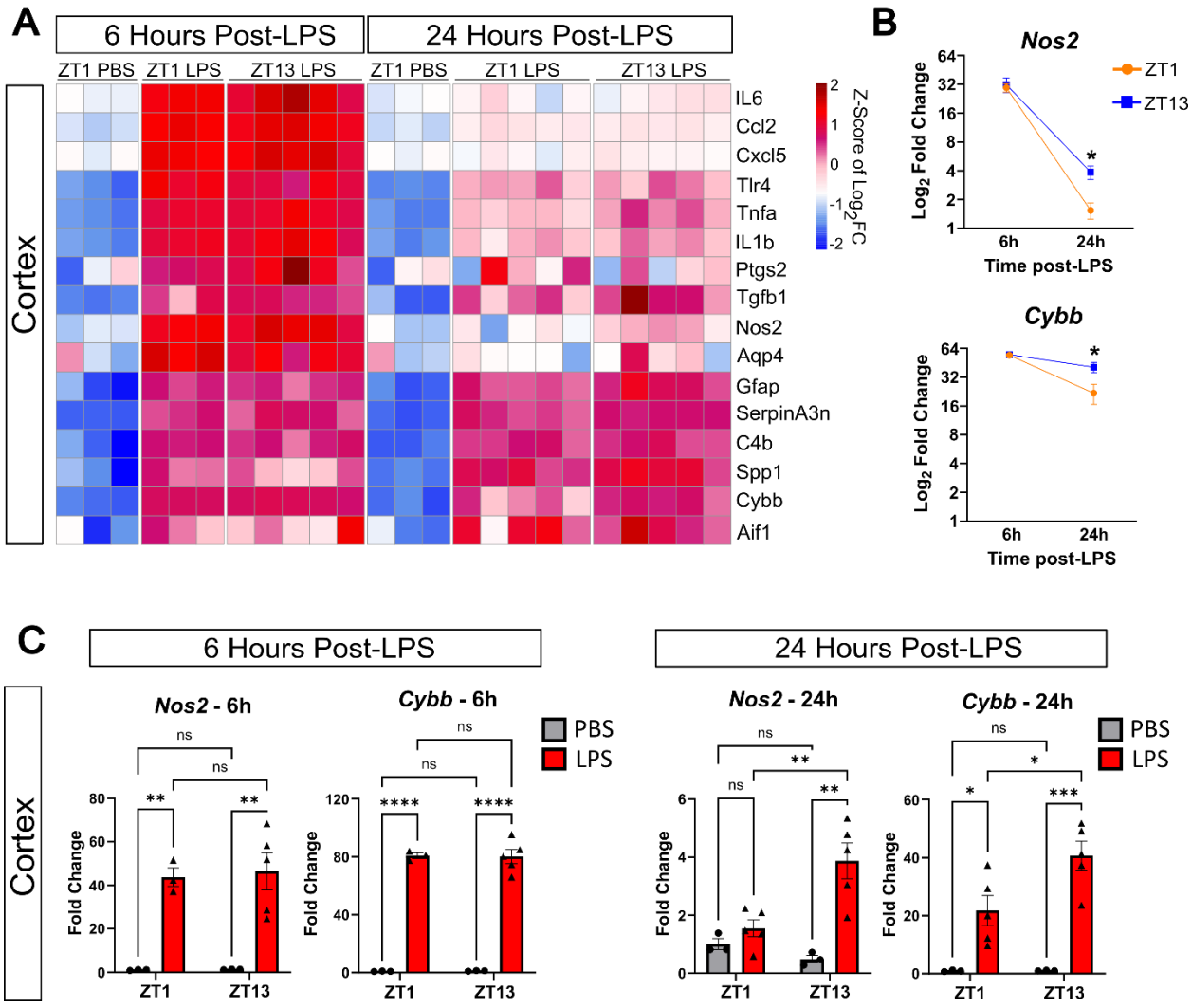

Figure 3.1: Evening LPS causes persisting expression of inflammatory and glial activation transcripts. (A) Heatmap of selected gene expression in mouse cortex 6- vs 24- hours after final LPS injection at ZT1 or ZT12. Gene expression is normalized to ZT1 PBS 6 hpi group, Transcripts with significant TOD effect at 24 hpi are denoted with *. Scale is Z-Score of Log2FC. (B) Nos2 and Cybb graphed across time (significant TOD effects are denoted with *). (C) Full graphs of Nos2 and Cybb, split across 6- and 24- hours post-LPS. n = 3-5 mice per group for all experiments. For 6 hr timepoint, only main effect of LPS was significant, while in 24 hrs timepoint main effect of LPS and interaction are significant for both genes, and post-hoc test results are shown. *p<0.05, **p<0.01, ***p<0.005, ****p<0.001.

In models of systemic LPS administration, peripheral cytokine mRNA levels peak between 0.5-3 hours post-LPS treatment, whereas BBB breakdown increases 6 hours post injection (hpi) (Ciesielska et al., 2021; Jangula & Murphy, 2013; Juskewitch et al., 2012; Singh & Jiang, 2004). To better characterize the diurnal dynamics of LPS-induced inflammation, we collected peripheral (lung) and CNS (cortex) tissue 6- and 24-hours after the final ZT1 or ZT13 dose of LPS (6 hour time points were 1pm (ZT7) or 1am (ZT17)), and examined inflammatory mRNA expression of a subset of transcripts by qPCR. We saw no diurnal differences in lung cytokine production or percent weight loss between the ZT1 and ZT13-injected groups at either 6 or 24 hours post-LPS, indicating that the CNS effects seen in this model of inflammation are not due to major diurnal variations in peripheral inflammatory response (Figure 3.2A, B). In cortical tissue, LPS strongly induced inflammatory gene expression at 6 hpi, but diurnal differences were not evident. However, at 24 hpi, several inflammatory genes (*Tnfa*, *Cxcl5*, and *Nos2*) showed increased expression in the Z13 LPS group – supporting our RNAseq data (Figure 3.1A). When comparing the 6 hpi to 24 hpi gene expression datasets, there is a sharp reduction in cortical inflammation at 24 hpi in all groups, though this resolution of inflammatory gene expression is mitigated in the ZT13 LPS group (Figure 3.1B, C). Conversely, markers of gliosis remain persistently elevated at both 6 and 24 hpi, with the microglial activation marker *Cybb* showing a diurnal difference 24 hours after LPS (Figure 3.1B, C). This indicates that the diurnal difference in inflammatory gene expression seen 24 hours after LPS administration may be due to decreased resolution of inflammation and microgliosis in mice treated with LPS at ZT13 compared to those at ZT1.

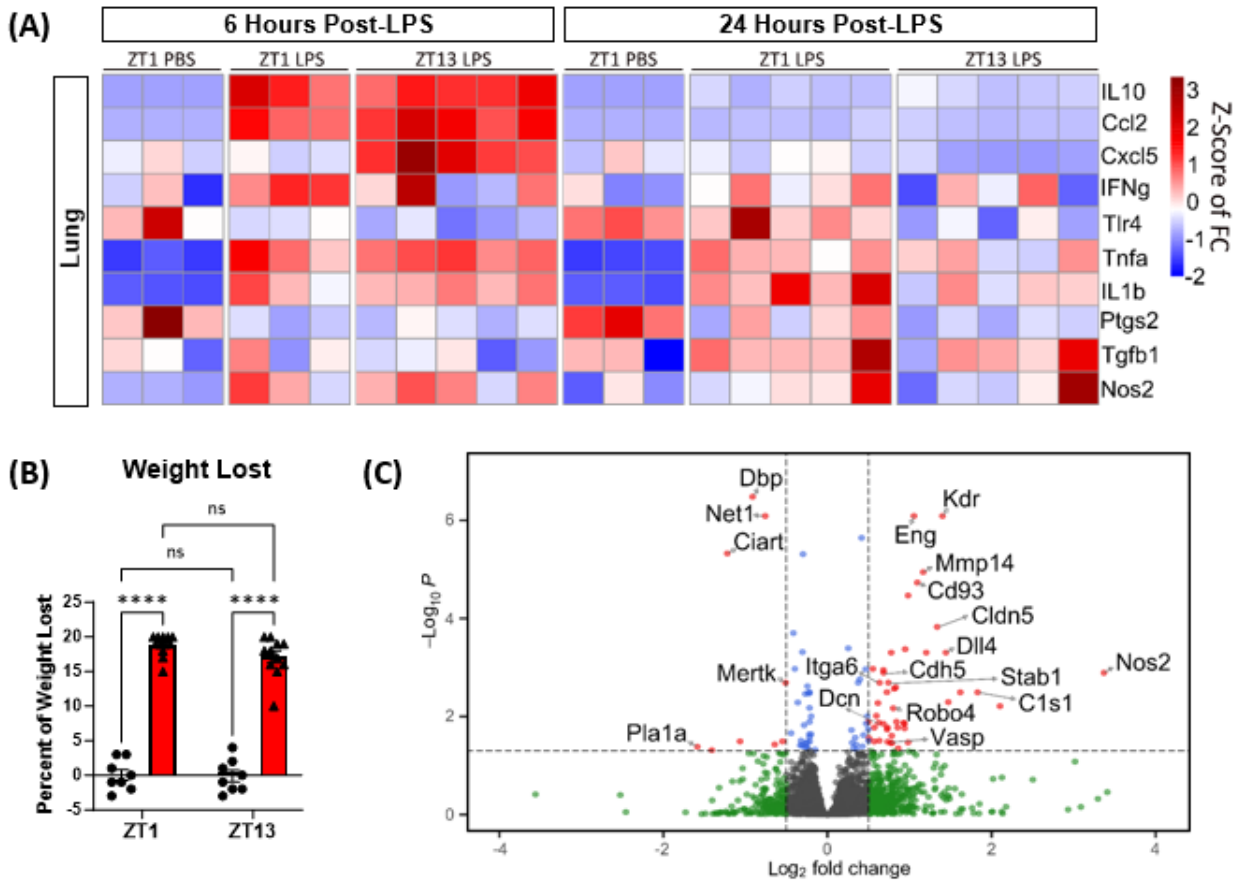

Figure 3.2: Absence of diurnal rhythms in peripheral immune activation at 6 or 24 hours post-LPS. (A) Heatmap of selected gene expression in mouse lung tissue 6- vs 24- hours after final LPS injection at ZT1 or ZT12. Gene expression is normalized to ZT1 PBS 6 hpi group, Transcripts with significant TOD effect at 24 hpi are denoted with *. Scale is Z-Score of FC. (B) Percent weight lost in PBS or LPS treated mice at ZT1 or ZT13. (C) Volcano plot of differentially expressed genes (DEGs) from bulk RNAseq in LPS-treated mouse cortex, with a significant TOD and treated interaction by 2-way ANOVA. Red dots indicate transcripts with adjusted P value <0.05 and fold change >1.75 fold, and right upper area indicates higher expression in mice treated at ZT13. Nos2 is one of the greatest differentially expressed genes in the cortex.

3.3.2 Evening LPS exposure induces increased hippocampal gliosis and perivascular microglial localization

We next quantified micro- and astrogliosis by immunohistochemistry in the same groups of mice (ZT1 or ZT3 LPS) sacrificed at 6 or 24 hpi. At 6 hpi there were no diurnal effects on microgliosis as measured by IBA1 percent area in the hippocampus, although there was a treatment effect at only ZT13 (Figure 3.3A, C). Similarly, using GFAP as a marker for

astrogliosis in the hippocampus, there were no LPS or time effects found at 6 hpi (Figure 3.3B, C). However, there was a significant diurnal effect on IBA1 and GFAP immunoreactivity 24 hours post LPS, the time at which we see robust BBB breakdown, with both microglia and astrocytes showing increased activation in the ZT13 LPS group (Figure 3.3C). Since the 24 hpi increase in astro- and micro-gliosis at ZT13 may also be coupled with changes in perivascular localization, we examined glial proximity to blood vessels at ZT13 (Mastorakos et al., 2021). We imaged $CD31^+$ blood vessels and quantified the percent of perivascular (within 8 um of CD31) vs total amount of IBA1 and GFAP. We saw that LPS did not change GFAP localization, but there was a significant increase in perivascular IBA1 (Figure 3.3D). These data suggest that microglia may play a critical role in LPS-induced BBB breakdown.

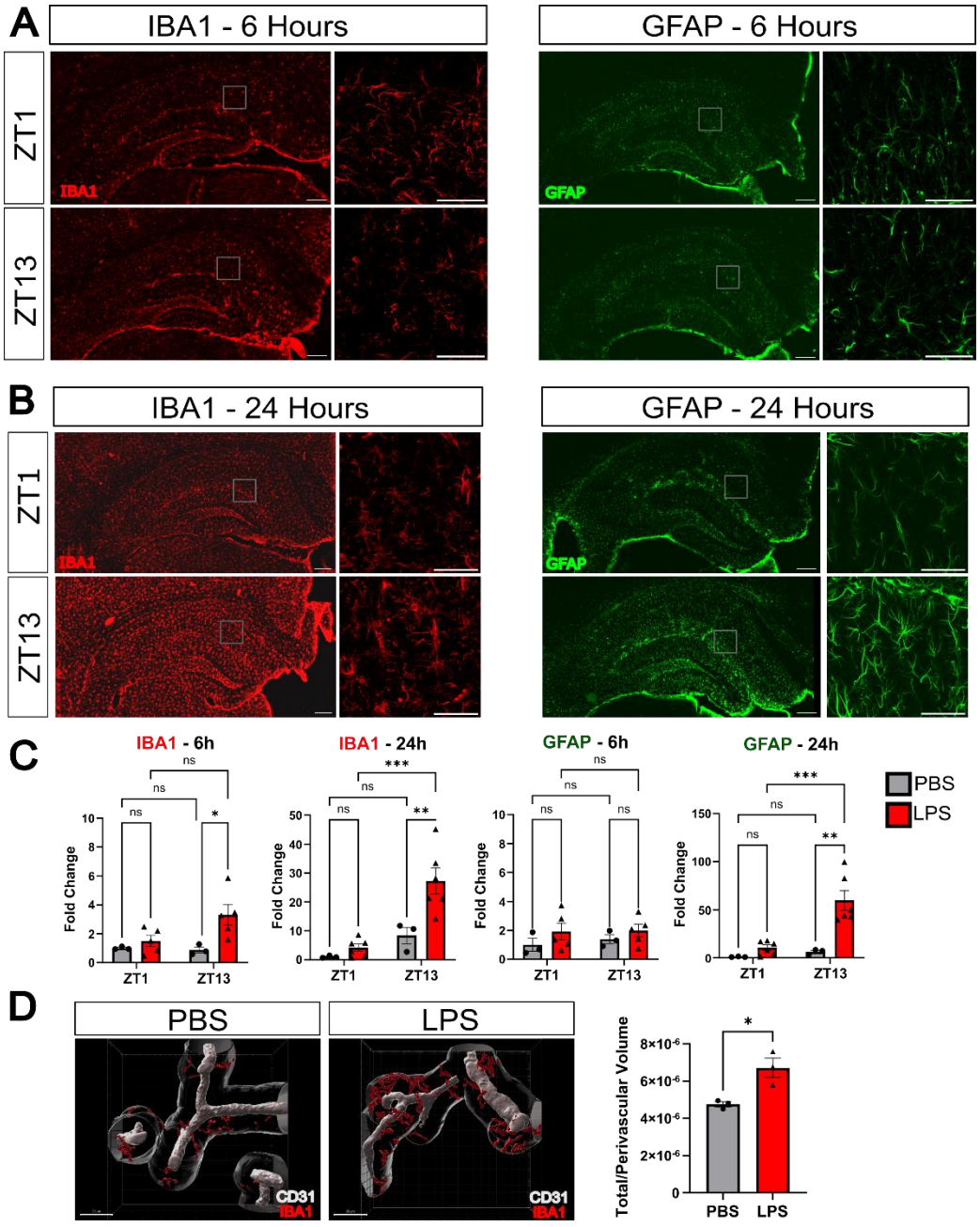

Figure 3.3: Evening LPS exposure induces increased hippocampal gliosis and perivascular microglial localization. (A) Representative images of IBA1 and GFAP after 6h of PBS or LPS treatment. (B) Representative images of IBA1 and GFAP after 24h of PBS or LPS treatment. (C) Quantification of IBA1 and GFAP percent area in the hippocampus 6 or 24 hours post-LPS, normalized to ZT1 PBS group. n = 3-5 mice per group. (D) Volume of IBA1 colocalized within 8µm of CD31, normalized to total volume, at ZT13 24 hpi. n = 3 mice per group; 3-6 vessels imaged per mouse. Inset images are of the hippocampus at 40x magnification. Scale bars: 200um in (A) and (B), inset is 50um; 20um in (D).

3.3.3 Microglia are Required for LPS-Induced Neuroinflammatory BBB Breakdown at ZT13

At baseline, capillary-associated microglia play an active role in maintaining BBB integrity. Ablating microglia with the CSFR1 antagonist Plexidartinib (PLX3397, referred to as PLX) alters vascular tone without changing pericyte coverage or astrocyte endfoot density (Bisht et al., 2021). During inflammation, PLX treatment protects against LPS-induced inner blood retinal barrier leak in the eye and microbubble-induced hemorrhage in the CNS (Kokona et al., 2018; Mastorakos et al., 2021). To determine if microglia are required for LPS-induced BBB breakdown, we treated mice for 2 weeks with PLX prior to LPS administration. Since there was no observed effect of LPS on the BBB at ZT1, we only treated PLX (or control chow) mice at the ZT13 time point. Of note, a previous study shows that PLX administration does not impact behavioral circadian rhythms in mice (Matsui et al., 2023). As previously reported, we found that PLX treatment completely ablated $IBA1^+$ cells (Figure 6B, C) in both PBS and LPS treated groups without altering peripheral immune responses or sickness behaviors (Figure 3.4A) (Vichaya et al., 2020). Despite microglia being the primary $TLR4^+$ CNS-resident cell, LPS-treated PLX mice had increased hippocampal GFAP (Figure 3.4B, C) as well as *Serpina3n* and *Gfap* upregulation (Figure 3.5A), suggesting that astrocyte activation in response to systemic LPS is independent of microglial function. However, despite these changes in astrocyte GFAP expression, ablating microglia through PLX administration reduced LPS-induced *TNFa* and *Nos2* in cerebral cortex and completely protected against NaFL leak, indicating that microglia are required for inflammatory BBB breakdown (Figure 3.4D, E).

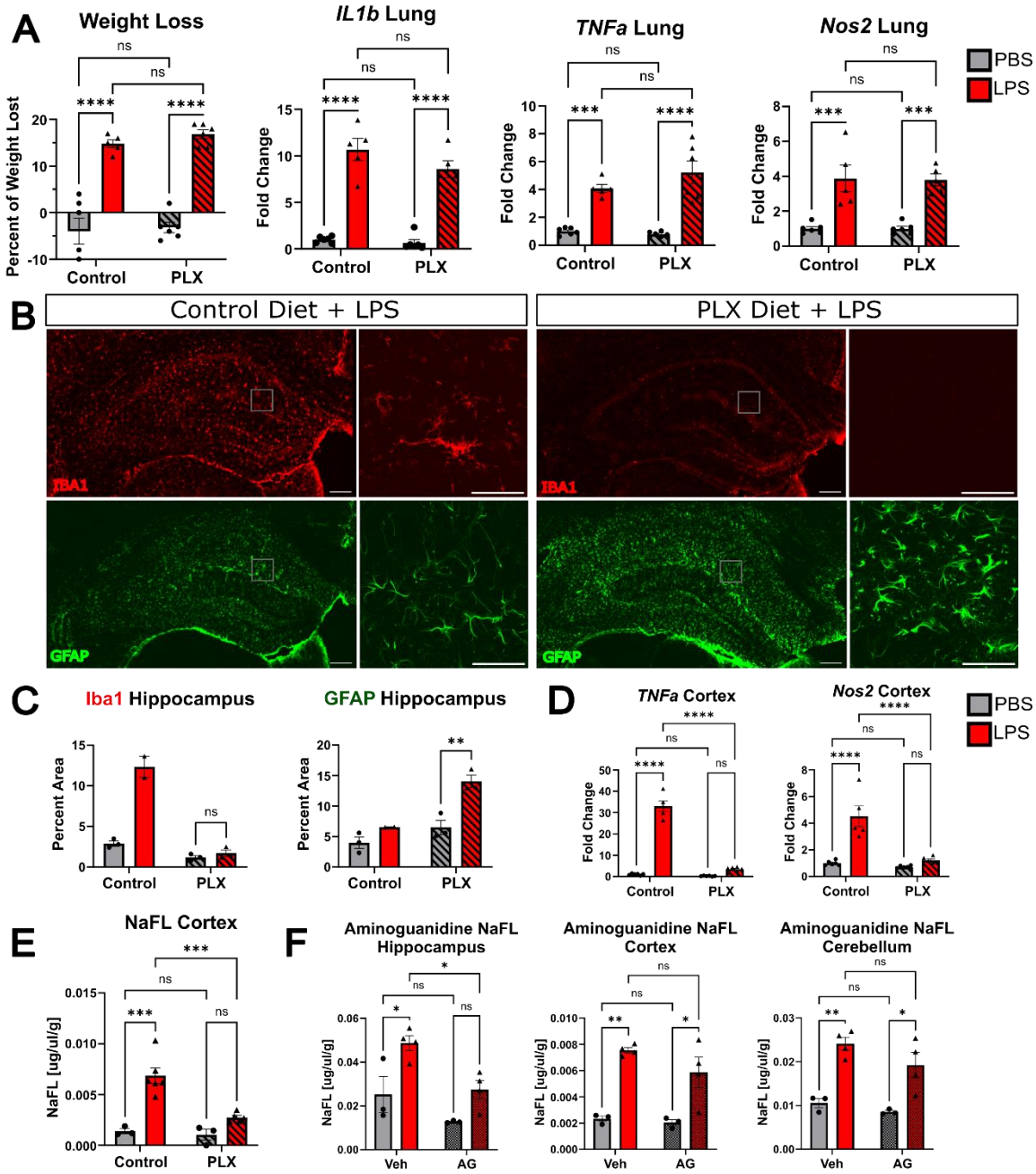

Figure 3.4: Microglia are required for LPS-induced inflammatory BBB breakdown at ZT13. (A) Peripheral cytokines and weight loss after 2 weeks of PLX3397 administration followed by 2d of PBS or LPS at ZT13. n = 5-6 mice per group. All graphs have significant main effect of LPS treatment only. (B) Representative images of hippocampal IBA1 and GFAP staining in control and PLX LPS-treated mice. Inset images are of the hippocampus at 40x magnification. (C) Quantification of IBA1 and GFAP hippocampal percent area. n = 2-3 mice per group. (D) LPS-induced cortical cytokine expression in PBS or LPS treated mice given control or PLX chow. n = 5-6 mice per group. (E) NaFL assay in PBS or LPS treated mice given either PLX or control chow. (F) NaFL assay from PBS or LPS treated mice given vehicle or aminoguanidine. Scale bars: 200um in (B), instep is 50um.

We next sought to manipulate astrocyte activation to determine its role in neuroinflammation caused by evening LPS exposure. Since astrocytes are known to mitigate microglial reactivity after CNS-injury and are in close proximity to blood vessels, they are a prime candidate to serve as the first responders to LPS-induced peripheral cytokines (Hu et al., 2023). Activation of the JAK2-STAT3 pathway is a critical step in astrocyte activation in disease models (Haim et al., 2015). *In vitro*, LPS-stimulation induces an astrocytic STAT3-dependent release of TNF, leading to a loss of endothelial cell barrier properties (H. Kim et al., 2022). Thus, we chose to target the astrocyte STAT3 pathway in our model, utilizing a previously described AAV9 viral vector which expresses a constitutively active form of JAK2 (JAK2ca) behind a truncated GFAP promoter (Ceyzériat et al., 2018). Activated JAK2 phosphorylates STAT3, which then translocates to the nucleus and regulates the transcription of pro- and anti-inflammatory cytokines, including *Tnf*, *Il-1b*, and *Il-6* (Minogue et al., 2012). To ensure global viral spread, we performed intracerebroventricular injections of this viral vector, or an identical control vector expressing eGFP instead of JAK2ca, at postnatal day 0 and waited until the mice were 2-months-old before administering i.p. LPS for two days at ZT13. Mice treated with AAV-GFAP-JAK2ca showed increased hippocampal IBA1 and GFAP in response to LPS as compared to AAV-GFAP-eGFP treated animals, demonstrating that activating astrocyte JAK2-STAT3 prior to LPS exposure enhances both micro- and astrogliosis in the brain (Figure 3.5B, C). However, we observed no increase in BBB permeability at baseline or in response to LPS in the AAV-GFAP-JAK2ca animals. (Figure 3.5D). This finding suggests that while astrocytes respond to LPS independently of microglia, astrocyte activation alone is insufficient to induce BBB breakdown at ZT13 – at least through the JAK2/STAT3 pathway.

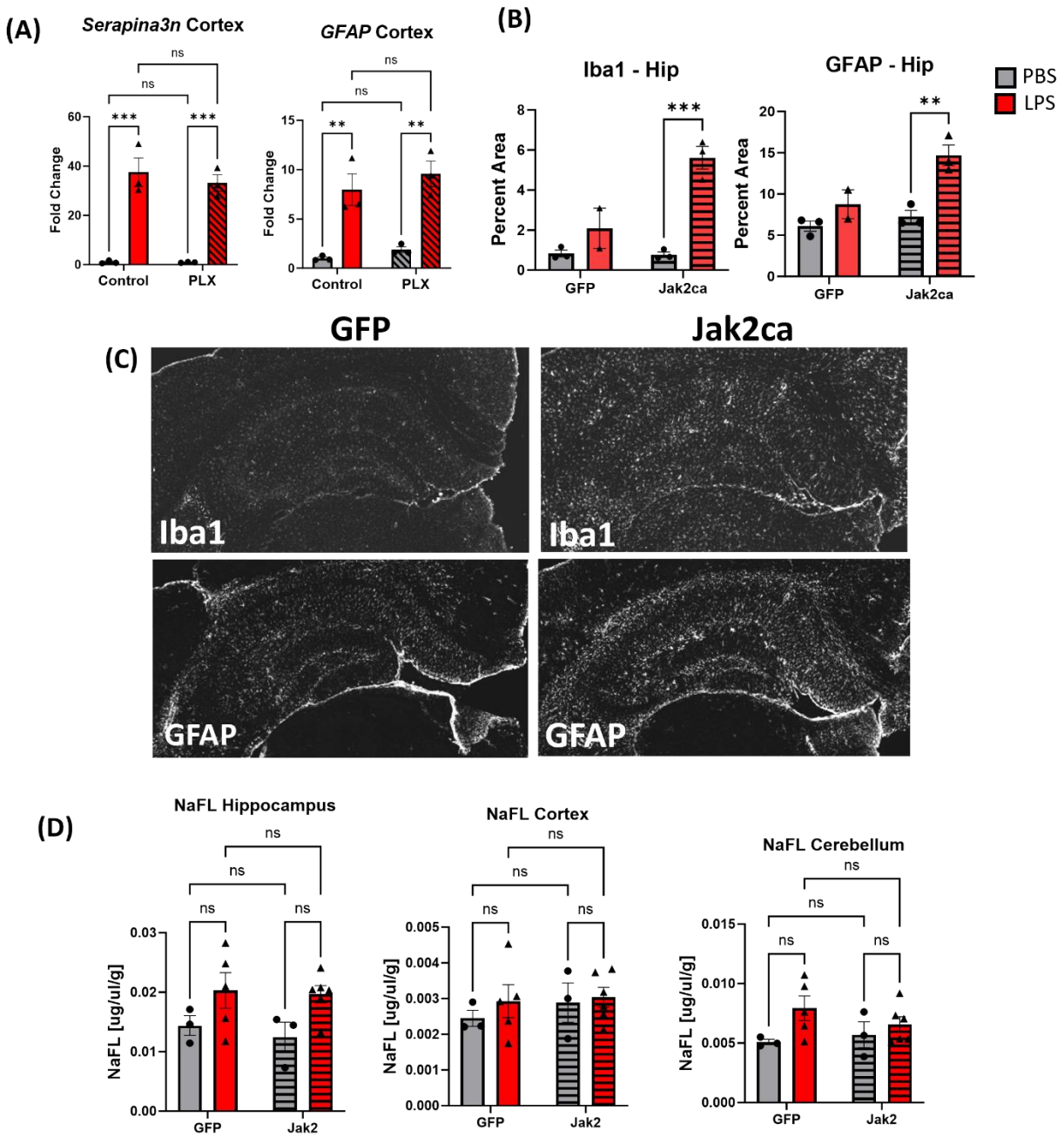

Figure 3.5: Astrocyte activation is insufficient to induce BBB breakdown. (A) *Serapina3n* and *Gfap* expression in PBS or LPS mice treated with 2 weeks of control or PLX chow. n = 3 mice per group. (B,C) Representative images of IBA1 and GFAP in hippocampus of LPS treated GFP or Jak2ca injected mice, and quantification. n = 2-3 mice per group. (D) NaFL assay in PBS or LPS treated Jak2ca or GFP injected mice. n = 3-5 mice per group.

Nos2 had the greatest fold change increase of any gene with a diurnal effect and was completely ablated with PLX treatment, so we next asked what role it plays in diurnal variation

in inflammatory BBB breakdown (Figure 2.5D and 3.4D). *Nos2* encodes inducible nitric oxide synthase (iNOS) which is highly expressed by microglia and known to induce BBB breakdown (Boje, 1996; Fan et al., 2011; Kong et al., 1996). To test the role of iNOS in LPS-mediated BBB breakdown at ZT13, we co-administered the iNOS inhibitor aminoguanidine (AG) with LPS in our typical paradigm. We found that AG co-administration for 2 days protected against inflammatory BBB breakdown at ZT13 in the hippocampus (Figure 3.4F). Although there is a similar trend, the protective effect of AG is not significant in the cortex or cerebellum – perhaps due to stronger LPS-induced leak in those areas (Figure 3.4F and 2.1C). Altogether these data suggest that microglia have an exaggerated response to peripheral inflammation in the evening, triggering increased cytokine production and altered endothelial cell function - potentially through *Nos2*.

2.4 Discussion

We found that TOD differences in inflammation only existed in cortical tissues 24 hours after LPS administration. While 6 hours post-LPS induced a robust, TOD-independent inflammatory response with a drastic increase in pro-inflammatory cytokine expression at both ZT1 and ZT13, by 24 hours post injection (hpi) there was a sharp reduction in neuroinflammation – with greater resolution in ZT13 LPS-treated mice. Interestingly, we found that this trend did not hold with glial activation genes, which remained high between both 6 and 24 hours post-LPS. We found that this persisting glial activation in response to evening LPS was associated with increased BBB permeability, which could be abrogated by microglial ablation or

iNOS inhibition but cannot be elicited through astrocyte activation. Thus, the time of day of an inflammatory insult influences neuroinflammatory response and BBB integrity.

Since LPS induces BBB breakdown both when administered systemically as well as directly to the CNS, it is difficult to disentangle the role of rhythms in peripheral and central inflammation (Banks et al., 2015; Mayhan, 1998). Brain endothelial cells (BECs) are $TLR4^+$ and trace amounts of LPS has been found in them up to 30 minutes after peripheral injection; however, LPS was not found directly in the brain parenchyma (Singh & Jiang, 2004). This indicates that rather than interacting directly with CNS-resident cells, LPS most likely acts indirectly on peripheral $TLR4^+$ cells – including leukocytes as well as BECs – producing cytokines which can readily cross the BBB. Additionally, existing circadian sequencing databases have found that there are no circadian rhythms in *TLR4* expression in BECs – suggesting that rhythmic neuroinflammatory responses to LPS occurs through CNS-resident cells (S. L. Zhang et al., 2021). Further supporting this claim, we found no diurnal variation in peripheral cytokines in our two-hit LPS model and observed that evening peripheral inflammation remains unaltered in PLX treated mice, despite the complete ablation of NaFL leak (Figure 3.4A,E). Additionally, astrocyte activation in the absence of $TLR4^+$ microglia indicates that astrocytes are responding to peripherally derived cytokines rather than parenchymal LPS.

Our data show that glia respond differently to LPS in the evening than in the morning, as both astrocytes and microglia showed increased reactivity 24 hours after evening LPS exposure. While microglia are not physically coupled to the NVU, they are still an intimate component of BBB function and increase perivascular localization during disease (Mastorakos et al., 2021). Using the CSFR1 antagonist PLX3397, we found that microglia are required for evening LPS-induced BBB breakdown – despite persisting astrogliosis. While PLX3397 can exert off-target

effects, including inhibition of Flt and C-kit, our observation that PLX3397 did not change LPS-induced inflammation in peripheral organs, but did impact the brain, strongly implicates microglia (Claeys et al., 2023). It is still possible other CNS-resident $CSFR1^{+}$ cells, such as perivascular macrophages (PVMs), play a role in LPS-induced inflammation. During many inflammatory diseases PVMs increase in number and vessel coverage; however, it is likely they are actually promoting vessel integrity, since their ablation increases leukocyte extravasation (Polfliet et al., 2001; T. Yang et al., 2019).

One way in which microglia impact BBB function is through the secretion of inflammatory mediators (R. Kang et al., 2020). Our data shows that the iNOS inhibitor aminoguanidine, given systemically, abrogated LPS-induced BBB breakdown at ZT13, suggesting that diurnal regulation of iNOS, particularly in microglia, may be a mechanism underlying the diurnal variation in susceptibility to inflammatory BBB breakdown. Our findings have several implications for human health. First, they might prompt investigation into diurnal variation in human BBB integrity in the setting of neuroinflammatory diseases. Second, the pathways that mediate this diurnal variation might be targeted therapeutically to prevent BBB breakdown in the setting of inflammatory diseases, particularly at times of peak vulnerability. Finally, diurnal susceptibility to inflammatory BBB permeability might be leveraged to allow better penetration of certain therapeutics, such as antibodies, into the brain. Chronotherapeutic regimens which incorporate information about diurnal BBB permeability dynamics may improve BBB penetration of anti-amyloid drugs, chemotherapies, and other agents. Our work, while a small first step, might open the door to such technologies.

2.5 Materials and Methods

BBB assays: 100uL of 100mg/ml sodium fluorescein (Sigma-Aldrich: F6377) diluted in sterile PBS was injected subcutaneously, 45 minutes later mice were deeply anesthetized with i.p. pentobarbital (150mg/kg). 100uL of blood was collected by cardiac puncture before they were perfused with ice-cold PBS containing 3g/l heparin. Both hemispheres were dissected into regions and stored in pre-weighed tubes filled with 500uL PBS on ice. A small piece of peripheral and brain tissues were removed, flash frozen, and stored at -80°C for RNA analysis as described below. Tissue was weighed then homogenized for 3 minutes in a bullet blender and serum was added to a serum separator tube (BD Microtainer: 365967) before being spun down and diluted 1:200, tissue supernatant and serum were incubated 1:1 in 2% Trichloroacetic acid (Millipore Sigma: T9159) overnight (4°C). The samples were spun down again and diluted 1:1 in Borate Buffer (Honeywell: 33650) before being read on a plate reader along with a standard curve. Fluorescence per gram of CNS tissue was compared to fluorescence per uL of serum to determine the absolute amount of NaFL that crossed from the periphery to the brain for each mouse.

4uL/g body weight of 2% Evans Blue (Sigma-Aldrich, E2129) was injected retro-orbitally, 15 minutes later the mice were deeply anesthetized and perfused as described above. Whole brains were dissected out and imaged.

Drug administration: LPS from *escherichia coli* O55:B5 (Sigma-Aldrich, L6529) was diluted to 2mg/ml in PBS and stored at -80°C. Immediately before each injection, LPS stock was thawed and diluted to 0.5mg/mL in PBS before being injected (i.p.) at a dose of 2mg/kg. Each LPS stock was not thawed more than twice before being discarded. To avoid batch effects, enough LPS was

purchased at each time for an average of 3 experimental cohorts to be treated from the same stock. Mice were weighed each day prior to injection and the weight at the first day was used to determine dosing for the entire experiment. Aminoguanidine hydrochloride (Sigma-Aldrich, 396494) was diluted in 5% DMSO in 0.9% Saline and injected (i.p.) at a dose of 150mg/kg.

Immunohistochemsitry and Imaging: Immunohistochemical antibodies used in this study include: IBA1 (rabbit, Wako, 019-19741, 1:1000), GFAP conjugated to Alexafluor-647 (mouse, Cell Signaling Technologies, 3657S, 1:800), CD31 (rat, BD Pharmingen, 5500274, 1:250), and CLDN5 (mouse, Invitrogen, 35-2500, 1:100).

Mice were anesthetized and perfused as described above. For immunohistochemistry experiments, one hemisphere was dissected into regions, flash frozen, and stored at -80°C for RNA analysis as described below. The other hemisphere was post-fixed in 4% paraformaldehyde for 12 hours (4°C), then cryoprotected with 30% sucrose in PBS (4°C) for 24 hours. Brains were then sectioned on a freezing sliding microtome in 50-micron serial coronal sections and stored in cryoprotectant solution (30% ethylene glycol, 15% sucrose, 15% phosphate buffer in ddH20). Sections were washed in TBS x 3, blocked for 60 minutes in TBSX (TBS+ 0.4% Triton X-100) containing 3% donkey serum, and incubated overnight at 4°C in primary antibodies diluted in TBSX containing 1% donkey serum. Sections were then incubated for 1 hour at room temperature in TBSX with 1:1000 donkey fluorescent secondary antibody and mounted on slides using Fluoromount-G (Southern Biotech 0100-01) before coverslipping. For all analyses of tight junction and endothelial markers, mice were perfused with 4% PFA for 3 minutes, the whole brain was collected, and post-fixed in 4% paraformaldehyde for 4 hours (4°C) before moving to 30% sucrose for 24 hours (4°C). Brains were sectioned and stored as described above. Sections were blocked overnight in 1% Bovine Serum Albumin, 0.75% Triton x100, 5% donkey serum in

PBS (4°C) before incubating in primary antibody diluted in PS/2 (0.5% BSA, 0.25% Triton x-100 in PBS) for 2 days (4°C). Sections were washed 3x in PS/2 then incubated for 2 hours at room temperature in PS/2 with 1:1000 donkey fluorescent secondary antibody, washed 2x in PS/2 and mounted as described above.

All fluorescent imaging was done on a Keyence BZ-X810 microscope. In general, laser intensity and exposure times were selected for each cohort of samples after a survey of the tissue, in order to select appropriate parameters that could then be held constant for all slides in that imaging session. These values varied by antibody, but all sections in a given cohort were imaged under identical conditions at the same magnification. For standard image analysis of epifluorescent images (such as determination of % area for antibodies such as anti-GFAP), TIFF image files were opened using ImageJ and converted to 8-bit greyscale files. Images with the dimmest and brightest intensity of staining, as well as some mid-range examples, were used to determine an appropriate threshold value that could optimally capture the intended staining across all conditions in that cohort, based on the judgment of the investigator. That threshold was then held constant across all images in the cohort, and black and white images of selected regions of interest were generated and quantified as % area stained using the Analyze Particles function. At least 2 adjacent sections per mouse per region were analyzed and averaged.

Perivascular gliosis analysis was done by taking 60x confocal images on a Zeiss LSM700 of blood vessels, the images were then exported and further analyzed using Imaris 10.0. In short, treatment groups were blinded to the investigator and 3D volumes for each channel were determined per image to account for LPS-effects on glial cell morphology, then an extended surface a distance of 8um away from blood vessels was applied. The volume of the channel colocalized to the extended surface compared to total channel volume as well as the volume of

the 8um extended surface were measured. 40x images were taken with confocal resolution imaging and 2D maximum intensity projects were used for representative Images.

Plexidartinib: Plexidartinib 3397 (PLX) was purchased from MedChemExpress (Hy-16749) and shipped to Research Diets, Inc (New Brunswick, NJ). PLX was formulated in AIN-76 diet at 400ppm and irradiated. PLX or control (AIN-76) chow were fed to mice ad libitum for 2 weeks prior to all PLX experiments.

RNA quantification: Tissue was homogenized in 500ul of Trizol with beads added before running in a bullet blender for 3 minutes. TRIzol samples were then subjected to chloroform extraction (1:6 chloroform:TRIzol, followed by thorough mixing, and centrifugation at (12500 x g for 15 minutes). RNA was then extracted from the aqueous layer using the PureLink RNA Mini Kit according to manufacturer's instructions. RNA concentration was measured on a Nanodrop spectrophotometer, then cDNA was made using a high-capacity RNA-cDNA reverse transcription kit (Applied Biosystems/Life Technologies) with 250ng-1 mg RNA per 20mL reaction. Real-time quantitative PCR was performed with ABI TaqMan primers and ABI PCR Master Mix buffer on ABI StepOnePLus or QuantStudio 12k thermocyclers. Taqman primers (Life Technologies) were used, and mRNA measurements were normalized to b-actin (Actb) mRNA for analysis. For larger experiments, microfluidic qPCR array measurements were performed by the Washington University Genome Technology Access Center using a Fluidigm Biomark HD system, again using Taqman primers. RNA sequencing was performed and values normalized as previously described (McKee et al., 2022). Volcano plots were made using Enhanced Volcano R package, heatmaps were made using the Pretty heatmap package, and X-Y

plots were made using ggplot. Over-representation analysis dot plots of KEGG pathways were generated using the ClusterProfiler and enrichplot R packages.

Viral vectors: Jak2 constitutively active viral vector was made at the Hope Center Viral Vector core using Mammalian Gene Collection cDNA for mouse Jak2 (Entrez ID 16452) generously gifted by Carole Escartin. Jak2ca cDNA was then packaged into an AAV9 envelope under expression of the truncated gfaABC1D promoter. A GFP tag was also included as a marker of Jak2ca expression. All viruses were administered via bilateral intracerebroventricular injection in newborn P0 pups as described previously (J.-Y. Kim et al., 2014). Two microliters of virus were injected at a concentration of $1.3x10^{13}$ gc/mL.

Statistics: In all figures, graphs depict the mean + SEM, and N generally indicates the number of animals, unless otherwise noted in the figure legend. For confocal images, each datapoint depicts the mean of two sections with 6 technical replicates taken per section, each mouse is considered an N of 1. For TEM experiment, each datapoint depicts the mean for 28-32 technical replicates from one mouse, and each of these mean values is considered an N of 1. An F test was first performed for datasets with a single dependent variable and 2 groups, to determine if variances were significantly different. If not, 2-tailed unpaired T-test was performed. For datasets with 2 dependent variables, 2-way ANOVA was performed, and if main effect was significant, Tukey multiple comparisons test was then added for appropriate sets of variables. Outliers were identified using Grubbs test and were excluded. Statistical tests were performed with GraphPad Prism software, version 10.0.2. P values greater than 0.1 were noted as not significant (NS). $P<0.05$ was considered significant and was note with asterisks indicating the p-value: *$P<0.05$, **<0.01, ***<0.005, ****<0.00

Study approval: All animal experiments were approved by the Washington University IACUC and were conducted in accordance with AALAC guidelines and under the supervision of the Washington University Department of Comparative Medicine. 7-week-old male C57/bl6J littermate mice were all obtained from Jackson Labs (Bar Harbor, ME) and allowed to acclimate for one week in our facilities before all experiments. For viral injection experiments embryonic day 18 timed-pregnant CD1 mice were ordered from Charles River (Wilmington, MA). Mice were housed in a 12-hour light/dark cycle (lights on at 6am and off at 6pm) and allowed ad libitum access to food and water unless otherwise stated.

Chapter 4: Astrocytic CXCL5 exacerbates plaque formation in a mouse mode of Alzheimer's Disease

4.1 Abstract

Alzheimer's disease (AD) is a devastating form of dementia and is the sixth-leading cause of death in the United States. AD is characterized by the accumulation of toxic protein aggregates – including extracellular amyloid-beta plaques and intracellular tau fibrils – as well as glial activation and neuronal cell death. Severe stages of AD are coupled with BBB disruption and peripheral immune cell infiltration. Sleep and circadian rhythms disruption, such as shift work, is associated with an increased risk of developing AD; however, AD patients also show altered circadian rhythms, suggesting there is a bidirectional relationship between circadian rhythms and AD. Previous studies from our lab have found that ablating the molecular clock protein *Bmal1* in astrocytes in a mouse model of AD protects against tau spread but does not alter amyloid plaque deposition. Since BMAL1 is a ubiquitous transcription factor, we considered that these discrepancies may be due to conflicting, non-circadian effects. To address this concern, we directly modulated one of the top dysregulated genes in an astrocyte *Bmal1* deficient mouse – the pro-inflammatory cytokine CXCL5. We found that overexpressing CXCL5 specifically in astrocytes significantly increased amyloid-beta (Aβ) percent area as well as Aβ plaque count, with an increase in the number of small plaques. This increase in amyloid-beta occurred independently of glial activation, with a trending decrease in markers of astro- and microgliosis when controlling for Aβ volume. Altogether, this data suggests *Cxcl5* overexpression alters microglial and astrocytic sensitivity to Aβ, rendering them unable to

perform protective functions, such as decreased clearance, uptake, or degradation – leading to increased plaque seeding.

4.2 Introduction

Alzheimer's disease (AD) is a progressive neurodegenerative disease, and it is currently the most common form of dementia as well as the sixth-leading cause of death in the United States ("2023 Alzheimer's Disease Facts and Figures," 2023). As the disease worsens, patients experience severe cognitive decline, including changes in behavior and mood and progressive memory loss (Long & Holtzman, 2019). The main pathology of AD includes the accumulation of extracellular misfolded amyloid-beta protein plaques and intracellular tau tangles, which ultimately result in neuronal death. However, neuroinflammation and amyloid-beta plaque deposition may long precede significant neuronal loss, tau pathology, and the onset of cognitive decline – leading to debate about the underlying mechanisms behind disease progression (Long & Holtzman, 2019; Majerova et al., 2019; Sofroniew & Vinters, 2010).

The central nervous system (CNS) is distinct from the periphery in that it lacks typical adaptive and innate immune cells at baseline. Instead, CNS homeostasis is maintained by glial cells, namely microglia, astrocytes, and oligodendrocytes. Microglia quickly respond to pathogens and injury in the CNS. For example, in response to neuronal death or injury, such as alpha-synuclein in Parkinson's Disease or amyloid-beta in Alzheimer's Disease, microglia adapt an activated, reactive state – termed microgliosis. Activated microglia release proinflammatory markers including TNF-alpha and interleukins (IL-6, IL-1, and IL-8) which in turn promote astrogliosis (J.-S. Park et al., 2021). When activated, astrocytes release additional

proinflammatory cytokines and may modulate extracellular tau spread through increased uptake or degradation – making them important players for mitigating or exacerbating AD pathology and neuronal damage (Sheehan et al., 2023). This increase in neuroinflammation may be the underlying trigger for cognitive decline in AD and can create a positive feedback loop through which neuronal death and plaque load are worsened (J.-S. Park et al., 2021; Sofroniew & Vinters, 2010). Astrocytes have a unique morphology, with a multitude of processes which both integrate into the synaptic cleft - potentially allowing them to modulate tau spread - as well as wrap around blood vessels (Allen et al., 2012; Blanco-Suarez et al., 2018; Christopherson et al., 2005; Ezan et al., 2012). These perivascular astroglial endfeet provide trophic support to the underlying endothelial and mural cells, together forming the blood-brain-barrier (BBB). The BBB serves as a selectively permeable barrier, preventing certain neurotoxic molecules and peripheral immune cells from entering the CNS (Mastorakos et al., 2021; Pulido et al., 2020). In cases of neural injury and neuroinflammation, the BBB can break down, disrupting CNS homeostasis (Erickson et al., 2023; Jana et al., 2022). It is hypothesized that BBB breakdown during these heightened states of neuroinflammation can contribute to increased infiltration of peripheral T cells, which may serve to further exacerbate AD pathology (X. Chen et al., 2023). Our lab focuses broadly on answering questions related to the role of circadian dysfunction, glia, and neuroinflammation in the development of neurodegenerative diseases. More specifically, we are interested in determining mechanisms by which circadian clock disruption in glia, including astrocytes, can mediate the breakdown of the blood-brain barrier, influence neuroinflammation, and affect plaque accumulation in mouse models of Alzheimer's disease.

Alzheimer's disease pathology is influenced by sleep and the body's natural circadian rhythms. Poor sleep and fragmentation of circadian rhythms have been shown to be associated

with amyloid-beta plaque deposition and tau accumulation (Ju et al., 2013; Musiek et al., 2018; Musiek & Ju, 2022). While the exact mechanism in unknown, this correlation could be due to disruption of circadian rhythms. Internal circadian rhythms are maintained by peripheral cellular clocks, which are regulated and tuned to daily light cycles by the pacemaker clock - the suprachiasmatic nucleus (SCN) within the brain. Molecularly, each circadian clock consists of a transcription-translation feedback loop (TTFL) with a positive arm and a negative arm. BMAL1 (ARNTL) is the core protein involved in the positive loop of the TTFL, which heterodimerizes to other transcription factors, CLOCK or NPAS2 to induce transcription of the Per and Cry genes. The PER, CRY, and REV-ERB proteins comprise the negative arm of the TTFL and inhibit activity of BMAL1 (for further discussion see 1.1.2 Circadian Rhythms – Entrainment and the Molecular Clock) (Kanan et al., 2024; McKee et al., 2022). These peripheral clocks regulate a variety of cellular functions and homeostasis including metabolism, inflammation, and oxidation (Bass & Takahashi, 2010; Kanan et al., 2024; Musiek et al., 2018). Notable, deletion of BMAL1 completely abrogates core clock function, and can be used as a genetic model of circadian rhythm disruption, though BMAL1 does have some non-circadian function (Lananna et al., 2018; Musiek et al., 2013). Currently, conflicting data exists about the specific role of BMAL1 in neurodegenerative diseases such as Alzheimer's disease. Previous literature has shown that global BMAL1 knockout increases amyloid-beta plaque burden (Kress et al., 2018). However, studies investigating astrocyte-specific BMAL1 knockout (BmKO) have found that while astrocytes appear more reactive, actual amyloid plaque burden does not change (McKee et al., 2022). Furthermore, astrocyte specific BmKO appears to be protective against tau accumulation by inducing protective astrocyte activation with increased autophagic function (Sheehan et al., 2023).

Although there was no change in plaque load in an astrocyte specific BmKO, it is possible that non-clock, transcription factor functions of BMAL1 may be causing conflicting results, or that BMAL1 might regulate some pro- and some anti-plaque pathways which counteract one another. To address this concern, we examined differentially expressed genes in an RNAseq dataset derived from bulk cortex tissue from astrocyte specific BmKO (Aldh1l1-CreERT2;Bmal1f/f) mice and Cre- control littermates (Fig. 4.1 A,B). We observed that *Cxcl5* is the fifth most upregulated gene in Cre+ mice, increasing by more than 10-fold, as compared to Cre- controls (Figure 4.1A, B). CXCL5 is chemokine and potent neutrophil chemoattractant that is necessary for neutrophil extravasation in peripheral lung tissue (Li et al., n.d.). Interestingly, neutrophils in an AD mouse model have also been shown to worsen plaque load and cognition (Zenaro et al., 2015). Furthermore, unpublished in vivo translating ribosome affinity purification-RNAseq (TRAP-seq) data from our lab reveals that the *Cxcl5* transcript shows circadian rhythms in astrocytes, and the amplitude of this rhythmicity increases in the presence of amyloid plaque pathology, as well as colocalization of CXCL5 and GFAP at the protein level using immunohistochemistry (Figure 4.1C). Because Cxcl5 was massively upregulated in astrocytes in response to *Bmal1* deletion, shows circadian rhythms in astrocytes in vivo, and has been implicated in neuroinflammation and BBB function, we hypothesized that Cxcl5 may mediate effects of astrocyte Bmal1 deletion on AD pathology. Thus, we examined the impact of astrocytic *Cxcl5* overexpression of AD pathology in a mouse amyloid plaque model.

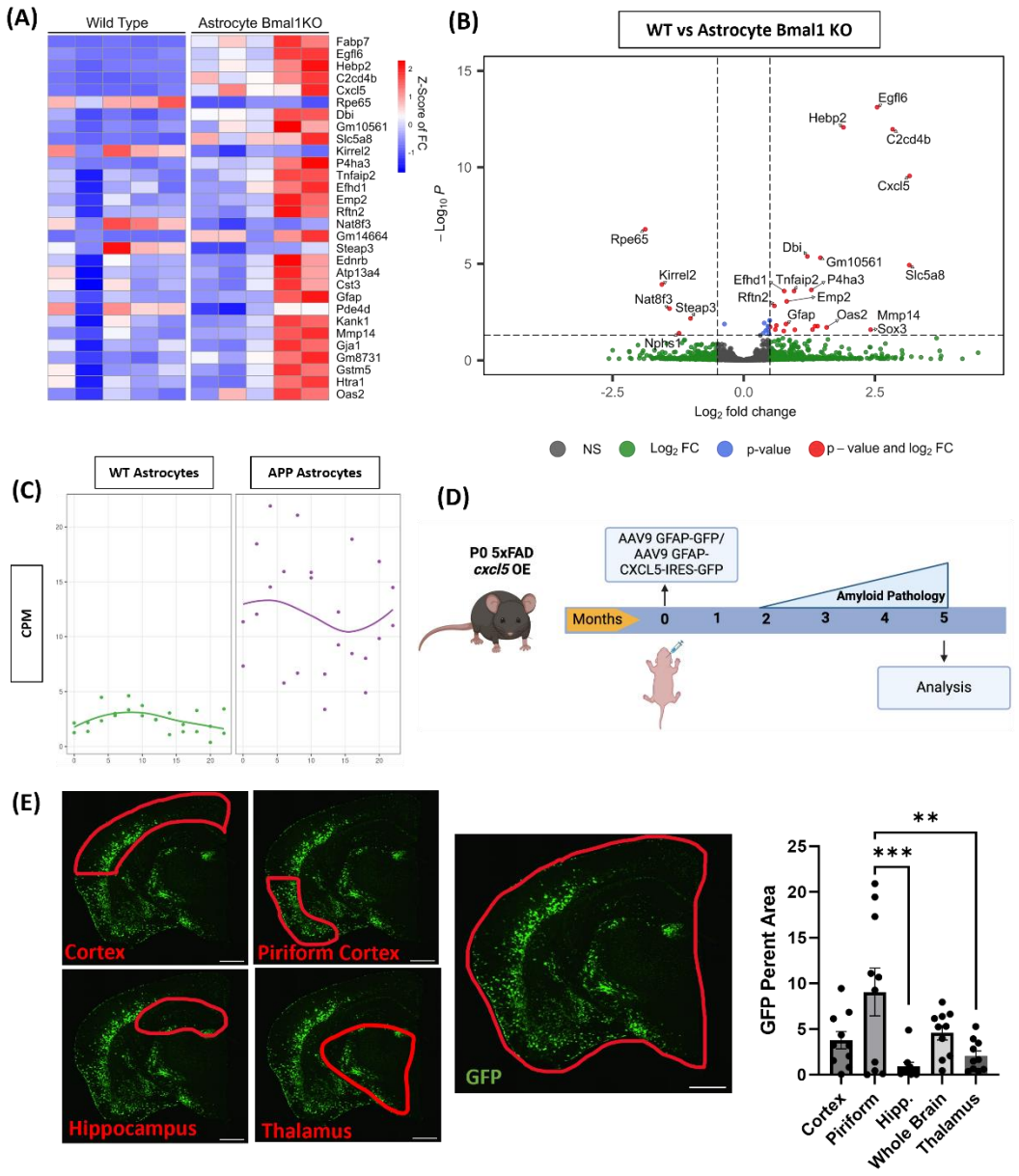

Figure 4.1: Astrocytic *Cxcl5* is rhythmic and under control of Bmal1. (A, B) Heatmap and volcano plots of differentially expressed genes under astrocyte-specific *Bmal1* deletion show that *cxcl5* is the fifth most upregulated gene. Figure from (McKee et al., 2022). (C) *Cxcl5* is rhythmically expressed in astrocytes and gains amplitude in the presence of Aβ. Figure from unpublished work by P. Sheehan. (D) 5xFAD mice were injected with *cxcl5*-overexpression virus at P0 and allowed to age to 5 months. (E) Representative images show the GFP viral tag within the whole brain, the piriform cortex, hippocampus, and cortex which were analyzed for changes in plaque deposition. n = 10 mice per group. Scale bar = 1000 µm.

4.3 Results

4.3.1 *Cxcl5* overexpression causes an increase in plaque deposition within the piriform cortex

To analyze how overexpression of astrocytic *Cxcl5* affects amyloid-beta (Aβ) plaque deposition and characterization in an AD model, we used 5xFAD mice, which express human amyloid precursor protein (APP) and presenilin 1 (PS1) genes bearing five mutations which cause familial Alzheimer's disease. These mice develop progressive amyloid plaque pathology and associated neuroinflammation starting around 3 months of age (Oakley et al., 2006). We performed intracerebroventricular injections of adeno-associated type 8 viral vector (AAV8) at postnatal day 0 (P0) in 5xFAD pups, ensuring global spread throughout the cortex (Figure 4.1D, E). Control mice were injected with an AAV8-GFAP-GFP virus, while experimental mice were injected with an AAV8-GFAP-CXCL5-IRES-GFP virus – the GFAP promoter allowed us to target specifically astrocytes. We sacrificed mice at 5 months and validated viral spread by quantifying the spread of GFP across brain regions (Figure 4.1D). We observed increased GFP fluorescence in cells that were morphologically consistent with astrocytes in the cortex, piriform cortex, thalamus, but not in the hippocampus (Figure 4.1E).

To determine the effect of *Cxcl5* overexpression (Cxcl5-OE) on plaque load, we aged male and female mice (13m/10f) to 5 months old, then stained sections for X34, a marker for fibrillar amyloid plaques. Using the regions of interest defined in Figure 4.1E, we quantified both percent area as well as individual plaque count and found that Cxcl5-OE mice had significantly greater X34 percent area across the whole brain – and that this difference was primarily driven by the piriform cortex (Figure 4.2A, B). We next sought to determine if Cxcl5-OE altered APP processing, which would suggest altered Aβ production, by examining a subset of transcripts by

qPCR. We saw no difference in APP processing genes or in transcripts related to inflammation (*Il6, Tnfa*) between the GFP and Cxcl5-OE groups (Figure 4.2C-E), despite the increase in Aβ plaque load. Cxcl5-OE mice did have a significant increase in *Cxcl5*, confirming the efficacy of the model described in Figure 4.1D.

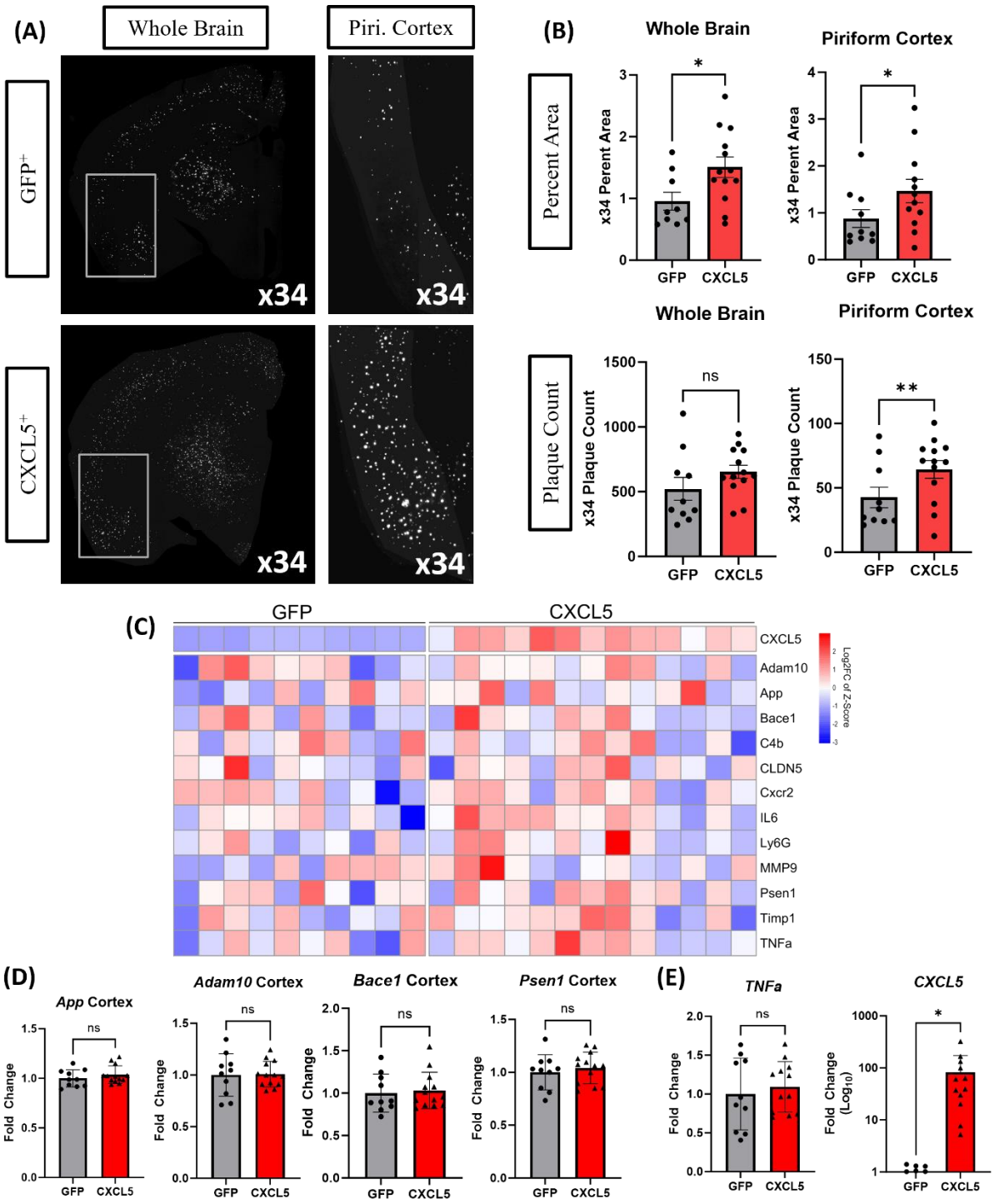

Figure 4.2: *Cxl5* overexpression causes an increase in plaque deposition. (A) Representative images of x34 in the whole brain, inset images are of the piriform cortex. (B) Quantification of x34 percent area and plaque count in the whole brain and piriform cortex. (C) Heatmap of inflammatory and APP processing genes from cortical tissue, scale is Z-Score of Log_2FC. (D) Two-tailed t-test of *APP*, *Adam10*, *Bace1*, and *Psen1* from GFP or CXCL5 injected mice. (E) Two-tailed t-test of *TNFa* and *Cxcl5* from GFP or CXCL5 injected mice *n* = 10-13 mice per group. Scale bars = 5 µm

4.3.2 Plaque deposition occurs independently of glial activation

To understand if the increase in plaque load is driven through decreased glial Aβ clearance or uptake in Cxcl5-OE mice, we next examined the response of glial cells. Similarly, to the chosen markers of APP processing and inflammation, we found that there was no significant effect of astrocytic *Cxcl5* overexpression on expression of transcripts related to gliosis (Figure 4.3A). However, there could be physiological effects of CXCL5 on astrocyte and microglial morphology and function that are not determined by gene expression alone. We quantified astro- and microgliosis through GFAP and IBA1 staining, respectively, in the piriform cortex. We saw that there were no differences in overall GFAP or IBA1 immunoreactivity, despite the significant increase in $X34^+$ plaque load in this region – suggesting that there may be a "glial fatigue" phenotype where glial cells interact less with their surrounding Aβ plaques (Figure 4.3B and C). To determine if there is an effect of Cxcl5-OE on astrocyte clustering, we measured the volume of total GFAP compared to peri-plaque GFAP (within a 20μm diameter of each plaque, quantifying 6 plaques per mouse. We found that there was no significant difference in astrocytic clustering around plaques (Figure 4.3.2D). Interestingly, we found that Cxcl5-OE mice have a significant positive correlation ($p = 0.0018$) of GFAP percent area and X34 plaque count, whereas the GFP group has a significant negative correlation ($p = 0.0588$) (Figure 4.3E). There was no effect of Cxcl5-OE on periplaque IBA1 clustering or correlation with $x34^+$ plaque count (data not shown).

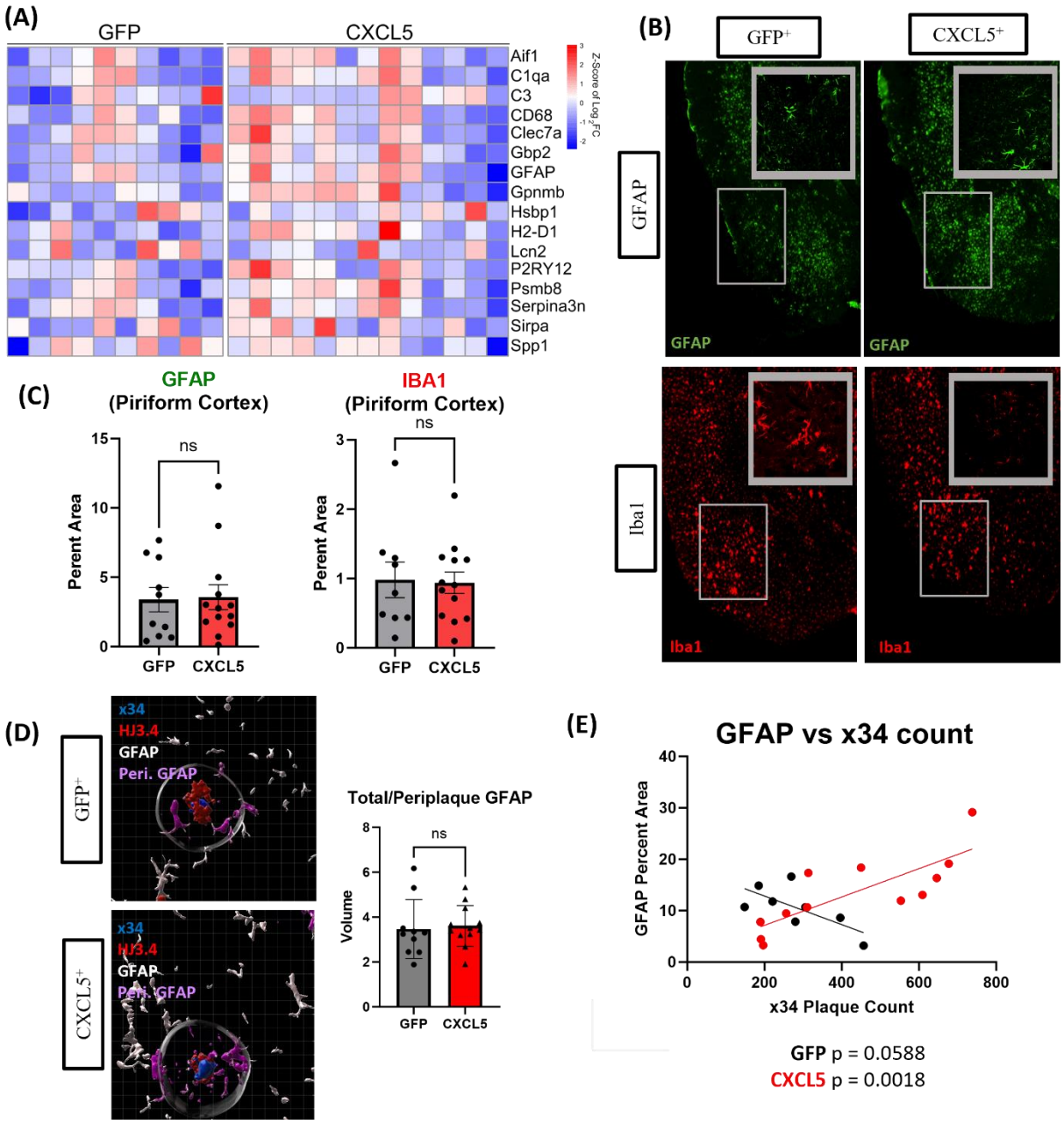

Figure 4.3: Increased plaque deposition in the piriform cortex occurs independently of glial activation. (A) Cortical GFP vs Cxcl5-OE gene expression data from select markers of astro- and micro-gliosis, scale is Z-Score of Log_2FC. (B) GFAP and IBA1 representative images and quantification in the piriform cortex. (C) Representative images of periplaque GFAP. (D) GFAP and IBA1 area correlated to x34 plaque count in the piriform cortex for both GFP and Cxcl5-OE mice. (E) Correlation between GFAP percent area and x34 plaque count in the piriform cortex per each mouse. *n* = 10-13 mice per group. Scale bars in (B) are 1000 µm, (D) are 50 µm

4.3.2 Astrocytic *Cxcl5* increases Aβ deposition without altering plaque morphology

We next characterized plaque morphology through co-staining with X34 and the anti-Aβ antibody HJ3.4 antibodies and conducting volumetric analysis on a per plaque basis. While X34 only labels the fibrillar compact core of the plaque, HJ3.4b labels the non-fibrillar amyloid as well, often labeling less compacted plaques material around the edges of the plaque (Mahan et al., 2022). We quantified the volume of both Aβ stains within the piriform cortex and found no significant difference between the control or Cxcl5-OE groups for either x34 or HJ3.4 volume on a per-plaque basis (Figure 4.4A). Upon further inspection of the z-stack confocal microscopy images, we noticed that the HJ3.4 antibody had not fully penetrated the entire amyloid-beta protein in each plaque and created a "halo" around the $x34^+$ portion of the plaque (Figure 4.4A). These "halos" were present using both Imaris and FIJI quantification software and persisted across multiple rounds of x34 and HJ3.4 co-stains, thus we determined these to be an artificial effect of poor penetration of the HJ3.4 antibody. To ensure there was no effect of Cxcl5-OE on HJ3.4 plaque penetration, we measured the colocalization of X34 and HJ3.4 found no significant difference (Figure 4.4A). To address this issue in our analysis, we compared x34 volume to the "Total Aβ" volume (the combined X34 and HJ3.4 volumes subtracted by the colocalization of the two). While we observed a slight trending increase in the X34:Total Aβ volume in the Cxcl5-OE mice, there was no overall statistically significant difference between the treatment groups (Figure 4.4B).

Since we found an increase in Aβ plaque count without a change in plaque composition, we next asked if there was an increase in the number of small Aβ plaques. We counted the number of individual plaques in both the whole brain and piriform cortex and binned the number of plaques based on size. When looking at the number of plaques in the smallest two bins

(approximately the lower 10% of all plaques) Cxcl5-OE mice had a significant increase in plaque count in both the piriform cortex and whole brain (Figure 4.4C and D).

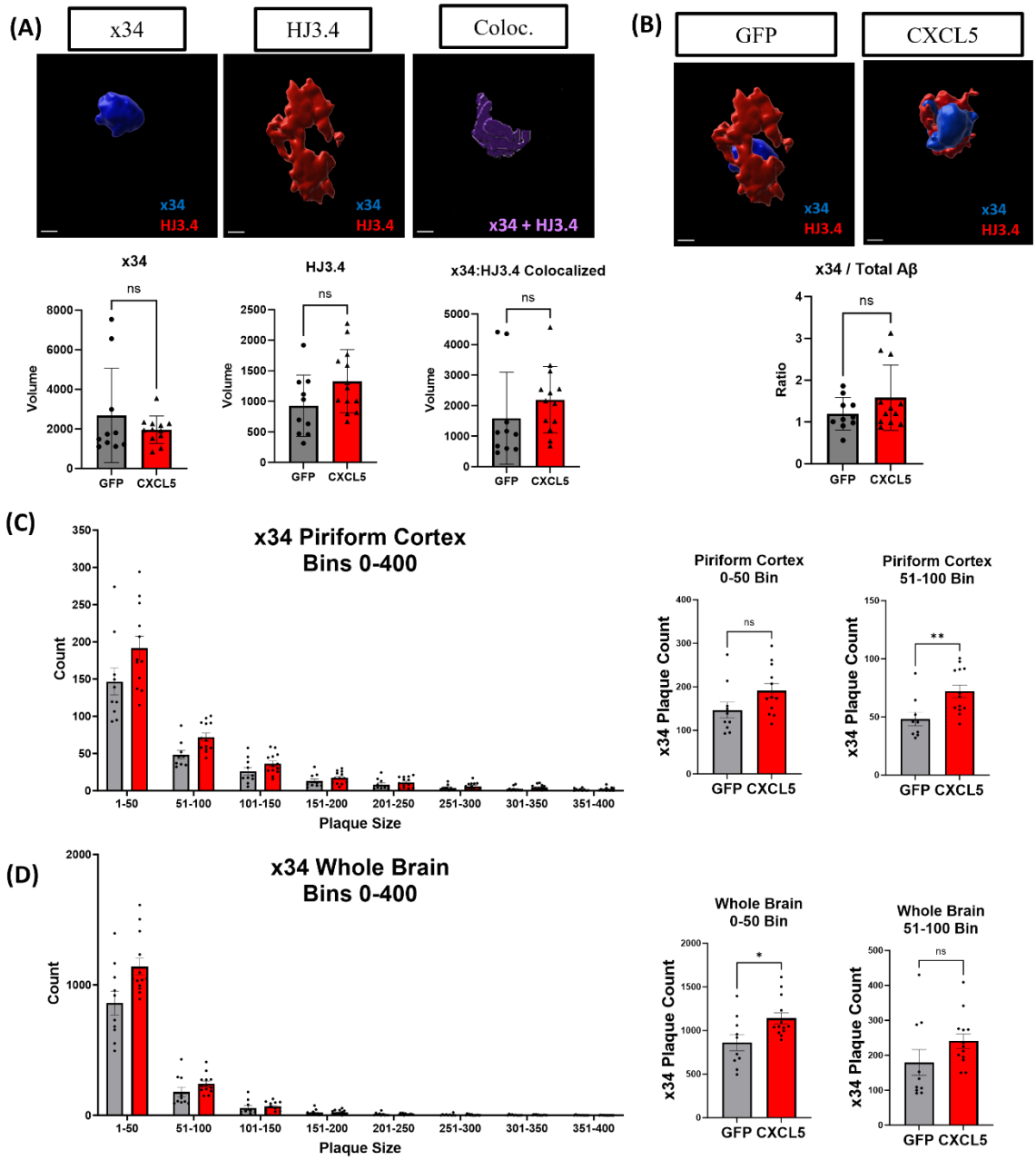

Figure 4.4: Astrocyte CXCL5 increases Aβ deposition without altering plaque morphology. (A) x34 and HJ3.4 co-staining and quantification. (B) Representative images and quantification of x34 and total Aβ ratio. (C) Histogram of x34 plaque counts of 8 out of 23 of the smallest sized plaques in the piriform cortex. Two-tailed t-test of the smallest two bins. (D) Histogram of x34 plaque counts of 8 out of 17 of the smallest sized plaques in the whole brain. Two-tailed t-test of the two smallest bins. *n* = 10-13 mice per group. Scale bars = 50 µm

4.4 Discussion

While previous studies from our lab have found that *Cxcl5* is rhythmically expressed in astrocytes and under BMAL1 control (McKee et al., 2022), it is still unknown what function CXCL5 serves during Alzheimer's disease (AD). Our current findings suggest that CXCL5 alters glial responsiveness to Aβ, causing an increase in plaque load. We found that there was the greatest viral expression in the piriform cortex and that this tracked as the region with the greatest Cxcl5-OE effect on X34 – both for percent area as well as number of individual plaques. This increase in Aβ in the piriform cortex occurred without an increase in APP processing genes or general markers of inflammation and gliosis. We also found that Cxcl5-OE did not increase glial clustering around plaques or change plaque morphology, although there was an astrocyte specific increase in positive correlation between GFAP and x34. This increase in astrocyte association with X34 plaque count was coupled with an increase in the number of small plaques – indicating either an increase in plaque condensation or deposition of nascent plaques.

The lack of increased gliosis or inflammation despite the increase in Aβ opposes the expected trend. Canonically, the greater the amount of AD pathology, the more inflammation and glial activation occurs. We propose that there may be an increase in glial "tolerance" for Aβ, where the increase in plaque pathology no longer induces the same increase in glial activation and release of pro-inflammatory cytokines. Additionally, Cxcl5-OE may be altering glial migration, leading to an absence of change in our periplaque clustering data. Mass production of the chemokine CXCL5 could induce widespread cell migration, causing there to be less focused glial clustering around plaques. However, the increase in positive correlation between GFAP and x34 suggests that Cxcl5-OE mice may have increased astrocyte sensitivity, since there was a stronger correlation between greater plaque burden and astrogliosis in these mice. Interestingly,

this correlation does not hold for IBA1, suggesting perhaps there is a cell-type specific effect of GFAP-specific *Cxcl5*-OE with increased astrocyte sensitivity to Aβ leading to disrupted cell migration and ultimately less microgliosis and pro-inflammatory cytokine release.

4.5 Materials and Methods

Mice: All mouse experiments were conducted in accordance with protocols approved by the Washington University in St. Louis Institutional Animal Care and Use Committee (IACUC). 5xFAD mice were obtained from The Jackson Laboratory (stock number: 034848-JAX) and were bred at Washington University in St. Louis. All cohorts of mice were mixed sex and consisted of only $5xFAD^+$ littermates from several breeding cages. All mice were housed under 12-h light/12-h dark conditions with food and water available ad libitum. 5xFAD mice were harvested at 5 months of age.

Viral vectors and administration: *Cxcl5* overexpression viral vector was made at the Hope Center Viral Vector core using Mammalian Gene Collection cDNA for mouse *Cxcl5* (Entrez ID 20311). *Cxcl5* cDNA was then packaged into an AAV8 envelope under expression of the full GFAP promoter. An eGFP tag was also included as a marker of *Cxcl5* expression. All viruses were administered via bilateral intracerebroventricular injection in newborn (P0) 5xFAD pups as described previously. Two microliters of virus were injected at a concentration of $1x10^{13}$gc/mL.

Immunohistochemistry and imaging: The following immunohistochemical antibodies used in this study include: x34 (in DMSO, Sigma-Aldrich, 1954-5MG, 1:2000), HJ3.4 (biotinylated, obtained from D. Holtzman, 1:2000), GFAP conjugated to Alexafluor-647 (mouse, Cell

Signaling Technologies, 3657S, 1:800), Iba1 (rabbit, Wako, 019-19741, 1:1000), DAPI (Thermo Fisher Scientific D1306).

Mice were anesthetized via intraperitoneal injection of pentobarbital (150 mg/kg) before they were perfused with ice-cold Phosphate Buffered Saline (PBS) containing 3 g/L heparin. One hemisphere was post-fixed in 4% paraformaldehyde (PFA) for 24 hours at 4ºC. The tissue was then cryoprotected with 30% sucrose in PBS at 4ºC for 48 hours. Brains were sectioned on a freezing sliding microtome in 50-micron serial coronal sections. Tissue sections were stored at 4ºC in a cryoprotectant solution containing 30% ethylene glycol, 15% sucrose, and 15% phosphate buffer in ddH_2O. For staining, tissues were washed 3x 15 minutes in TBS, then incubated at room temperature for 1 hour in 0.25% TBSX (TBS and Triton X) containing 3% donkey or goat serum. Tissues were incubated at 4ºC overnight in 0.25% TBSX containing 1% donkey or goat serum and diluted primary antibodies. The next day, sections were washed 3x 15 minutes in TBS, then incubated at room temperature in 0.25% TBSX containing diluted fluorescent secondary antibodies (1:1000). Sections were mounted on slides using Fluoromount-G (Southern Biotech 0100-01) before coverslipping. For x34 staining, sections were incubated at room temperature for 20 minutes in x34-containing staining buffer (1:500 10N NaOH added to an aliquot of x34 Wash Buffer). Sections were then washed 3x 2 minutes at room temperature in x34 Wash Buffer (60% PBS, 40% EtOH) followed by 2x 5 minutes in PBS.

All fluorescent imaging was done using a Keyence BZ-X810 microscope. Values for laser intensity and exposure time varied by antibody, but all sections in a given IHC cohort were imaged under identical conditions at the same magnification. To choose laser intensity and exposure time, the tissue was widely surveyed to pick parameters that would result in the clearest images for each antibody in the cohort. For image analysis of plaque and glial cell count and

percent area, TIFF images were opened in FIJI and converted to grey-scale 8-bit files. Appropriate threshold levels were utilized to capture the intended staining across all files, as determined by the investigator. The selected threshold remained constant for all images in the cohort, and regions of interest (ROIs) were created for brain regions including the whole brain, the cortex, the hippocampus, the thalamus, and the piriform cortex. ROIs were quantified as percent area using the Analyze Particles function on FIJI.

40x confocal images were taken using the ZENS Software on a ZEISS Zens confocal laser scanning microscope. Confocal images were saves as .lsm files and analyzed using the IMARIS visualization and analysis software at the Washington University Center for Cellular Imaging (Version 10.0, Bitplane, South Windsor, CT, USA). To quantify volumes of each antibody (GFAP x34 and HJ3.4), 3D surfaces with detail ranging from 0.4 to 0.8 microns were made for each marker. The Batch Process Colocalization function was used to colocalize volumes of x34, HJ3.4, and GFAP. The Intensity Mean function was used for GFAP periplaque analysis. For each mouse, the volume for each antibody marker was averaged over three plaques across two independent tissue sections for a technical replicate of 6.

Rna quantification and fluidigm analysis: 500 μL of TRIzol was added to Eppendorf SafeLock tubes containing beads and tissue samples. Tissue was homogenized in a bullet blender at speed level 8 for 3 minutes. The TRIzol tissue samples were then subjected to chloroform extraction (1:6 chloroform:TRIzol), followed by mixing and centrifugation at 12500g for 15 minutes. RNA was extracted from the aqueous layer using the manufacturer's instructions included in the PureLink RNA Mini Kit. RNA concentration was measured on a Nanodrop spectrophotometer. From the RNA, cDNA was made using an RNA-cDNA reverse transcription kit (Applied

Biosystems/Life Technologies) with 0.5-2.2 μL of RNA per 20 μL reaction. Quantitative PCR (qPCR) was performed with ABI Taqman primers and ABI PCR Master Mix Buffer on ABI StepOnePlus or QuantStudio 12k thermocyclers. Taqman primers (Life Technologies) were used and mRNA measurements were normalized to b-Actin (Actb) for analysis. The microfluidic qPCR array measurements were performed by the Washington University Genome Technology Access Center using a Fluidigm Biomark HD program and Taqman primers. Heatmaps were created using the Pretty heatmap package on R, and the volcano plot was created with the Enhanced Volcano R package.

Statistics: For all figures, statistical 2-tailed T tests were performed with GraphPad Prism software version 10.1.2. Outliers were determined using the Grubb's test with a significance level of Alpha = 0.05 and were excluded. Graphs depict the mean + SEM, and significance level is depicted with asterisks. P-values greater than 0.1 were denoted as not-significant (ns), while P-values less than 0.05 were denoted as significant (*P < 0.05; **P<0.01).

Chapter 5: Future Directions

Light, sleep, and internal circadian rhythms all play critical roles in basic biological function as well as regulating inflammation and disease progression. In this thesis, we addressed how light and circadian rhythms drive neuroinflammation during acute innate immune activation as well as how cell-intrinsic circadian rhythms impact chronic neurodegenerative disease pathology. Here we will describe the main findings from each project and discuss future directions and potential additional experiments that may address unanswered questions.

In the first project, we examined the role of circadian rhythms and light in driving diurnal variations in inflammatory blood-brain barrier (BBB) disruption. Using a two-hit LPS model, we found inflammatory BBB breakdown induced the leak of small, inert tracers and that there was significantly greater leak following LPS exposure in the evening compared to the morning. Interestingly, this diurnal variation in small molecule leak persisted in mice kept in an inverted light cycle for 1 day; however, keeping the mice in constant darkness completely protected against this effect. Together these experiments suggest an interaction between both light and circadian rhythms in driving inflammatory BBB breakdown. While genetic manipulation of clock proteins, such as BMAL1, may have off-target non-circadian effects, using a BMAL1 deficient mouse could further disentangle cellular circadian rhythms from the presence of zeitgebers. We considered using cell-specific BMAL1 knockout models; however, since previous literature suggests that brain-specific BMAL1 deficient mice have BBB dysfunction at baseline (Nakazato et al., 2017) we determined altered light schedules were the optimal method. Beyond understanding the upstream circadian cause for time-of-day differences in BBB dysregulation, additional experiments may also allow us to better understand the mechanism. We

found increased plasma membrane ruffling and vesicle formation in mice treated with LPS in the evening. By doing additional ultrastructural analysis coupled with injecting electron dense tracers, such as horseradish peroxidase, we could confirm that endothelial cells are increasing luminal uptake through transcytosis. Size exclusion or timing assays could also give us insight into the kinetics of the leak. Using various sized fluorescent dextrans would provide spatial resolution, while perfusing mice at various time points after tracer administration would address how quickly tracers are able to leak across the BBB. Finally, while bulk tissue RNA-sequencing was able to identify inflammatory and BBB associated genes as the most dysregulated pathways during evening LPS exposure, cell-specific transcriptomic analysis may provide further insight into the cell type involved in this phenomenon. Single cell RNA-sequencing would allow profiling for microglial subpopulations; however, astrocytic RNA is harder to capture. We would suggest using a cell-specific system such as translating ribosome affinity purification (including peripherally associated processes) or transgenic astrocyte cell labeling prior to cell sorting and sequencing.

The second project was a continuation of the first, where we answered questions around what cell types are involved in inflammatory BBB dysregulation and how peripheral LPS administration triggers widespread neuroinflammation. We found that peripheral and central markers of inflammation peak 6 hours after LPS exposure, and that 18 hours later (24 hours post injection) there is a sharp decline in peripheral and central inflammation – with reduced neuroinflammatory resolution in mice treated with LPS during the evening. This data suggests that, in this two-hit model of LPS, time-of-day differences in inflammatory BBB breakdown occur independently of rhythms in peripheral inflammation. An interesting next step may be to isolate the neuroinflammatory response by using a CNS-specific inflammatory stimuli such as

stereotactic LPS injections or traumatic brain injury. However, it is important to consider the high baseline BBB disruption in these models may create a ceiling effect where it is impossible to distinguish a time-of-day increase. Notably, we found that the diurnal variation in neuroinflammatory resolution did not hold for markers of glial activation which remained similarly upregulated between 6 and 24 hours post-LPS.

In addition to the persisting upregulation of glial activation genes, we also found increased hippocampal astro- and micro- gliosis 24 hours post-LPS. This gliosis was coupled by increased microglial perivascular localization, with microglial ablation completely protecting against evening LPS-induced BBB breakdown. Further characterization of microglia such as branching analysis, ultrastructural characterization of cortical capillaries in PLX-treated mice, or single-cell RNAseq may provide additional mechanistic insights. Additionally, there are possible off-target effects PLX treatment, either due to the high sucrose chow the drug is formulated in or the ablation of other $CSFR1^{+}$ CNS-resident immune cells. To address these concerns, we suggest alternate genetic microglial ablation methods such as using the diphtheria toxin Cx3cr1-DTR model or using the *fms*-intronic regulatory element ($Csf1r^{\Delta FIRE/\Delta FIRE}$) mice. Additionally, while PLX protecting against all LPS-induced BBB leak without altering peripheral immune responses suggests that inflammatory BBB breakdown is due to CNS-specific responses, it is possible that the protective effects of systemic aminoguanidine (AG) administration are due to a dampened peripheral immune response. Since global *Nos2*-deficient mice are LPS-lethal, a strategy for isolating the central and peripheral immune response could be central inhibition of iNOS, either through central administration of AG by microdialysis, or via the generation of a cell-specific *Nos2*-deficient mouse.

The third chapter of this thesis moved away from peripheral models of acute inflammation, and instead focused on chronic neurodegeneration using the 5xFAD mouse model of Alzheimer's disease (AD). Using existing RNA-sequencing databases we selected *Cxcl5* as a candidate gene due to its strong upregulation in a *Bmal1*-deficient animal as well as its rhythmicity in specifically astrocytes. We found that *Cxcl5* overexpression (Cxcl5-OE) in astrocytes increased amyloid-beta (Aβ) plaque pathology in the piriform cortex and that this may be due to increased astrocyte sensitivity to Aβ and decreased uptake or degradation. There are many questions that have yet to be answered regarding the role of CXCL5 in AD pathology. CXCL5 is primarily known as a potent neutrophil chemokine, a cell type which is known to be deleterious for AD pathology (Zenaro et al., 2015). An interesting next step would be developing an *in vitro* migration assay to test if Aβ-induced CXCL5 production from astrocytes attracts neutrophils. One could then repeat the Cxcl5-OE viral injection model in 5xFAD mice to quantify neutrophil infiltration *in vivo*, either through immunohistochemistry or flow cytometry. Another question prompted by our data is the underlying mechanism at play for this increase in plaque load. We propose conducting *in vitro* uptake assays, to determine if knocking down or overexpressing *Cxcl5* alters astrocyte or microglial phagocytosis of Aβ. Additionally, there could be further characterization of this model through quantifying markers of neuronal cell death or looking at a lesser-known function of CXCL5 – BBB breakdown (Haarmann et al., 2019).

Altogether, I hope that this thesis has substantially contributed to the field of circadian and neuroinflammatory research. Our data highlights the importance of considering time-of-day when conducting neuroimmunology experiments and provides evidence to suggest that both light and circadian rhythms control glial cell function and cerebrovascular structure. We hope that this body of work can help provide translational insights, such as what is the impact of light and

circadian rhythm disturbances to patients in the ICU with neurovascular injuries or those hospitalized with chronic neuroinflammatory diseases.

References

2023 Alzheimer's disease facts and figures. (2023). *Alzheimer's & Dementia: The Journal of the Alzheimer's Association*, *19*(4), 1598–1695. https://doi.org/10.1002/alz.13016

Alcolado, R., Weller, R. O., Parrish, E. P., & Garrod, D. (1988). The cranial arachnoid and pia mater in man: Anatomical and ultrastructural observations. *Neuropathology and Applied Neurobiology*, *14*(1), 1–17. https://doi.org/10.1111/j.1365-2990.1988.tb00862.x

Allen, N. J., Bennett, M. L., Foo, L. C., Wang, G. X., Chakraborty, C., Smith, S. J., & Barres, B. A. (2012). Astrocyte glypicans 4 and 6 promote formation of excitatory synapses via GluA1 AMPA receptors. *Nature*, *486*(7403), 410–414. https://doi.org/10.1038/nature11059

Almalki, W. H., Ghoneim, M. M., Alshehri, S., Imam, S. S., Kazmi, I., & Gupta, G. (2022). Sepsis triggered oxidative stress-inflammatory axis: The pathobiology of reprogramming in the normal sleep–wake cycle. *Molecular and Cellular Biochemistry*, *477*(9), 2203–2211. https://doi.org/10.1007/S11010-022-04432-1/METRICS

Ameen, R. W., Warshawski, A., Fu, L., & Antle, M. C. (2022). Early life circadian rhythm disruption in mice alters brain and behavior in adulthood. *Scientific Reports 2022 12:1*, *12*(1), 1–13. https://doi.org/10.1038/s41598-022-11335-0

Artiushin, G., Zhang, S. L., Tricoire, H., & Sehgal, A. (2018). Endocytosis at the Drosophila blood-brain barrier as a function for sleep. *eLife*, *7*, e43326. https://doi.org/10.7554/eLife.43326

Banks, W. A. (2005). Blood-brain barrier transport of cytokines: A mechanism for neuropathology. *Current Pharmaceutical Design*, *11*(8), 973–984. https://doi.org/10.2174/1381612053381684

Banks, W. A., Gray, A. M., Erickson, M. A., Salameh, T. S., Damodarasamy, M., Sheibani, N., Meabon, J. S., Wing, E. E., Morofuji, Y., Cook, D. G., & Reed, M. J. (2015). Lipopolysaccharide-induced blood-brain barrier disruption: Roles of cyclooxygenase, oxidative stress, neuroinflammation, and elements of the neurovascular unit. *Journal of Neuroinflammation*, *12*(1). https://doi.org/10.1186/S12974-015-0434-1

Barca-Mayo, O., Boender, A. J., Armirotti, A., & De Pietri Tonelli, D. (2020). Deletion of astrocytic BMAL1 results in metabolic imbalance and shorter lifespan in mice. *Glia*, *68*(6), 1131–1147. https://doi.org/10.1002/glia.23764

Barca-Mayo, O., Pons-Espinal, M., Follert, P., Armirotti, A., Berdondini, L., & De Pietri Tonelli, D. (2017). Astrocyte deletion of Bmal1 alters daily locomotor activity and cognitive functions via GABA signalling. *Nature Communications*, *8*, 14336. https://doi.org/10.1038/ncomms14336

Bass, J., & Takahashi, J. S. (2010). Circadian Integration of Metabolism and Energetics. *Science (New York, N.Y.)*, *330*(6009), 1349–1354. https://doi.org/10.1126/science.1195027

Beaulé, C., Swanstrom, A., Leone, M. J., & Herzog, E. D. (2009). Circadian Modulation of Gene Expression, but not Glutamate Uptake, in Mouse and Rat Cortical Astrocytes. *PLoS ONE*, *4*(10), e7476. https://doi.org/10.1371/journal.pone.0007476

Becquet, D., Girardet, C., Guillaumond, F., François-Bellan, A.-M., & Bosler, O. (2008). Ultrastructural plasticity in the rat suprachiasmatic nucleus. Possible involvement in clock entrainment. *Glia*, *56*(3), 294–305. https://doi.org/10.1002/glia.20613

Bedussi, B., van Lier, M. G. J. T. B., Bartstra, J. W., de Vos, J., Siebes, M., VanBavel, E., & Bakker, E. N. T. P. (2015). Clearance from the mouse brain by convection of interstitial

fluid towards the ventricular system. *Fluids and Barriers of the CNS*, *12*, 23. https://doi.org/10.1186/s12987-015-0019-5

Bellesi, M., Pfister-Genskow, M., Maret, S., Keles, S., Tononi, G., & Cirelli, C. (2013). Effects of sleep and wake on oligodendrocytes and their precursors. *The Journal of Neuroscience: The Official Journal of the Society for Neuroscience*, *33*(36), 14288–14300. https://doi.org/10.1523/JNEUROSCI.5102-12.2013

Bennett, F. C., Bennett, M. L., Yaqoob, F., Mulinyawe, S. B., Grant, G. A., Gephart, M. H., Plowey, E. D., & Barres, B. A. (2018). A combination of ontogeny and CNS environment establishes microglial identity. *Neuron*, *98*(6), 1170-1183.e8. https://doi.org/10.1016/j.neuron.2018.05.014

Bennett, S. R. (2015). Sepsis in the intensive care unit. *Surgery (Oxford, Oxfordshire)*, *33*(11), 565–571. https://doi.org/10.1016/j.mpsur.2015.08.002

Berg, R. M., Plovsing, R. R., Evans, K. A., Christiansen, C. B., Bailey, D. M., Holstein-Rathlou, N.-H., & Møller, K. (2013). Lipopolysaccharide infusion enhances dynamic cerebral autoregulation without affecting cerebral oxygen vasoreactivity in healthy volunteers. *Critical Care*, *17*(5), R238. https://doi.org/10.1186/cc13062

Bergles, D. E., Roberts, J. D., Somogyi, P., & Jahr, C. E. (2000). Glutamatergic synapses on oligodendrocyte precursor cells in the hippocampus. *Nature*, *405*(6783), 187–191. https://doi.org/10.1038/35012083

Bhatwadekar, A. D., Beli, E., Diao, Y., Chen, J., Luo, Q., Alex, A., Caballero, S., Dominguez, J. M., Salazar, T. E., Busik, J. V., Segal, M. S., & Grant, M. B. (2017). Conditional Deletion of Bmal1 Accentuates Microvascular and Macrovascular Injury. *The American Journal of Pathology*, *187*(6), 1426–1435. https://doi.org/10.1016/j.ajpath.2017.02.014

Bisht, K., Okojie, K. A., Sharma, K., Lentferink, D. H., Sun, Y.-Y., Chen, H.-R., Uweru, J. O., Amancherla, S., Calcuttawala, Z., Campos-Salazar, A. B., Corliss, B., Jabbour, L., Benderoth, J., Friestad, B., Mills, W. A., Isakson, B. E., Tremblay, M.-È., Kuan, C.-Y., & Eyo, U. B. (2021). Capillary-associated microglia regulate vascular structure and function through PANX1-P2RY12 coupling in mice. *Nature Communications*, *12*(1), Article 1. https://doi.org/10.1038/s41467-021-25590-8

Blacher, E., Tsai, C., Litichevskiy, L., Shipony, Z., Iweka, C. A., Schneider, K. M., Chuluun, B., Heller, H. C., Menon, V., Thaiss, C. A., & Andreasson, K. I. (2022). Aging disrupts homeostatic circadian gene regulation and function in macrophages. *Nature Immunology*, *23*(2), 229–236. https://doi.org/10.1038/s41590-021-01083-0

Blanco-Suarez, E., Liu, T.-F., Kopelevich, A., & Allen, N. J. (2018). Astrocyte-secreted chordin like 1 drives synapse maturation and limits plasticity by increasing synaptic GluA2 AMPA receptors. *Neuron*, *100*(5), 1116-1132.e13. https://doi.org/10.1016/j.neuron.2018.09.043

Boivin, D. B., James, F. O., Wu, A., Cho-Park, P. F., Xiong, H., & Sun, Z. S. (2003). Circadian clock genes oscillate in human peripheral blood mononuclear cells. *Blood*, *102*(12), 4143–4145. https://doi.org/10.1182/BLOOD-2003-03-0779

Boje, K. M. K. (1996). Inhibition of nitric oxide synthase attenuates blood-brain barrier disruption during experimental meningitis. *Brain Research*, *720*(1), 75–83. https://doi.org/10.1016/0006-8993(96)00142-4

Bollinger, T., Leutz, A., Leliavski, A., Skrum, L., Kovac, J., Bonacina, L., Benedict, C., Lange, T., Westermann, J., Oster, H., & Solbach, W. (2011). Circadian Clocks in Mouse and

Human CD4+ T Cells. *PLoS ONE*, *6*(12), 29801. https://doi.org/10.1371/JOURNAL.PONE.0029801

Brahmachari, S., Fung, Y. K., & Pahan, K. (2006). Induction of glial fibrillary acidic protein expression in astrocytes by nitric oxide. *The Journal of Neuroscience: The Official Journal of the Society for Neuroscience*, *26*(18), 4930–4939. https://doi.org/10.1523/JNEUROSCI.5480-05.2006

Brancaccio, M., Edwards, M. D., Patton, A. P., Smyllie, N. J., Chesham, J. E., Maywood, E. S., & Hastings, M. H. (2019). Cell-autonomous clock of astrocytes drives circadian behavior in mammals. *Science (New York, N.Y.)*, *363*(6423), 187–192. https://doi.org/10.1126/science.aat4104

Buckley, M. W., & McGavern, D. B. (2022). Immune dynamics in the CNS and its barriers during homeostasis and disease*. *Immunological Reviews*, *306*(1), 58–75. https://doi.org/10.1111/imr.13066

Butt, A. M., Fern, R. F., & Matute, C. (2014). Neurotransmitter signaling in white matter. *Glia*, *62*(11), 1762–1779. https://doi.org/10.1002/glia.22674

Ceyzériat, K., Ben Haim, L., Denizot, A., Pommier, D., Matos, M., Guillemaud, O., Palomares, M.-A., Abjean, L., Petit, F., Gipchtein, P., Gaillard, M.-C., Guillermier, M., Bernier, S., Gaudin, M., Aurégan, G., Joséphine, C., Déchamps, N., Veran, J., Langlais, V., … Escartin, C. (2018). Modulation of astrocyte reactivity improves functional deficits in mouse models of Alzheimer's disease. *Acta Neuropathologica Communications*, *6*, 104. https://doi.org/10.1186/s40478-018-0606-1

Chelluboina, B., Klopfenstein, J. D., Pinson, D. M., Wang, D. Z., Vemuganti, R., & Veeravalli, K. K. (2015). Matrix Metalloproteinase-12 Induces Blood–Brain Barrier Damage After

Focal Cerebral Ischemia. *Stroke*, *46*(12), 3523–3531. https://doi.org/10.1161/STROKEAHA.115.011031

Chen, W., Ju, X.-Z., Lu, Y., Ding, X.-W., Miao, C.-H., & Chen, J.-W. (2019). Propofol improved hypoxia-impaired integrity of blood-brain barrier via modulating the expression and phosphorylation of zonula occludens-1. *CNS Neuroscience & Therapeutics*, *25*(6), 704–713. https://doi.org/10.1111/cns.13101

Chen, X., Firulyova, M., Manis, M., Herz, J., Smirnov, I., Aladyeva, E., Wang, C., Bao, X., Finn, M. B., Hu, H., Shchukina, I., Kim, M. W., Yuede, C. M., Kipnis, J., Artyomov, M. N., Ulrich, J. D., & Holtzman, D. M. (2023). Microglia-mediated T cell infiltration drives neurodegeneration in tauopathy. *Nature*, *615*(7953), Article 7953. https://doi.org/10.1038/s41586-023-05788-0

Chen, Y., & Liu, L. (2012). Modern methods for delivery of drugs across the blood–brain barrier. *Advanced Drug Delivery Reviews*, *64*(7), 640–665. https://doi.org/10.1016/j.addr.2011.11.010

Choi, M., Ku, T., Chong, K., Yoon, J., & Choi, C. (2011). Minimally invasive molecular delivery into the brain using optical modulation of vascular permeability. *Proceedings of the National Academy of Sciences*, *108*(22), 9256–9261. https://doi.org/10.1073/pnas.1018790108

Christopherson, K. S., Ullian, E. M., Stokes, C. C. A., Mullowney, C. E., Hell, J. W., Agah, A., Lawler, J., Mosher, D. F., Bornstein, P., & Barres, B. A. (2005). Thrombospondins are astrocyte-secreted proteins that promote CNS synaptogenesis. *Cell*, *120*(3), 421–433. https://doi.org/10.1016/j.cell.2004.12.020

Chung, A. W., Anand, K., Anselme, A. C., Chan, A. A., Gupta, N., Venta, L. A., Schwartz, M. R., Qian, W., Xu, Y., Zhang, L., Kuhn, J., Patel, T., Rodriguez, A. A., Belcheva, A., Darcourt, J., Ensor, J., Bernicker, E., Pan, P.-Y., Chen, S. H., … Chang, J. C. (2021). A phase 1/2 clinical trial of the nitric oxide synthase inhibitor L-NMMA and taxane for treating chemoresistant triple-negative breast cancer. *Science Translational Medicine*, *13*(624), eabj5070. https://doi.org/10.1126/scitranslmed.abj5070

Ciesielska, A., Matyjek, M., & Kwiatkowska, K. (2021). TLR4 and CD14 trafficking and its influence on LPS-induced pro-inflammatory signaling. *Cellular and Molecular Life Sciences: CMLS*, *78*(4), 1233–1261. https://doi.org/10.1007/s00018-020-03656-y

Claeys, W., Verhaege, D., Van Imschoot, G., Van Wonterghem, E., Van Acker, L., Amelinck, L., De Ponti, F. F., Scott, C., Geerts, A., Van Steenkiste, C., Van Hoecke, L., & Vandenbroucke, R. E. (2023). Limitations of PLX3397 as a microglial investigational tool: Peripheral and off-target effects dictate the response to inflammation. *Frontiers in Immunology*, *14*.

Colwell, C. S., & Ghiani, C. A. (2019). Potential Circadian Rhythms in Oligodendrocytes? Working together through time. *Neurochemical Research*, 10.1007/s11064-019-02778–5. https://doi.org/10.1007/s11064-019-02778-5

Conroy, D. A., Spielman, A. J., & Scott, R. Q. (2005). Daily rhythm of cerebral blood flow velocity. *Journal of Circadian Rhythms*, *3*(1), 3. https://doi.org/10.1186/1740-3391-3-3

Cox, S. L., O'Siorain, J. R., Fagan, L. E., Curtis, A. M., & Carroll, R. G. (2022). Intertwining roles of circadian and metabolic regulation of the innate immune response. *Seminars in Immunopathology*, *44*(2), 225–237. https://doi.org/10.1007/S00281-021-00905-5/FIGURES/2

Curtis, A. M., Bellet, M. M., Sassone-Corsi, P., & O'Neill, L. A. J. (2014). Circadian Clock Proteins and Immunity. *Immunity, 40*(2), 178–186. https://doi.org/10.1016/j.immuni.2014.02.002

Daneman, R. (2012). The blood-brain barrier in health and disease. *Annals of Neurology, 72*(5), 648–672. https://doi.org/10.1002/ana.23648

Davis, F. C., & Menaker, M. (1981). Development of the Mouse Circadian Pacemaker: Independence from Environmental Cycles. *Journal of Comparative Physiology, 143*(4), 527. https://doi.org/10.1007/BF00609919

Davis, K. L., Stewart, D. G., Friedman, J. I., Buchsbaum, M., Harvey, P. D., Hof, P. R., Buxbaum, J., & Haroutunian, V. (2003). White matter changes in schizophrenia: Evidence for myelin-related dysfunction. *Archives of General Psychiatry, 60*(5), 443–456. https://doi.org/10.1001/archpsyc.60.5.443

De Angelis, F., Bernardo, A., Magnaghi, V., Minghetti, L., & Tata, A. M. (2012). Muscarinic receptor subtypes as potential targets to modulate oligodendrocyte progenitor survival, proliferation, and differentiation. *Developmental Neurobiology, 72*(5), 713–728. https://doi.org/10.1002/dneu.20976

de Boer, A. G., & Gaillard, P. J. (2007). Drug targeting to the brain. *Annual Review of Pharmacology and Toxicology, 47*, 323–355. https://doi.org/10.1146/annurev.pharmtox.47.120505.105237

Dean, T., Koffi, A. V., Goldstein, E., Ghaemmaghami, J., & Gallo, V. (2022). Endogenous Circadian Clock Machinery in Cortical NG2-Glia Regulates Cellular Proliferation. *eNeuro, 9*(5). https://doi.org/10.1523/ENEURO.0110-22.2022

Druzd, D., Matveeva, O., Ince, L., Harrison, U., He, W., Schmal, C., Herzel, H., Tsang, A. H., Kawakami, N., Leliavski, A., Uhl, O., Yao, L., Sander, L. E., Chen, C. S., Kraus, K., de Juan, A., Hergenhan, S. M., Ehlers, M., Koletzko, B., … Scheiermann, C. (2017). Lymphocyte Circadian Clocks Control Lymph Node Trafficking and Adaptive Immune Responses. *Immunity*, *46*(1), 120–132. https://doi.org/10.1016/j.immuni.2016.12.011

Dwork, A. J., Mancevski, B., & Rosoklija, G. (2007). White matter and cognitive function in schizophrenia. *The International Journal of Neuropsychopharmacology*, *10*(4), 513–536. https://doi.org/10.1017/S1461145707007638

Ebihara, S., Tsuji, K., & Kondo, K. (1978). Strain differences of the mouse's free-running circadian rhythm in continuous darkness. *Physiology & Behavior*, *20*(6), 795–799. https://doi.org/10.1016/0031-9384(78)90308-6

Elherik, K., Khan, F., McLaren, M., Kennedy, G., & Belch, J. J. F. (2002). Circadian variation in vascular tone and endothelial cell function in normal males. *Clinical Science (London, England: 1979)*, *102*(5), 547–552.

Engelhardt, B., & Ransohoff, R. M. (2012). Capture, crawl, cross: The T cell code to breach the blood-brain barriers. *Trends in Immunology*, *33*(12), 579–589. https://doi.org/10.1016/j.it.2012.07.004

Epelman, S., Lavine, K. J., & Randolph, G. J. (2014). Origin and Functions of Tissue Macrophages. *Immunity*, *41*(1), 21–35. https://doi.org/10.1016/j.immuni.2014.06.013

Erickson, M. A., Shulyatnikova, T., Banks, W. A., & Hayden, M. R. (2023). Ultrastructural Remodeling of the Blood–Brain Barrier and Neurovascular Unit by Lipopolysaccharide-Induced Neuroinflammation. *International Journal of Molecular Sciences*, *24*(2), Article 2. https://doi.org/10.3390/ijms24021640

Espinal, E. R., Matthews, T., Holder, B. M., Bee, O. B., Humber, G. M., Brook, C. E., Divyapicigil, M., Sharp, J., & Kim, B. J. (2022). Group B Streptococcus-Induced Macropinocytosis Contributes to Bacterial Invasion of Brain Endothelial Cells. *Pathogens*, *11*(4), 474. https://doi.org/10.3390/pathogens11040474

Etain, B., Milhiet, V., Bellivier, F., & Leboyer, M. (2011). Genetics of circadian rhythms and mood spectrum disorders. *European Neuropsychopharmacology*, *21*(SUPPL.4), S676–S682. https://doi.org/10.1016/J.EURONEURO.2011.07.007

Eum, S. Y., Schurhoff, N., Teglas, T., Wolff, G., & Toborek, M. (2023). Circadian disruption alters gut barrier integrity via a ß-catenin-MMP-related pathway. *Molecular and Cellular Biochemistry*, *478*(3), 581–595. https://doi.org/10.1007/s11010-022-04536-8

Ezan, P., André, P., Cisternino, S., Saubaméa, B., Boulay, A.-C., Doutremer, S., Thomas, M.-A., Quenech'du, N., Giaume, C., & Cohen-Salmon, M. (2012). Deletion of astroglial connexins weakens the blood-brain barrier. *Journal of Cerebral Blood Flow and Metabolism: Official Journal of the International Society of Cerebral Blood Flow and Metabolism*, *32*(8), 1457–1467. https://doi.org/10.1038/jcbfm.2012.45

Fan, D., Gu, Y., Lv, H., Tang, T., Xu, Z., Song, Z., & Tong, X. (2011). The protective mechanism for the blood-brain barrier induced by aminoguanidine in surgical brain injury in rats. *Cellular and Molecular Neurobiology*, *31*(8), 1213–1219. https://doi.org/10.1007/s10571-011-9723-0

Fernández-Castañeda, A., Chappell, M. S., Rosen, D. A., Seki, S. M., Beiter, R. M., Johanson, D. M., Liskey, D., Farber, E., Onengut-Gumuscu, S., Overall, C. C., Dupree, J. L., & Gaultier, A. (2020). The active contribution of OPCs to neuroinflammation is mediated

by LRP1. *Acta Neuropathologica*, *139*(2), 365–382. https://doi.org/10.1007/s00401-019-02073-1

Fernandez-Galaz, M. C., Martinez Muñoz, R., Villanua, M. A., & Garcia-Segura, L. M. (1999). Diurnal oscillation in glial fibrillary acidic protein in a perisuprachiasmatic area and its relationship to the luteinizing hormone surge in the female rat. *Neuroendocrinology*, *70*(5), 368–376. https://doi.org/10.1159/000054498

Fischer, H., Gottschlich, R., & Seelig, A. (1998). Blood-Brain Barrier Permeation: Molecular Parameters Governing Passive Diffusion. *The Journal of Membrane Biology*, *165*(3), 201–211. https://doi.org/10.1007/s002329900434

Fonken, L. K., Frank, M. G., Kitt, M. M., Barrientos, R. M., Watkins, L. R., & Maier, S. F. (2015). Microglia inflammatory responses are controlled by an intrinsic circadian clock. *Brain, Behavior, and Immunity*, *45*, 171–179. https://doi.org/10.1016/j.bbi.2014.11.009

Fonken, L. K., Kitt, M. M., Gaudet, A. D., Barrientos, R. M., Watkins, L. R., & Maier, S. F. (2016). Diminished circadian rhythms in hippocampal microglia may contribute to age-related neuroinflammatory sensitization. *Neurobiology of Aging*, *47*, 102–112. https://doi.org/10.1016/j.neurobiolaging.2016.07.019

Gaucher, J., Montellier, E., & Sassone-Corsi, P. (2018). Molecular Cogs: Interplay between Circadian Clock and Cell Cycle. *Trends in Cell Biology*, *28*(5), 368–379. https://doi.org/10.1016/j.tcb.2018.01.006

Geiger, S. S., Traba, J., Richoz, N., Farley, T. K., Brooks, S. R., Petermann, F., Wang, L., Gonzalez, F. J., Sack, M. N., & Siegel, R. M. (2021). Feeding-induced resistance to acute lethal sepsis is dependent on hepatic BMAL1 and FXR signalling. *Nature Communications*, *12*(1), Article 1. https://doi.org/10.1038/s41467-021-22961-z

Gerhardt, H., & Betsholtz, C. (2003). Endothelial-pericyte interactions in angiogenesis. *Cell and Tissue Research*, *314*(1), 15–23. https://doi.org/10.1007/s00441-003-0745-x

Gibbs, J. E., Blaikley, J., Beesley, S., Matthews, L., Simpson, K. D., Boyce, S. H., Farrow, S. N., Else, K. J., Singh, D., Ray, D. W., & Loudon, A. S. I. (2012). The nuclear receptor REV-ERBα mediates circadian regulation of innate immunity through selective regulation of inflammatory cytokines. *Proceedings of the National Academy of Sciences*, *109*(2), 582–587. https://doi.org/10.1073/pnas.1106750109

Gibbs, J., Ince, L., Matthews, L., Mei, J., Bell, T., Yang, N., Saer, B., Begley, N., Poolman, T., Pariollaud, M., Farrow, S., Demayo, F., Hussell, T., Worthen, G. S., Ray, D., & Loudon, A. (2014). An epithelial circadian clock controls pulmonary inflammation and glucocorticoid action. *Nature Medicine*, *20*(8), 919–926. https://doi.org/10.1038/nm.3599

Greter, M., Heppner, F. L., Lemos, M. P., Odermatt, B. M., Goebels, N., Laufer, T., Noelle, R. J., & Becher, B. (2005). Dendritic cells permit immune invasion of the CNS in an animal model of multiple sclerosis. *Nature Medicine*, *11*(3), 328–334. https://doi.org/10.1038/nm1197

Griffin, P., Dimitry, J. M., Sheehan, P. W., Lananna, B. V., Guo, C., Robinette, M. L., Hayes, M. E., Cedeño, M. R., Nadarajah, C. J., Ezerskiy, L. A., Colonna, M., Zhang, J., Bauer, A. Q., Burris, T. P., & Musiek, E. S. (2019). Circadian clock protein Rev-erbα regulates neuroinflammation. *Proceedings of the National Academy of Sciences of the United States of America*, *116*(11), 5102–5107. https://doi.org/10.1073/pnas.1812405116

Griffin, P., Sheehan, P. W., Dimitry, J. M., Guo, C., Kanan, M. F., Lee, J., Zhang, J., & Musiek, E. S. (2020). REV-ERBα mediates complement expression and diurnal regulation of microglial synaptic phagocytosis. *eLife*, *9*, e58765. https://doi.org/10.7554/eLife.58765

Guzmán-Ruiz, M. A., Guerrero-Vargas, N. N., Lagunes-Cruz, A., González-González, S., García-Aviles, J. E., Hurtado-Alvarado, G., Mendez-Hernández, R., Chavarría-Krauser, A., Morin, J.-P., Arriaga-Avila, V., Buijs, R. M., & Guevara-Guzmán, R. (2023). Circadian modulation of microglial physiological processes and immune responses. *Glia*, *71*(2), 155–167. https://doi.org/10.1002/glia.24261

Haarmann, A., Schuhmann, M. K., Silwedel, C., Monoranu, C. M., Stoll, G., & Buttmann, M. (2019). Human brain endothelial CXCR2 is inflammation-inducible and mediates CXCL5-and CXCL8-triggered paraendothelial barrier breakdown. *International Journal of Molecular Sciences*, *20*(3). https://doi.org/10.3390/ijms20030602

Hablitz, L. M., Plá, V., Giannetto, M., Vinitsky, H. S., Stæger, F. F., Metcalfe, T., Nguyen, R., Benrais, A., & Nedergaard, M. (2020). Circadian control of brain glymphatic and lymphatic fluid flow. *Nature Communications*, *11*, 4411. https://doi.org/10.1038/s41467-020-18115-2

Haim, L. B., Ceyzériat, K., Sauvage, M. A. C., Aubry, F., Auregan, G., Guillermier, M., Ruiz, M., Petit, F., Houitte, D., Faivre, E., Vandesquille, M., Aron-Badin, R., Dhenain, M., Déglon, N., Hantraye, P., Brouillet, E., Bonvento, G., & Escartin, C. (2015). The JAK/STAT3 Pathway Is a Common Inducer of Astrocyte Reactivity in Alzheimer's and Huntington's Diseases. *Journal of Neuroscience*, *35*(6), 2817–2829. https://doi.org/10.1523/JNEUROSCI.3516-14.2015

Halberg, F., Johnson, E. A., Brown, B. W., & Bittner, J. J. (1960). Susceptibility Rhythm to E. coli Endotoxin and Bioassay. *Proceedings of the Society for Experimental Biology and Medicine*, *103*(1), 142–144. https://doi.org/10.3181/00379727-103-25439

Hamanaka, G., Ohtomo, R., Takase, H., Lok, J., & Arai, K. (2018). Role of oligodendrocyte-neurovascular unit in white matter repair. *Neuroscience Letters, 684*, 175–180. https://doi.org/10.1016/j.neulet.2018.07.016

Hannocks, M.-J., Pizzo, M. E., Huppert, J., Deshpande, T., Abbott, N. J., Thorne, R. G., & Sorokin, L. (2018). Molecular characterization of perivascular drainage pathways in the murine brain. *Journal of Cerebral Blood Flow & Metabolism*, *38*(4), 669–686. https://doi.org/10.1177/0271678X17749689

Hartsock, A., & Nelson, W. J. (2008). Adherens and Tight Junctions: Structure, Function and Connections to the Actin Cytoskeleton. *Biochimica et Biophysica Acta*, *1778*(3), 660–669. https://doi.org/10.1016/j.bbamem.2007.07.012

Hasel, P., Rose, I. V. L., Sadick, J. S., Kim, R. D., & Liddelow, S. A. (2021). Neuroinflammatory astrocyte subtypes in the mouse brain. *Nature Neuroscience*, *24*(10), 1475–1487. https://doi.org/10.1038/s41593-021-00905-6

Haspel, J. A., Chettimada, S., Shaik, R. S., Chu, J.-H., Raby, B. A., Cernadas, M., Carey, V., Process, V., Hunninghake, G. M., Ifedigbo, E., Lederer, J. A., Englert, J., Pelton, A., Coronata, A., Fredenburgh, L. E., & Choi, A. M. K. (2014). Circadian rhythm reprogramming during lung inflammation. *Nature Communications*, *5*, 4753. https://doi.org/10.1038/ncomms5753

Hattar, S., Liao, H.-W., Takao, M., Berson, D. M., & Yau, K.-W. (2002). Melanopsin-Containing Retinal Ganglion Cells: Architecture, Projections, and Intrinsic Photosensitivity. *Science (New York, N.Y.)*, *295*(5557), 1065–1070. https://doi.org/10.1126/science.1069609

Hayashi, Y., Koyanagi, S., Kusunose, N., Okada, R., Wu, Z., Tozaki-Saitoh, H., Ukai, K., Kohsaka, S., Inoue, K., Ohdo, S., & Nakanishi, H. (2013). The intrinsic microglial molecular clock controls synaptic strength via the circadian expression of cathepsin S. *Scientific Reports*, *3*, 2744. https://doi.org/10.1038/srep02744

Hendrickson, A. E., Wagoner, N., & Cowan, W. M. (1972). An autoradiographic and electron microscopic study of retino-hypothalamic connections. *Zeitschrift Für Zellforschung Und Mikroskopische Anatomie*, *135*(1), 1–26. https://doi.org/10.1007/BF00307084/METRICS

Hp, G., V, S., M, S., S, I.-J., Po, F., K, B., C, H., P, R., T, S., U, G., M, H., S, R., A, Z., S, S., R, N., J, N., & N, J. (2023). Delivery of the Brainshuttle™ amyloid-beta antibody fusion trontinemab to non-human primate brain and projected efficacious dose regimens in humans. *mAbs*, *15*(1). https://doi.org/10.1080/19420862.2023.2261509

Hu, X., Li, S., Shi, Z., Lin, W.-J., Yang, Y., Li, Y., Li, H., Xu, Y., Zhou, M., & Tang, Y. (2023). Partial Ablation of Astrocytes Exacerbates Cerebral Infiltration of Monocytes and Neuronal Loss After Brain Stab Injury in Mice. *Cellular and Molecular Neurobiology*, *43*(2), 893–905. https://doi.org/10.1007/s10571-022-01224-5

Huang, S., Wu, T., Lau, A. Y., Au, C., Huang, H., Wang, X., & Kim, J. Y. (2021). Attention to time-of-day variability improves the reproducibility of gene expression patterns in multiple sclerosis. *iScience*, *24*(11), 103247. https://doi.org/10.1016/J.ISCI.2021.103247

Hudson, N., Celkova, L., Hopkins, A., Greene, C., Storti, F., Ozaki, E., Fahey, E., Theodoropoulou, S., Kenna, P. F., Humphries, M. M., Curtis, A. M., Demmons, E., Browne, A., Liddie, S., Lawrence, M. S., Grimm, C., Cahill, M. T., Humphries, P., Doyle, S. L., & Campbell, M. (2019). Dysregulated claudin-5 cycling in the inner retina

causes retinal pigment epithelial cell atrophy. *JCI Insight*, *4*(15). https://doi.org/10.1172/jci.insight.130273

Ibuka, N., & Kawamura, H. (1975). Loss of circadian rhythm in sleep-wakefulness cycle in the rat by suprachiasmatic nucleus lesions. *Brain Research*, *96*(1), 76–81. https://doi.org/10.1016/0006-8993(75)90574-0

Iliff, J. J., Wang, M., Liao, Y., Plogg, B. A., Peng, W., Gundersen, G. A., Benveniste, H., Vates, G. E., Deane, R., Goldman, S. A., Nagelhus, E. A., & Nedergaard, M. (2012). A Paravascular Pathway Facilitates CSF Flow Through the Brain Parenchyma and the Clearance of Interstitial Solutes, Including Amyloid β. *Science Translational Medicine*, *4*(147), 147ra111. https://doi.org/10.1126/scitranslmed.3003748

Iweka, C. A., Seigneur, E., Hernandez, A. L., Paredes, S. H., Cabrera, M., Blacher, E., Pasternak, C. T., Longo, F. M., de Lecea, L., & Andreasson, K. I. (2023). Myeloid deficiency of the intrinsic clock protein BMAL1 accelerates cognitive aging by disrupting microglial synaptic pruning. *Journal of Neuroinflammation*, *20*(1), 48. https://doi.org/10.1186/s12974-023-02727-8

Jana, A., Wang, X., Leasure, J. W., Magana, L., Wang, L., Kim, Y.-M., Dodiya, H., Toth, P. T., Sisodia, S. S., & Rehman, J. (2022). Increased Type I interferon signaling and brain endothelial barrier dysfunction in an experimental model of Alzheimer's disease. *Scientific Reports*, *12*(1), Article 1. https://doi.org/10.1038/s41598-022-20889-y

Jangula, A., & Murphy, E. J. (2013). Lipopolysaccharide-induced blood brain barrier permeability is enhanced by alpha-synuclein expression. *Neuroscience Letters*, *551*, 23–27. https://doi.org/10.1016/j.neulet.2013.06.058

Jin, W.-N., Shi, S. X.-Y., Li, Z., Li, M., Wood, K., Gonzales, R. J., & Liu, Q. (2017). Depletion of microglia exacerbates postischemic inflammation and brain injury. *Journal of Cerebral Blood Flow and Metabolism: Official Journal of the International Society of Cerebral Blood Flow and Metabolism*, *37*(6), 2224–2236. https://doi.org/10.1177/0271678X17694185

Ju, Y.-E. S., McLeland, J. S., Toedebusch, C. D., Xiong, C., Fagan, A. M., Duntley, S. P., Morris, J. C., & Holtzman, D. M. (2013). Sleep quality and preclinical Alzheimer disease. *JAMA Neurology*, *70*(5), 587–593. https://doi.org/10.1001/jamaneurol.2013.2334

Juskewitch, J. E., Knudsen, B. E., Platt, J. L., Nath, K. A., Knutson, K. L., Brunn, G. J., & Grande, J. P. (2012). LPS-Induced Murine Systemic Inflammation Is Driven by Parenchymal Cell Activation and Exclusively Predicted by Early MCP-1 Plasma Levels. *The American Journal of Pathology*, *180*(1), 32–40. https://doi.org/10.1016/j.ajpath.2011.10.001

Kalayci, R., Kaya, M., Ahishali, B., Arican, N., Elmas, I., & Kucuk, M. (2006). Long-term l-NAME treatment potentiates the blood–brain barrier disruption during pentylenetetrazole-induced seizures in rats. *Life Sciences*, *79*(1), 16–20. https://doi.org/10.1016/j.lfs.2005.12.034

Kanan, M. K., Sheehan, P. W., Haines, J. N., Gomez, P. G., Dhuler, A., Nadarajah, C. J., Wargel, Z. M., Freeberg, B. M., Nelvagal, H. R., Izumo, M., Takahashi, J. S., Cooper, J. D., Davis, A. A., & Musiek, E. S. (2024). Neuronal deletion of the circadian clock gene *Bmal1* induces cell-autonomous dopaminergic neurodegeneration. *JCI Insight*, *9*(2). https://doi.org/10.1172/jci.insight.162771

Kang, R., Gamdzyk, M., Lenahan, C., Tang, J., Tan, S., & Zhang, J. H. (2020). The Dual Role of Microglia in Blood-Brain Barrier Dysfunction after Stroke. *Current Neuropharmacology*, *18*(12), 1237–1249. https://doi.org/10.2174/1570159X18666200529150907

Kang, S. S., Ebbert, M. T. W., Baker, K. E., Cook, C., Wang, X., Sens, J. P., Kocher, J.-P., Petrucelli, L., & Fryer, J. D. (2018). Microglial translational profiling reveals a convergent APOE pathway from aging, amyloid, and tau. *The Journal of Experimental Medicine*, *215*(9), 2235–2245. https://doi.org/10.1084/jem.20180653

Keller, M., Mazuch, J., Abraham, U., Eom, G. D., Herzog, E. D., Volk, H. D., Kramer, A., & Maier, B. (2009). A circadian clock in macrophages controls inflammatory immune responses. *Proceedings of the National Academy of Sciences of the United States of America*, *106*(50), 21407. https://doi.org/10.1073/PNAS.0906361106

Kim, H., Leng, K., Park, J., Sorets, A. G., Kim, S., Shostak, A., Embalabala, R. J., Mlouk, K., Katdare, K. A., Rose, I. V. L., Sturgeon, S. M., Neal, E. H., Ao, Y., Wang, S., Sofroniew, M. V., Brunger, J. M., McMahon, D. G., Schrag, M. S., Kampmann, M., & Lippmann, E. S. (2022). Reactive astrocytes transduce inflammation in a blood-brain barrier model through a TNF-STAT3 signaling axis and secretion of alpha 1-antichymotrypsin. *Nature Communications*, *13*(1), Article 1. https://doi.org/10.1038/s41467-022-34412-4

Kim, J.-Y., Grunke, S. D., Levites, Y., Golde, T. E., & Jankowsky, J. L. (2014). Intracerebroventricular viral injection of the neonatal mouse brain for persistent and widespread neuronal transduction. *Journal of Visualized Experiments: JoVE*, *91*, 51863. https://doi.org/10.3791/51863

Knowland, D., Arac, A., Sekiguchi, K. J., Hsu, M., Lutz, S. E., Perrino, J., Steinberg, G. K., Barres, B. A., Nimmerjahn, A., & Agalliu, D. (2014). Stepwise recruitment of

transcellular and paracellular pathways underlies blood-brain barrier breakdown in stroke. *Neuron*, *82*(3), 603–617. https://doi.org/10.1016/j.neuron.2014.03.003

Kokona, D., Ebneter, A., Escher, P., & Zinkernagel, M. S. (2018). Colony-stimulating factor 1 receptor inhibition prevents disruption of the blood-retina barrier during chronic inflammation. *Journal of Neuroinflammation*, *15*(1), 340. https://doi.org/10.1186/s12974-018-1373-4

Kong, L.-Y., McMillian, M. K., Maronpot, R., & Hong, J.-S. (1996). Protein tyrosine kinase inhibitors suppress the production of nitric oxide in mixed glia, microglia-enriched or astrocyte-enriched cultures. *Brain Research*, *729*(1), 102–109. https://doi.org/10.1016/0006-8993(96)00417-9

Kraft, P., Benz, P. M., Austinat, M., Brede, M. E., Schuh, K., Walter, U., Stoll, G., & Kleinschnitz, C. (2010). Deficiency of Vasodilator-Stimulated Phosphoprotein (VASP) Increases Blood-Brain-Barrier Damage and Edema Formation after Ischemic Stroke in Mice. *PLoS ONE*, *5*(12), e15106. https://doi.org/10.1371/journal.pone.0015106

Kress, G. J., Liao, F., Dimitry, J., Cedeno, M. R., FitzGerald, G. A., Holtzman, D. M., & Musiek, E. S. (2018). Regulation of amyloid-β dynamics and pathology by the circadian clock. *Journal of Experimental Medicine*, *215*(4), 1059–1068. https://doi.org/10.1084/jem.20172347

Kunieda, T., Minamino, T., Miura, K., Katsuno, T., Tateno, K., Miyauchi, H., Kaneko, S., Bradfield, C. A., FitzGerald, G. A., & Komuro, I. (2008). Reduced Nitric Oxide Causes Age-Associated Impairment of Circadian Rhythmicity. *Circulation Research*, *102*(5), 607–614. https://doi.org/10.1161/CIRCRESAHA.107.162230

Lajoie, J. M., & Shusta, E. V. (2015). Targeting Receptor-Mediated Transport for Delivery of Biologics Across the Blood-Brain Barrier. *Annual Review of Pharmacology and Toxicology*, *55*(1), 613–631. https://doi.org/10.1146/annurev-pharmtox-010814-124852

Lananna, B. V., Nadarajah, C. J., Izumo, M., Cedeño, M. R., Xiong, D. D., Dimitry, J., Tso, C. F., McKee, C. A., Griffin, P., Sheehan, P. W., Haspel, J. A., Barres, B. A., Liddelow, S. A., Takahashi, J. S., Karatsoreos, I. N., & Musiek, E. S. (2018). Cell-Autonomous Regulation of Astrocyte Activation by the Circadian Clock Protein BMAL1. *Cell Reports*, *25*(1), 1-9.e5. https://doi.org/10.1016/j.celrep.2018.09.015

Lang, V., Ferencik, S., Ananthasubramaniam, B., Kramer, A., & Maier, B. (2021). Susceptibility rhythm to bacterial endotoxin in myeloid clock-knockout mice. *eLife*, *10*. https://doi.org/10.7554/ELIFE.62469

Lavialle, M., & Servière, J. (1993). Circadian fluctuations in GFAP distribution in the Syrian hamster suprachiasmatic nucleus. *Neuroreport*, *4*(11), 1243–1246. https://doi.org/10.1097/00001756-199309000-00008

Leal, E. C., Manivannan, A., Hosoya, K.-I., Terasaki, T., Cunha-Vaz, J., Ambrósio, A. F., & Forrester, J. V. (2007). Inducible nitric oxide synthase isoform is a key mediator of leukostasis and blood-retinal barrier breakdown in diabetic retinopathy. *Investigative Ophthalmology & Visual Science*, *48*(11), 5257–5265. https://doi.org/10.1167/iovs.07-0112

Lee, J., Dimitry, J. M., Song, J. H., Son, M., Sheehan, P. W., King, M. W., Travis Tabor, G., Goo, Y. A., Lazar, M. A., Petrucelli, L., & Musiek, E. S. (2023). Microglial REV-ERBα regulates inflammation and lipid droplet formation to drive tauopathy in male mice. *Nature Communications*, *14*(1), 5197. https://doi.org/10.1038/s41467-023-40927-1

Lee, J., Kim, D. E., Griffin, P., Sheehan, P. W., Kim, D.-H., Musiek, E. S., & Yoon, S.-Y. (2020). Inhibition of REV-ERBs stimulates microglial amyloid-beta clearance and reduces amyloid plaque deposition in the 5XFAD mouse model of Alzheimer's disease. *Aging Cell*, *19*(2), e13078. https://doi.org/10.1111/acel.13078

Lee, J.-T., Pamir, N., Liu, N.-C., Kirk, E. A., Averill, M. M., Becker, L., Larson, I., Hagman, D. K., Foster-Schubert, K. E., van Yserloo, B., Bornfeldt, K. E., LeBoeuf, R. C., Kratz, M., & Heinecke, J. W. (2014). Macrophage Metalloelastase (MMP12) Regulates Adipose Tissue Expansion, Insulin Sensitivity, and Expression of Inducible Nitric Oxide Synthase. *Endocrinology*, *155*(9), 3409–3420. https://doi.org/10.1210/en.2014-1037

LeGates, T. A., & Altimus, C. M. (2011). Measuring Circadian and Acute Light Responses in Mice using Wheel Running Activity. *Journal of Visualized Experiments : JoVE*, *48*(48). https://doi.org/10.3791/2463

Leone, M. J., Beaule, C., Marpegan, L., Simon, T., Herzog, E. D., & Golombek, D. A. (2015). Glial and light-dependent glutamate metabolism in the suprachiasmatic nuclei. *Chronobiology International*, *32*(4), 573–578. https://doi.org/10.3109/07420528.2015.1006328

Li, W., Chen, Z., Chin, I., Chen, Z., & Dai, H. (2018). The Role of VE-cadherin in Blood-brain Barrier Integrity under Central Nervous System Pathological Conditions. *Current Neuropharmacology*, *16*(9), 1375–1384. https://doi.org/10.2174/1570159X16666180222164809

Li, W., Hsiao, H.-M., Higashikubo, R., Saunders, B. T., Bharat, A., Goldstein, D. R., Krupnick, A. S., Gelman, A. E., Lavine, K. J., & Kreisel, D. (n.d.). Heart-resident CCR2+

macrophages promote neutrophil extravasation through TLR9/MyD88/CXCL5 signaling. *JCI Insight*, *1*(12), e87315. https://doi.org/10.1172/jci.insight.87315

Lin, S., & Bergles, D. E. (2004). Synaptic signaling between GABAergic interneurons and oligodendrocyte precursor cells in the hippocampus. *Nature Neuroscience*, *7*(1), 24–32. https://doi.org/10.1038/nn1162

Lin, X. P., Mintern, J. D., & Gleeson, P. A. (2020). Macropinocytosis in Different Cell Types: Similarities and Differences. *Membranes*, *10*(8), 177. https://doi.org/10.3390/membranes10080177

Liu, T., Zhang, M., Mukosera, G. T., Borchardt, D., Li, Q., Tipple, T. E., Ishtiaq Ahmed, A. S., Power, G. G., & Blood, A. B. (2019). L-NAME releases nitric oxide and potentiates subsequent nitroglycerin-mediated vasodilation. *Redox Biology*, *26*, 101238. https://doi.org/10.1016/j.redox.2019.101238

Liu, Y., Zhang, Y., Li, T., Han, J., & Wang, Y. (2020). The tight junction protein TJP1 regulates the feeding-modulated hepatic circadian clock. *Nature Communications*, *11*(1), 589. https://doi.org/10.1038/s41467-020-14470-2

Lo, E. H. (2008). A new penumbra: Transitioning from injury into repair after stroke. *Nature Medicine*, *14*(5), 497–500. https://doi.org/10.1038/nm1735

Lo, E. H. (2014). 2013 Thomas Willis Award Lecture: Causation and Collaboration for Stroke Research. *Stroke; a Journal of Cerebral Circulation*, *45*(1), 305–308. https://doi.org/10.1161/STROKEAHA.113.001269

Lodygin, D., Odoardi, F., Schläger, C., Körner, H., Kitz, A., Nosov, M., van den Brandt, J., Reichardt, H. M., Haberl, M., & Flügel, A. (2013). A combination of fluorescent NFAT

and H2B sensors uncovers dynamics of T cell activation in real time during CNS autoimmunity. *Nature Medicine*, *19*(6), 784–790. https://doi.org/10.1038/nm.3182

Long, J. M., & Holtzman, D. M. (2019). Alzheimer Disease: An Update on Pathobiology and Treatment Strategies. *Cell*, *179*(2), 312–339. https://doi.org/10.1016/j.cell.2019.09.001

Louer, E. M. M., Günzel, D., Rosenthal, R., Carmone, C., Yi, G., Stunnenberg, H. G., den Hollander, A. I., & Deen, P. M. T. (2020). Differential day-night expression of tight junction components in murine retinal pigment epithelium. *Experimental Eye Research*, *193*, 107985. https://doi.org/10.1016/j.exer.2020.107985

Louveau, A., Herz, J., Alme, M. N., Salvador, A. F., Dong, M. Q., Viar, K. E., Herod, G., Knopp, J., Setliff, J., Lupi, A. L., Mesquita, S. D., Frost, E. L., Gaultier, A., Harris, T. H., Cao, R., Hu, S., Lukens, J. R., Smirnov, I., Overall, C. C., … Kipnis, J. (2018). CNS lymphatic drainage and neuroinflammation are regulated by meningeal lymphatic vasculature. *Nature Neuroscience*, *21*(10), 1380. https://doi.org/10.1038/s41593-018-0227-9

Lowrey, P. L., & Takahashi, J. S. (2004). MAMMALIAN CIRCADIAN BIOLOGY: ELUCIDATING GENOME-WIDE LEVELS OF TEMPORAL ORGANIZATION. *Annual Review of Genomics and Human Genetics*, *5*, 407. https://doi.org/10.1146/ANNUREV.GENOM.5.061903.175925

Mahan, T. E., Wang, C., Bao, X., Choudhury, A., Ulrich, J. D., & Holtzman, D. M. (2022). Selective reduction of astrocyte apoE3 and apoE4 strongly reduces Aβ accumulation and plaque-related pathology in a mouse model of amyloidosis. *Molecular Neurodegeneration*, *17*(1), 13. https://doi.org/10.1186/s13024-022-00516-0

Majerova, P., Michalicova, A., Cente, M., Hanes, J., Vegh, J., Kittel, A., Kosikova, N., Cigankova, V., Mihaljevic, S., Jadhav, S., & Kovac, A. (2019). Trafficking of immune cells across the blood-brain barrier is modulated by neurofibrillary pathology in tauopathies. *PloS One*, *14*(5), e0217216. https://doi.org/10.1371/journal.pone.0217216

Marpegan, L., Swanstrom, A. E., Chung, K., Simon, T., Haydon, P. G., Khan, S. K., Liu, A. C., Herzog, E. D., & Beaulé, C. (2011). Circadian Regulation of ATP Release in Astrocytes. *The Journal of Neuroscience*, *31*(23), 8342–8350. https://doi.org/10.1523/JNEUROSCI.6537-10.2011

Maruo, T., Nakatani, S., Kanzaki, H., Kakuchi, H., Yamagishi, M., Kitakaze, M., Ohe, T., & Miyatake, K. (2006). Circadian variation of endothelial function in idiopathic dilated cardiomyopathy. *The American Journal of Cardiology*, *97*(5), 699–702. https://doi.org/10.1016/j.amjcard.2005.09.118

Mastorakos, P., & McGavern, D. (2019). The anatomy and immunology of vasculature in the central nervous system. *Science Immunology*, *4*(37), eaav0492. https://doi.org/10.1126/sciimmunol.aav0492

Mastorakos, P., Mihelson, N., Luby, M., Burks, S. R., Johnson, K., Hsia, A. W., Witko, J., Frank, J. A., Latour, L., & McGavern, D. B. (2021). Temporally Distinct Myeloid Cell Reponses Mediate Damage and Repair After Cerebrovascular Injury. *Nature Neuroscience*, *24*(2), 245–258. https://doi.org/10.1038/s41593-020-00773-6

Mastrullo, V., van der Veen, D. R., Gupta, P., Matos, R. S., Johnston, J. D., McVey, J. H., Madeddu, P., Velliou, E. G., & Campagnolo, P. (2022). Pericytes' Circadian Clock Affects Endothelial Cells' Synchronization and Angiogenesis in a 3D Tissue Engineered

Scaffold. *Frontiers in Pharmacology*, *13*, 867070. https://doi.org/10.3389/fphar.2022.867070

Mathiisen, T. M., Lehre, K. P., Danbolt, N. C., & Ottersen, O. P. (2010). The perivascular astroglial sheath provides a complete covering of the brain microvessels: An electron microscopic 3D reconstruction. *Glia*, *58*(9), 1094–1103. https://doi.org/10.1002/glia.20990

Matsui, F., Yamaguchi, S. T., Kobayashi, R., Ito, S., Nagashima, S., Zhou, Z., & Norimoto, H. (2023). Ablation of microglia does not alter circadian rhythm of locomotor activity. *Molecular Brain*, *16*, 34. https://doi.org/10.1186/s13041-023-01021-1

Matsumoto, Y., Tsunekawa, Y., Nomura, T., Suto, F., Matsumata, M., Tsuchiya, S., & Osumi, N. (2011). Differential proliferation rhythm of neural progenitor and oligodendrocyte precursor cells in the young adult hippocampus. *PloS One*, *6*(11), e27628. https://doi.org/10.1371/journal.pone.0027628

Matyszak, M. K., & Perry, V. H. (1998). Bacillus Calmette-Guérin sequestered in the brain parenchyma escapes immune recognition. *Journal of Neuroimmunology*, *82*(1), 73–80. https://doi.org/10.1016/S0165-5728(97)00190-2

Mayhan, W. G. (1998). Effect of lipopolysaccharide on the permeability and reactivity of the cerebral microcirculation: Role of inducible nitric oxide synthase. *Brain Research*, *792*(2), 353–357. https://doi.org/10.1016/S0006-8993(98)00259-5

Mazzitelli, J. A., Smyth, L. C. D., Cross, K. A., Dykstra, T., Sun, J., Du, S., Mamuladze, T., Smirnov, I., Rustenhoven, J., & Kipnis, J. (2022). Cerebrospinal fluid regulates skull bone marrow niches via direct access through dural channels. *Nature Neuroscience*, *25*(5), 555–560. https://doi.org/10.1038/s41593-022-01029-1

McKee, C. A., Lee, J., Cai, Y., Saito, T., Saido, T., & Musiek, E. S. (2022). Astrocytes deficient in circadian clock gene Bmal1 show enhanced activation responses to amyloid-beta pathology without changing plaque burden. *Scientific Reports*, *12*(1), Article 1. https://doi.org/10.1038/s41598-022-05862-z

McKee, C. A., Polino, A. J., King, M. W., & Musiek, E. S. (2023). Circadian clock protein BMAL1 broadly influences autophagy and endolysosomal function in astrocytes. *Proceedings of the National Academy of Sciences of the United States of America*, *120*(20), e2220551120. https://doi.org/10.1073/pnas.2220551120

Merlini, M., Rafalski, V. A., Ma, K., Kim, K.-Y., Bushong, E. A., Rios Coronado, P. E., Yan, Z., Mendiola, A. S., Sozmen, E. G., Ryu, J. K., Haberl, M. G., Madany, M., Sampson, D. N., Petersen, M. A., Bardehle, S., Tognatta, R., Dean, T., Acevedo, R. M., Cabriga, B., … Akassoglou, K. (2021). Microglial Gi-dependent dynamics regulate brain network hyperexcitability. *Nature Neuroscience*, *24*(1), 19–23. https://doi.org/10.1038/s41593-020-00756-7

Mestre, H., Hablitz, L. M., Xavier, A. L., Feng, W., Zou, W., Pu, T., Monai, H., Murlidharan, G., Castellanos Rivera, R. M., Simon, M. J., Pike, M. M., Plá, V., Du, T., Kress, B. T., Wang, X., Plog, B. A., Thrane, A. S., Lundgaard, I., Abe, Y., … Nedergaard, M. (n.d.). Aquaporin-4-dependent glymphatic solute transport in the rodent brain. *eLife*, *7*, e40070. https://doi.org/10.7554/eLife.40070

Minogue, A. M., Barrett, J. P., & Lynch, M. A. (2012). LPS-induced release of IL-6 from glia modulates production of IL-1β in a JAK2-dependent manner. *Journal of Neuroinflammation*, *9*(1), 126. https://doi.org/10.1186/1742-2094-9-126

Mohn, C., Lomniczi, A., Faletti, A., Scorticati, C., Elverdin, J. C., McCann, S. M., & Rettori, V. (2002). Effects of Aminoguanidine and Meloxicam on Nitric Oxide and Prostaglandin E Production Induced by Lipopolysaccharide in the Hypothalamus and Anterior Pituitary of the Rat. *Neuroimmunomodulation*, *9*(5), 276–285. https://doi.org/10.1159/000054290

Moore, R. Y. (2007). Suprachiasmatic nucleus in sleep–wake regulation. *Sleep Medicine*, *8*(SUPPL. 3), 27–33. https://doi.org/10.1016/J.SLEEP.2007.10.003

Moore, R. Y., & Eichler, V. B. (1972). Loss of a circadian adrenal corticosterone rhythm following suprachiasmatic lesions in the rat. *Brain Research*, *42*(1), 201–206. https://doi.org/10.1016/0006-8993(72)90054-6

Moore, R. Y., & Lenn, N. J. (1972). A retinohypothalamic projection in the rat. *Journal of Comparative Neurology*, *146*(1), 1–14. https://doi.org/10.1002/CNE.901460102

Moriguchi, K., Miyamoto, K., Fukumoto, Y., & Kusunoki, S. (2021). Change in light-dark cycle affects experimental autoimmune encephalomyelitis. *Journal of Neuroimmunology*, *353*. https://doi.org/10.1016/J.JNEUROIM.2021.577495

Moskowitz, M. A., Lo, E. H., & Iadecola, C. (2010). The Science of Stroke: Mechanisms in Search of Treatments. *Neuron*, *67*(2), 181–198. https://doi.org/10.1016/j.neuron.2010.07.002

Munford, R. S. (2010). Murine responses to endotoxin: Another dirty little secret? *The Journal of Infectious Diseases*, *201*(2), 175–177. https://doi.org/10.1086/649558

Murphy, K. M., & Weaver, C. (2017). Janeway's immunobiology.

Musiek, E. S., Bhimasani, M., Zangrilli, M. A., Morris, J. C., Holtzman, D. M., & Ju, Y.-E. S. (2018). Circadian Rest-Activity Pattern Changes in Aging and Preclinical Alzheimer

Disease. *JAMA Neurology*, *75*(5), 582–590. https://doi.org/10.1001/jamaneurol.2017.4719

Musiek, E. S., & Ju, Y.-E. S. (2022). Targeting Sleep and Circadian Function in the Prevention of Alzheimer Disease. *JAMA Neurology*, *79*(9), 835–836. https://doi.org/10.1001/jamaneurol.2022.1732

Musiek, E. S., Lim, M. M., Yang, G., Bauer, A. Q., Qi, L., Lee, Y., Roh, J. H., Ortiz-Gonzalez, X., Dearborn, J. T., Culver, J. P., Herzog, E. D., Hogenesch, J. B., Wozniak, D. F., Dikranian, K., Giasson, B. I., Weaver, D. R., Holtzman, D. M., & FitzGerald, G. A. (2013). Circadian clock proteins regulate neuronal redox homeostasis and neurodegeneration. *Journal of Clinical Investigation*, *123*(12), 5389–5400. https://doi.org/10.1172/JCI70317

Nakazato, R., Kawabe, K., Yamada, D., Ikeno, S., Mieda, M., Shimba, S., Hinoi, E., Yoneda, Y., & Takarada, T. (2017). Disruption of Bmal1 impairs blood-brain barrier integrity via pericyte dysfunction. *Journal of Neuroscience*, *37*(42), 10052–10062. https://doi.org/10.1523/JNEUROSCI.3639-16.2017

Nakazato, R., Takarada, T., Yamamoto, T., Hotta, S., Hinoi, E., & Yoneda, Y. (2011). Selective upregulation of Per1 mRNA expression by ATP through activation of P2X7 purinergic receptors expressed in microglial cells. *Journal of Pharmacological Sciences*, *116*(4), 350–361. https://doi.org/10.1254/jphs.11069fp

Ni, J., Wu, Z., Meng, J., Saito, T., Saido, T. C., Qing, H., & Nakanishi, H. (2019). An impaired intrinsic microglial clock system induces neuroinflammatory alterations in the early stage of amyloid precursor protein knock-in mouse brain. *Journal of Neuroinflammation*, *16*, 173. https://doi.org/10.1186/s12974-019-1562-9

Nico, B., Mangieri, D., Crivellato, E., Longo, V., De Giorgis, M., Capobianco, C., Corsi, P., Benagiano, V., Roncali, L., & Ribatti, D. (2007). HIF Activation and VEGF Overexpression are Coupled with ZO-1 Up-phosphorylation in the Brain of Dystrophic MDX Mouse. *Brain Pathology*, *17*(4), 399–406. https://doi.org/10.1111/j.1750-3639.2007.00090.x

Nonaka, H., Emoto, N., Ikeda, K., Fukuya, H., Rohman, M. S., Raharjo, S. B., Yagita, K., Okamura, H., & Yokoyama, M. (2001). Angiotensin II induces circadian gene expression of clock genes in cultured vascular smooth muscle cells. *Circulation*, *104*(15), 1746–1748. https://doi.org/10.1161/hc4001.098048

Noya, S. B., Colameo, D., Brüning, F., Spinnler, A., Mircsof, D., Opitz, L., Mann, M., Tyagarajan, S. K., Robles, M. S., & Brown, S. A. (2019). The forebrain synaptic transcriptome is organized by clocks but its proteome is driven by sleep. *Science*, *366*(6462), eaav2642. https://doi.org/10.1126/science.aav2642

Oakley, H., Cole, S. L., Logan, S., Maus, E., Shao, P., Craft, J., Guillozet-Bongaarts, A., Ohno, M., Disterhoft, J., Van Eldik, L., Berry, R., & Vassar, R. (2006). Intraneuronal beta-amyloid aggregates, neurodegeneration, and neuron loss in transgenic mice with five familial Alzheimer's disease mutations: Potential factors in amyloid plaque formation. *The Journal of Neuroscience: The Official Journal of the Society for Neuroscience*, *26*(40), 10129–10140. https://doi.org/10.1523/JNEUROSCI.1202-06.2006

Oh-oka, K., Kono, H., Ishimaru, K., Miyake, K., Kubota, T., Ogawa, H., Okumura, K., Shibata, S., & Nakao, A. (2014). Expressions of Tight Junction Proteins Occludin and Claudin-1 Are under the Circadian Control in the Mouse Large Intestine: Implications in Intestinal

Permeability and Susceptibility to Colitis. *PLOS ONE*, *9*(5), e98016. https://doi.org/10.1371/journal.pone.0098016

Onnink, A. M. H., Zwiers, M. P., Hoogman, M., Mostert, J. C., Dammers, J., Kan, C. C., Vasquez, A. A., Schene, A. H., Buitelaar, J., & Franke, B. (2015). Deviant white matter structure in adults with attention-deficit/hyperactivity disorder points to aberrant myelination and affects neuropsychological performance. *Progress in Neuro-Psychopharmacology & Biological Psychiatry*, *63*, 14–22. https://doi.org/10.1016/j.pnpbp.2015.04.008

Otto, M. E., Svatikova, A., Barretto, R. B. de M., Santos, S., Hoffmann, M., Khandheria, B., & Somers, V. (2004). Early morning attenuation of endothelial function in healthy humans. *Circulation*, *109*(21), 2507–2510. https://doi.org/10.1161/01.CIR.0000128207.26863.C4

Ouyang, Y., Andersson, C. R., Kondo, T., Golden, S. S., & Johnson, C. H. (1998). Resonating circadian clocks enhance fitness in cyanobacteria. *Proceedings of the National Academy of Sciences of the United States of America*, *95*(15), 8660. https://doi.org/10.1073/PNAS.95.15.8660

Paladino, N., Leone, M. J., Plano, S. A., & Golombek, D. A. (2010). Paying the circadian toll: The circadian response to LPS injection is dependent on the Toll-like receptor 4. *Journal of Neuroimmunology*, *225*(1–2), 62–67. https://doi.org/10.1016/J.JNEUROIM.2010.04.015

Pan, W., Cornélissen, G., Halberg, F., & Kastin, A. J. (2002). Selected Contribution: Circadian rhythm of tumor necrosis factor-α uptake into mouse spinal cord. *Journal of Applied Physiology*, *92*(3), 1357–1362. https://doi.org/10.1152/japplphysiol.00915.2001

Pan, W., & Kastin, A. J. (2001). Diurnal variation of leptin entry from blood to brain involving partial saturation of the transport system. *Life Sciences*, *68*(24), 2705–2714. https://doi.org/10.1016/S0024-3205(01)01085-2

Paolicelli, R. C., Bolasco, G., Pagani, F., Maggi, L., Scianni, M., Panzanelli, P., Giustetto, M., Ferreira, T. A., Guiducci, E., Dumas, L., Ragozzino, D., & Gross, C. T. (2011). Synaptic pruning by microglia is necessary for normal brain development. *Science (New York, N.Y.)*, *333*(6048), 1456–1458. https://doi.org/10.1126/science.1202529

Pardridge, W. M. (1992). Recent Developments in Peptide Drug Delivery to the Brain. *Pharmacology & Toxicology*, *71*(1), 3–10. https://doi.org/10.1111/j.1600-0773.1992.tb00512.x

Park, J., Jung, M. S., Moon, E., Lim, H. J., Oh, C. E., & Lee, J. H. (2021). Prediction of Locomotor Activity by Infrared Motion Detector on Sleep-wake State in Mice. *Clinical Psychopharmacology and Neuroscience*, *19*(2), 303. https://doi.org/10.9758/CPN.2021.19.2.303

Park, J.-S., Kam, T.-I., Lee, S., Park, H., Oh, Y., Kwon, S.-H., Song, J.-J., Kim, D., Kim, H., Jhaldiyal, A., Na, D. H., Lee, K. C., Park, E. J., Pomper, M. G., Pletnikova, O., Troncoso, J. C., Ko, H. S., Dawson, V. L., Dawson, T. M., & Lee, S. (2021). Blocking microglial activation of reactive astrocytes is neuroprotective in models of Alzheimer's disease. *Acta Neuropathologica Communications*, *9*(1), 78. https://doi.org/10.1186/s40478-021-01180-z

Paschos, G. K., & FitzGerald, G. A. (2010). Circadian clocks and vascular function. *Circulation Research*, *106*(5), 833–841. https://doi.org/10.1161/CIRCRESAHA.109.211706

Peng, X., Luo, Z., He, S., Zhang, L., & Li, Y. (2021). Blood-Brain Barrier Disruption by Lipopolysaccharide and Sepsis-Associated Encephalopathy. *Frontiers in Cellular and Infection Microbiology*, *11*.

Persidsky, Y., Ramirez, S. H., Haorah, J., & Kanmogne, G. D. (2006). Blood-brain barrier: Structural components and function under physiologic and pathologic conditions. *Journal of Neuroimmune Pharmacology: The Official Journal of the Society on NeuroImmune Pharmacology*, *1*(3), 223–236. https://doi.org/10.1007/s11481-006-9025-3

Pizarro, A., Hayer, K., Lahens, N. F., & Hogenesch, J. B. (2013). CircaDB: A database of mammalian circadian gene expression profiles. *Nucleic Acids Research*, *41*(Database issue), D1009-1013. https://doi.org/10.1093/nar/gks1161

Podbielska, M., Banik, N. L., Kurowska, E., & Hogan, E. L. (2013). Myelin Recovery in Multiple Sclerosis: The Challenge of Remyelination. *Brain Sciences*, *3*(3), 1282–1324. https://doi.org/10.3390/brainsci3031282

Polfliet, M. M. J., Zwijnenburg, P. J. G., van Furth, A. M., van der Poll, T., Döpp, E. A., Renardel de Lavalette, C., van Kesteren-Hendrikx, E. M. L., van Rooijen, N., Dijkstra, C. D., & van den Berg, T. K. (2001). Meningeal and Perivascular Macrophages of the Central Nervous System Play a Protective Role During Bacterial Meningitis. *The Journal of Immunology*, *167*(8), 4644–4650. https://doi.org/10.4049/jimmunol.167.8.4644

Prolo, L. M., Takahashi, J. S., & Herzog, E. D. (2005). Circadian rhythm generation and entrainment in astrocytes. *The Journal of Neuroscience: The Official Journal of the Society for Neuroscience*, *25*(2), 404–408. https://doi.org/10.1523/JNEUROSCI.4133-04.2005

Pulido, R. S., Munji, R. N., Chan, T. C., Quirk, C. R., Weiner, G. A., Weger, B. D., Rossi, M. J., Elmsaouri, S., Malfavon, M., Deng, A., Profaci, C. P., Blanchette, M., Qian, T., Foreman, K. L., Shusta, E. V., Gorman, M. R., Gachon, F., Leutgeb, S., & Daneman, R. (2020). Neuronal Activity Regulates Blood-Brain Barrier Efflux Transport through Endothelial Circadian Genes. *Neuron*, *108*(5), 937-952.e7. https://doi.org/10.1016/j.neuron.2020.09.002

Pulido-Salgado, M., Vidal-Taboada, J. M., Barriga, G. G.-D., Solà, C., & Saura, J. (2018). RNA-Seq transcriptomic profiling of primary murine microglia treated with LPS or LPS + IFNγ. *Scientific Reports*, *8*(1), 16096. https://doi.org/10.1038/s41598-018-34412-9

Quartin, A. A., Calonge, R. O., Schein, R. M. H., & Crandall, L. A. (2008). Influence of critical illness on physicians' prognoses for underlying disease: A randomized study using simulated cases. *Critical Care Medicine*, *36*(2), 462–470. https://doi.org/10.1097/01.CCM.0B013E3181611F968

Radulovic, K., Mak'Anyengo, R., Kaya, B., Steinert, A., & Niess, J. H. (2018). Injections of Lipopolysaccharide into Mice to Mimic Entrance of Microbial-derived Products After Intestinal Barrier Breach. *Journal of Visualized Experiments : JoVE*, *135*, 57610. https://doi.org/10.3791/57610

Ramkisoensing, A., & Meijer, J. H. (2015). Synchronization of Biological Clock Neurons by Light and Peripheral Feedback Systems Promotes Circadian Rhythms and Health. *Frontiers in Neurology*, *6*, 128. https://doi.org/10.3389/fneur.2015.00128

Ransohoff, R. M. (2016). A polarizing question: Do M1 and M2 microglia exist? *Nature Neuroscience*, *19*(8), Article 8. https://doi.org/10.1038/nn.4338

Rojo, D., Badner, A., & Gibson, E. M. (2022). Circadian control of glial cell homeodynamics. *Journal of Biological Rhythms*, *37*(6), 593–608. https://doi.org/10.1177/07487304221120966

Rojo, D., Cengio, L. D., Badner, A., Kim, S., Sakai, N., Greene, J., Dierckx, T., Mehl, L. C., Eisinger, E., Ransom, J., Arellano-Garcia, C., Gumma, M. E., Soyk, R. L., Lewis, C. M., Lam, M., Weigel, M. K., Damonte, V. M., Yalçın, B., Jones, S. E., … Gibson, E. M. (2023). BMAL1 loss in oligodendroglia contributes to abnormal myelination and sleep. *Neuron*, *0*(0). https://doi.org/10.1016/j.neuron.2023.08.002

Saunders, N. R., Dziegielewska, K. M., Møllgård, K., & Habgood, M. D. (2015). Markers for blood-brain barrier integrity: How appropriate is Evans blue in the twenty-first century and what are the alternatives? *Frontiers in Neuroscience*, *9*.

Schafer, D. P., Lehrman, E. K., Kautzman, A. G., Koyama, R., Mardinly, A. R., Yamasaki, R., Ransohoff, R. M., Greenberg, M. E., Barres, B. A., & Stevens, B. (2012). Microglia Sculpt Postnatal Neural Circuits in an Activity and Complement-Dependent Manner. *Neuron*, *74*(4), 691. https://doi.org/10.1016/j.neuron.2012.03.026

Scheiermann, C., Kunisaki, Y., Lucas, D., Chow, A., Jang, J.-E., Zhang, D., Hashimoto, D., Merad, M., & Frenette, P. S. (2012). Adrenergic nerves govern circadian leukocyte recruitment to tissues. *Immunity*, *37*(2), 290–301. https://doi.org/10.1016/j.immuni.2012.05.021

Seemann, S., Zohles, F., & Lupp, A. (2017). Comprehensive comparison of three different animal models for systemic inflammation. *Journal of Biomedical Science*, *24*(1), 60. https://doi.org/10.1186/s12929-017-0370-8

Sehgal, A. (2017). Physiology Flies with Time. *Cell*, *171*(6), 1232–1235. https://doi.org/10.1016/J.CELL.2017.11.028

Shackelford, P. G., & Feigin, R. D. (1973). Periodicity of susceptibility to pneumococcal infection: Influence of light and adrenocortical secretions. *Science (New York, N.Y.)*, *182*(4109), 285–287. https://doi.org/10.1126/SCIENCE.182.4109.285

Sheehan, P. W., Nadarajah, C. J., Kanan, M. F., Patterson, J. N., Novotny, B., Lawrence, J. H., King, M. W., Brase, L., Inman, C. E., Yuede, C. M., Lee, J., Patel, T. K., Harari, O., Benitez, B. A., Davis, A. A., & Musiek, E. S. (2023). An astrocyte BMAL1-BAG3 axis protects against alpha-synuclein and tau pathology. *Neuron*, *111*(15), 2383-2398.e7. https://doi.org/10.1016/j.neuron.2023.05.006

Silva, A. Y. O., Amorim, É. A., Barbosa-Silva, M. C., Lima, M. N., Oliveira, H. A., Granja, M. G., Oliveira, K. S., Fagundes, P. M., Neris, R. L. S., Campos, R. M. P., Moraes, C. A., Vallochi, A. L., Rocco, P. R. M., Bozza, F. A., Castro-Faria-Neto, H. C., & Maron-Gutierrez, T. (2020). Mesenchymal Stromal Cells Protect the Blood-Brain Barrier, Reduce Astrogliosis, and Prevent Cognitive and Behavioral Alterations in Surviving Septic Mice. *Critical Care Medicine*, *48*(4), e290. https://doi.org/10.1097/CCM.0000000000004219

Silver, A. C., Arjona, A., Hughes, M. E., Nitabach, M. N., & Fikrig, E. (2012). Circadian expression of clock genes in mouse macrophages, dendritic cells, and B cells. *Brain, Behavior, and Immunity*, *26*(3), 407–413. https://doi.org/10.1016/J.BBI.2011.10.001

Silver, A. C., Buckley, S. M., Hughes, M. E., Hastings, A. K., Nitabach, M. N., & Fikrig, E. (2018). Daily oscillations in expression and responsiveness of Toll-like receptors in

splenic immune cells. *Heliyon*, *4*(3), e00579. https://doi.org/10.1016/j.heliyon.2018.e00579

Singh, A. K., & Jiang, Y. (2004). How does peripheral lipopolysaccharide induce gene expression in the brain of rats? *Toxicology*, *201*(1), 197–207. https://doi.org/10.1016/j.tox.2004.04.015

Sladojevic, N., Stamatovic, S. M., Johnson, A. M., Choi, J., Hu, A., Dithmer, S., Blasig, I. E., Keep, R. F., & Andjelkovic, A. V. (2019). Claudin-1-Dependent Destabilization of the Blood–Brain Barrier in Chronic Stroke. *The Journal of Neuroscience*, *39*(4), 743–757. https://doi.org/10.1523/JNEUROSCI.1432-18.2018

Sofroniew, M. V., & Vinters, H. V. (2010). Astrocytes: Biology and pathology. *Acta Neuropathologica*, *119*(1), 7–35. https://doi.org/10.1007/s00401-009-0619-8

Stephan, F. K., & Zucker, I. (1972). Circadian Rhythms in Drinking Behavior and Locomotor Activity of Rats Are Eliminated by Hypothalamic Lesions. *Proceedings of the National Academy of Sciences*, *69*(6), 1583–1586. https://doi.org/10.1073/PNAS.69.6.1583

Stevenson, P. G., Hawke, S., Sloan, D. J., & Bangham, C. R. (1997). The immunogenicity of intracerebral virus infection depends on anatomical site. *Journal of Virology*, *71*(1), 145–151.

Takahashi, J. S. (2017). Transcriptional architecture of the mammalian circadian clock. *Nature Reviews. Genetics*, *18*(3), 164. https://doi.org/10.1038/NRG.2016.150

Takahashi, J. S., Hong, H. K., Ko, C. H., & McDearmon, E. L. (2008). The genetics of mammalian circadian order and disorder: Implications for physiology and disease. *Nature Reviews Genetics 2008 9:10*, *9*(10), 764–775. https://doi.org/10.1038/nrg2430

Takeda, M., Mori, F., Yoshida, A., Takamiya, A., Nakagomi, S., Sato, E., & Kiyama, H. (2001). Constitutive nitric oxide synthase is associated with retinal vascular permeability in early diabetic rats. *Diabetologia*, *44*(8), 1043–1050. https://doi.org/10.1007/s001250100588

Takeda, N., & Maemura, K. (2016). Circadian clock and the onset of cardiovascular events. *Hypertension Research*, *39*(6), Article 6. https://doi.org/10.1038/hr.2016.9

Thiel, V. E., & Audus, K. L. (2001). Nitric oxide and blood-brain barrier integrity. *Antioxidants & Redox Signaling*, *3*(2), 273–278. https://doi.org/10.1089/152308601300185223

Tiedt, S., Buchan, A. M., Dichgans, M., Lizasoain, I., Moro, M. A., & Lo, E. H. (2022). The neurovascular unit and systemic biology in stroke—Implications for translation and treatment. *Nature Reviews. Neurology*, *18*(10), 597–612. https://doi.org/10.1038/s41582-022-00703-z

Trontinemab | ALZFORUM. (n.d.). Retrieved January 23, 2024, from https://www.alzforum.org/therapeutics/trontinemab

Tso, C. F., Simon, T., Greenlaw, A. C., Puri, T., Mieda, M., & Herzog, E. D. (2017). Astrocytes regulate daily rhythms in the suprachiasmatic nucleus and behavior. *Current Biology : CB*, *27*(7), 1055–1061. https://doi.org/10.1016/j.cub.2017.02.037

Utepbergenov, D. I., Fanning, A. S., & Anderson, J. M. (2006). Dimerization of the scaffolding protein ZO-1 through the second PDZ domain. *The Journal of Biological Chemistry*, *281*(34), 24671–24677. https://doi.org/10.1074/jbc.M512820200

van Furth, R., & Cohn, Z. A. (1968). The origin and kinetics of mononuclear phagocytes. *The Journal of Experimental Medicine*, *128*(3), 415–435. https://doi.org/10.1084/jem.128.3.415

Vichaya, E. G., Malik, S., Sominsky, L., Ford, B. G., Spencer, S. J., & Dantzer, R. (2020). Microglia depletion fails to abrogate inflammation-induced sickness in mice and rats. *Journal of Neuroinflammation*, *17*(1), 172. https://doi.org/10.1186/s12974-020-01832-2

Wang, C., Li, J., Zhao, L., & Qian, P. (2022). Shape transformations of red blood cells in the capillary and their possible connections to oxygen transportation. *Journal of Biological Physics*, *48*(1), 79–92. https://doi.org/10.1007/s10867-021-09594-5

Wang, X.-L., Kooijman, S., Gao, Y., Tzeplaeff, L., Cosquer, B., Milanova, I., Wolff, S. E. C., Korpel, N., Champy, M.-F., Petit-Demoulière, B., Goncalves Da Cruz, I., Sorg-Guss, T., Rensen, P. C. N., Cassel, J.-C., Kalsbeek, A., Boutillier, A.-L., & Yi, C.-X. (2021). Microglia-specific knock-down of Bmal1 improves memory and protects mice from high fat diet-induced obesity. *Molecular Psychiatry*, *26*(11), 6336–6349. https://doi.org/10.1038/s41380-021-01169-z

Wee, R., Castrucci, A. M., Provencio, I., Gan, L., & Van Gelder, R. N. (2002). Loss of Photic Entrainment and Altered Free-Running Circadian Rhythms in math5−/− Mice. *The Journal of Neuroscience*, *22*(23), 10427. https://doi.org/10.1523/JNEUROSCI.22-23-10427.2002

Wiedrick, J., Meza-Romero, R., Gerstner, G., Seifert, H., Chaudhary, P., Headrick, A., Kent, G., Maestas, A., Offner, H., & Vandenbark, A. A. (2021). Sex differences in EAE reveal common and distinct cellular and molecular components. *Cellular Immunology*, *359*, 104242. https://doi.org/10.1016/j.cellimm.2020.104242

Williamson, A. V., Mellor, J. R., Grant, A. L., & Randall, A. D. (1998). Properties of GABA(A) receptors in cultured rat oligodendrocyte progenitor cells. *Neuropharmacology*, *37*(7), 859–873. https://doi.org/10.1016/s0028-3908(98)00016-1

Wolburg, H., Wolburg-Buchholz, K., & Engelhardt, B. (2005). Diapedesis of mononuclear cells across cerebral venules during experimental autoimmune encephalomyelitis leaves tight junctions intact. *Acta Neuropathologica*, *109*(2), 181–190. https://doi.org/10.1007/s00401-004-0928-x

Womac, A. D., Burkeen, J. F., Neuendorff, N., Earnest, D. J., & Zoran, M. J. (2009). Circadian Rhythms of Extracellular ATP Accumulation in SCN Cells and Cultured Astrocytes. *The European Journal of Neuroscience*, *30*(5), 869–876. https://doi.org/10.1111/j.1460-9568.2009.06874.x

Wong, K. H., Riaz, M. K., Xie, Y., Zhang, X., Liu, Q., Chen, H., Bian, Z., Chen, X., Lu, A., & Yang, Z. (2019). Review of Current Strategies for Delivering Alzheimer's Disease Drugs across the Blood-Brain Barrier. *International Journal of Molecular Sciences*, *20*(2), Article 2. https://doi.org/10.3390/ijms20020381

Yang, A. C., Stevens, M. Y., Chen, M. B., Lee, D. P., Stähli, D., Gate, D., Contrepois, K., Chen, W., Iram, T., Zhang, L., Vest, R. T., Chaney, A., Lehallier, B., Olsson, N., du Bois, H., Hsieh, R., Cropper, H. C., Berdnik, D., Li, L., … Wyss-Coray, T. (2020). Physiological blood-brain transport is impaired with age by a shift in transcytosis. *Nature*, *583*(7816), 425–430. https://doi.org/10.1038/s41586-020-2453-z

Yang, T., Guo, R., & Zhang, F. (2019). Brain perivascular macrophages: Recent advances and implications in health and diseases. *CNS Neuroscience & Therapeutics*, *25*(12), 1318–1328. https://doi.org/10.1111/cns.13263

Yao, L., Xue, X., Yu, P., Ni, Y., & Chen, F. (2018). Evans Blue Dye: A Revisit of Its Applications in Biomedicine. *Contrast Media & Molecular Imaging*, *2018*, 7628037. https://doi.org/10.1155/2018/7628037

You, S., Yu, A. M., Roberts, M. A., Joseph, I. J., & Jackson, F. R. (2021). Circadian regulation of the Drosophila astrocyte transcriptome. *PLoS Genetics*, *17*(9), e1009790. https://doi.org/10.1371/journal.pgen.1009790

Yuan, S. Y., & Rigor, R. R. (2010). Structure and Function of Exchange Microvessels. In *Regulation of Endothelial Barrier Function*. Morgan & Claypool Life Sciences. https://www.ncbi.nlm.nih.gov/books/NBK54123/

Zenaro, E., Pietronigro, E., Bianca, V. D., Piacentino, G., Marongiu, L., Budui, S., Turano, E., Rossi, B., Angiari, S., Dusi, S., Montresor, A., Carlucci, T., Nanì, S., Tosadori, G., Calciano, L., Catalucci, D., Berton, G., Bonetti, B., & Constantin, G. (2015). Neutrophils promote Alzheimer's disease-like pathology and cognitive decline via LFA-1 integrin. *Nature Medicine*, *21*(8), 880–886. https://doi.org/10.1038/nm.3913

Zhang, R., Lahens, N. F., Ballance, H. I., Hughes, M. E., & Hogenesch, J. B. (2014). A circadian gene expression atlas in mammals: Implications for biology and medicine. *Proceedings of the National Academy of Sciences of the United States of America*, *111*(45), 16219–16224. https://doi.org/10.1073/pnas.1408886111

Zhang, S. L., Lahens, N. F., Yue, Z., Arnold, D. M., Pakstis, P. P., Schwarz, J. E., & Sehgal, A. (2021). A circadian clock regulates efflux by the blood-brain barrier in mice and human cells. *Nature Communications*, *12*(1), 617. https://doi.org/10.1038/s41467-020-20795-9

Zhang, S. L., Yue, Z., Arnold, D. M., Artiushin, G., & Sehgal, A. (2018). A Circadian Clock in the Blood-Brain Barrier Regulates Xenobiotic Efflux. *Cell*, *173*(1), 130-139.e10. https://doi.org/10.1016/j.cell.2018.02.017

Zhang, Y., & Pardridge, W. M. (2001). Rapid transferrin efflux from brain to blood across the blood-brain barrier. *Journal of Neurochemistry*, *76*(5), 1597–1600. https://doi.org/10.1046/j.1471-4159.2001.00222.x

Zhang, Z., Yu, B., Wang, X., Luo, C., Zhou, T., Zheng, X., & Ding, J. (2020). Circadian rhythm and atherosclerosis (Review). *Experimental and Therapeutic Medicine*, *20*(5), 96. https://doi.org/10.3892/etm.2020.9224

Zheng, B., Larkin, D. W., Albrecht, U., Sun, Z. S., Sage, M., Eichele, G., Lee, C. C., & Bradley, A. (1999). The mPer2 gene encodes a functional component of the mammalian circadian clock. *Nature*, *400*(6740), Article 6740. https://doi.org/10.1038/22118